REDOX SIGNALING IN AN IN VIVO FLOW MODEL OF LOW MAGNITUDE OSCILLATORY WALL SHEAR STRESS

A Dissertation
Presented to
The Academic Faculty

by

Nick J. Willett

In Partial Fulfillment
of the Requirements for the Degree
Doctor in Philosophy in the
Wallace H. Coulter Department of Biomedical Engineering

Georgia Institute of Technology
May 2010

REDOX SIGNALING IN AN IN VIVO FLOW MODEL OF LOW MAGNITUDE OSCILLATORY WALL SHEAR STRESS

Approved by:

W. Robert Taylor, M.D., Ph.D., Advisor
School of Medicine
Emory University

Don P. Giddens, Ph.D.
School of Biomedical Engineering
Georgia Institute of Technology

John Oshinski, Ph.D.
School of Biomedical Engineering
Georgia Institute of Technology

Roy L. Sutliff, Ph.D.
School of Medicine
Emory University

Dr. Hanjoong Jo, Ph.D.
School of Biomedical Engineering
Georgia Institute of Technology

Date Approved: March, 10, 2010

ACKNOWLEDGEMENTS

This thesis is the cumulative product of much excellent collaboration over the last five years. The biomedical engineering department collaboration between Emory and Georgia Tech truly provides an environment conducive to success. From the administrative management to the PI's, everyone in this department has been immensely helpful along my journey. For this I am immensely grateful and I will try to express the depth and reach of the support that I have received over the last five years.

First and foremost, I would like to thank my advisor, Bob Taylor. Bob has been an outstanding advisor and I cannot express how lucky I am to have worked under him for the past five years. I came to graduate school with a background entirely composed of engineering and little to no knowledge of the biological world around me. Bob is one of the few MD's that I have met that takes an active interest in engineering and is truly an engineer at heart. Though I may have not realized this at the time, I believe that this trait was an immediate connection that made me feel comfortable in my transition into a new field. Furthermore, Bob's laid back attitude seemed to match mine incredibly well. In particular, I appreciate the fact that although Bob is now Chair of Cardiology he still resents wearing ties and takes his off as soon as we get into a meeting. Though this may seem small, it has been these small things that have made me feels so comfortable and fostered an excellent relationship between advisor and advisee. Beyond the work environment, I am ever amazed at the wealth of knowledge that Bob retains. Be it the location of a 10 year old piece of equipment located in the cupboard of a back corner of the lab or an unknown cd-something molecule that I can never keep straight. Bob has

amazing insight into every project and presentation. Thank you for your excellent guidance during the course of my work. Thank you for your support in helping develop into the scientist that I now am. I truly admire you and you have been an inspiration to me over the last five years.

I would like to thank my thesis committee, Roy Sutliff, John Oshinski, Hanjoong Jo, and Don Giddens. Thank you all for the advice and guidance that you have provided over the years. I was able to put my committee together early in my thesis work, and you all have provided immensely valuable support in the direction of my work. Additionally, I have collaborated with everyone of you in one way or another during my thesis work. To Roy, thank you for helping with the blood pressure measurements. Those were a pain and I hope you never have to do those again. To John, thank you for your help with the CFD and MR. I appreciate the access to your computers and the guidance you have provided during interpretation of the data. To Dr. Jo, thank you for your help with sharing resources, antibodies, and mice. Your work has truly gone hand in hand with mine and I look forward to seeing where your leadership takes the field. To Don, thank you for the guidance and friendship you have provided. I know you are busy as a dean and I appreciate you taking time and a special interest in my project. Thank you for providing resources to help me develop the CFD part of work. Thank you committee members, you all have been instrumental in the success of my thesis work.

I must also thank my other collaborators. Thank you to Bob Long for your help in the animal imaging with the MR. Thank you to Bob Guldberg and Angela Lin for help with the μCT imaging. I also did a rotation with Bob Guldberg and will be pursuing a post-doc in his lab. Bob, I look forward to continued work with you. Thank you to Niren

Murthy and Kousik Kundu for help with the hydrocyanine dyes. In particular I would like to express my gratitude to Kousik who made dyes for me on a single day of notice and would even bring them to me at Emory. Thank you.

During my rotation with Bob, I know that Bob expected me to pursue a different direction, one with an engineering emphasis, but it was the amazing environment that Bob has cultivated in his lab that attracted me. The lab has a wealth of expertise with people coming from all backgrounds and a wealth of diversity with members from all over the globe. The lab has had many people come and go over the last five years and they have all provided support and friendship for me. First, I must thank Daiana Weiss. Daiana knows absolutely everything there is to know about working with mice. She helped me develop my coarctation surgery which is the basis for this entire thesis. She has also been a great friend over the last five years. Thank you Daiana. I would also like to particularly thank Dardo Ferrara. Dardo developed the en face staining techniwue and began the entire shear stress project that my thesis was built upon. Thank you for all your hard work before I started in the lab and for teaching me the techniques.

To the current postdocs in the lab, Sarah Knight, Natalia Landazari, and recently Alicia Lyle, thank you for the mentorship that you have provided for me. To Sarah, thank you for all the hard work that you have put into developing the hydrocyanines and nurturing the collaboration with the Murthy lab. To Natalia, thank you for your help in the animal surgery room. To Ali, thank you for the support during the days of writing this thesis. It was great to have someone to discuss the pain that is writing a 200+ page thesis and for the little bits of advice after having just gone through the whole process.

Next, I must thank my fellow graduate students, Brian Clark, Ian Campbell, Ebony Washington, Scott Robinson and former graduate students Katie Rafferty, Craig Duvall, and Matt Whalin. You all have provided such great support and friendship during graduate school. We have had great times from the many lunches, to late nights and early mornings in the lab, to birthday parties, concerts, sporting events, etc., and even doing research together. Firstly, to Katie, thank you for mentoring me during my rotation. I enjoyed learning how to do scientific research with animals and it was your mentorship that led me to join the lab. Thank you for your continued friendship and best of luck in Cincinnati. To Craig, you were a great friend when I joined the lab and have continued to be to this day. You are truly an inspiration in the success that you have had and I wish you the best of luck. To Matt, thank you for introducing me to 312. I have valued are continued friendship, particularly on the soccer field. To Scott, your dedication and perseverance have been inspirational and I still can't believe that you are about to go on and start med school. I wish you the best of luck. Thank you for the friendship you have provided over the years. To Ebony, it was great having another student join at the same time as me. During the initial lab "hazing" period I had someone to conspire with and share the burden. To Ian, thank you for your help with the CFD work. I appreciate your effort getting everything up and running in Oshinskiville and working to learn the software and help me with it. I have thoroughly enjoyed all our discussion over beer and talk of brewing. It has been a great outlet during long days at work. To Brian, I wish you luck in the lab and it has been great to see a new and still inspired face around the lab. Thanks to all my fellow students.

Additionally, I would like to thank the rest of the Taylor lab including, Dianne Sutcliffe, Giji Joseph, Rachel Ransom, Aaron Fan. I have enjoyed the years in lab with you. Thanks for your help during staining, suggestions and advice during lab meetings, and for helping to maintain working order in the lab. I wish you all best of luck in your future endeavors. I wish to also thank all the previous members of the Taylor lab.

Finally, I would like to thank those closest to me, my family. Ben, Jesse, John and Judy thank you so much for being a wonderful, loving, and supportive family. Seeing you guys is always such a relief, and a welcome break from the tough days at works. I love spending vacation and holidays with all of you and hope that we can continue our traditions even as our family expands. To Ben and Jess, thank you for being such great siblings. It was great having you guys out in Colorado (though Jess came after I graduated). It is amazing how similar we all are yet can have such completely different directions in life. I wish you both the best of luck. To my parents, I can't thank you enough for the support you have provided over the years. Thank you for providing me with the excellent opportunities that I have had throughout my life. I am so grateful. I love you both very much. I would also like to thank my grandparents Gram and Marty, Grandpa Bill and Carol, and the late Peg and Ward (Gamma and Gamp). I love you all. Lastly, I would like to thank my ever supportive girlfriend, Amber Hudson. You have been so wonderful to me over the last three years and in particular the last couple of months. I am so happy that I will be staying in Atlanta to be with you as you finish your PhD. I hope that I can provide the same support that you have given to me both in and out of work.

TABLE OF CONTENTS

LIST OF FIGURES

LIST OF ABBREVIATIONS

1-D	1-Dimensional
3-D	3-Dimensional
AAA	Abdominal Aortic Aneurysm
AEBSF	4-(2-Aminoethyl)benzenesulfonylfluoride
AHA	American Heart Association
Ang II	Angiotensin II
ANOVA	Analysis of Variances
apoE	Apolipoprotein E
AT_1R	Angiotensin I Receptor
BAECS	Bovine Aortic Endothelial Cells
βAPN	Beta-aminopropionitrile Fumarate
BMP4	Bone Morphogenic Protein 4
BSA	Bovine Serum Albumen
CFD	Computational Fluid Dynamics
CVD	Cardiovascular Disease
DCF-DA	Dichlorofluorescein Diacetate
DHE	Dihydroethidium
DNA	Deoxyribonucleic Acid
DPI	Diphenyleneiodonium
ECM	Extracellular Matrix
EGFR	Epidermal Growth Factor Receptor
eNOS	endothelial nitric oxide synthase (NOS III)
ESR	Electron Spin Resonance

GPx	Glutathione Peroxidase
GTP	Guanosine Triphosphate
HPLC	High Performance Liquid Chromatography
HUVECS	Human Umbilical Vein Endothelial Cells
ICAM-1	Intracellular Adhesion Molecule-1
IL-1	Interleukin 1
LFA-1	Lymphocyte Function Associated Molecule-1
L-NAME	L-arginine methyl ester
MAC-1	Macrophage-1 Antigen
MAECS	Mouse Aortic Endothelial Cells
μCT	Micro-Computed Tomography
MRI	Magnetic Resonance Imaging
mRNA	Messenger Ribonucleic Acid
MPO	Myloperoxidase
NADP	Nicotinamide Adenine Dinucleotide Phosphate
NFκB	Nuclear Factor Kappa B-cell
NO	Nitric Oxide
Nox	NADPH Oxidase
OSI	Oscillatory Shear Index
PBS	Phosphate Buffered Saline
PECAM-1	Platelet Endothelial Cell Adhesion Molecule-1
PEG-SOD	Polyethylene Glycol Superoxide Dismutase
Re	Reynold's Number
ROS	Reactive Oxygen Species
SEM	Standard Error of the Mean

siRNA	Small Interfering Ribonucleic Acid
SMP	Shape Memory Polymer
SOD	Superoxide Dismutase
TNF-alpha	Tumor Necrosis Factor-Alpha
VCAM-1	Vascular Cell Adhesion Molecule-1
VE Cadherin	Vascular Endothelial Cadherin
VEGF-R	Vascular Endothelial Growth Factor Receptor
VLA-4	Very Late Activation Antigen-4
WSS	Wall Shear Stress
XDH	Xanthine Dehydrogenase
XO	Xanthine Oxidase

LIST OF SYMBOLS

μ	Viscosity
ρ	Density
υ	Kinematic Viscosity
ω	Angular Frequency
α	Womersley Number
τ	Shear Stress
$O_2^{\cdot -}$	Superoxide

SUMMARY

Atherosclerosis is a multifactorial inflammatory disease that occurs in predisposed locations in the vasculature where blood flow is disturbed. *In vitro* studies have implicated reactive oxygen species as important mediators of pathologic WSS signaling. *In vitro* studies have implicated reactive oxygen species as mediators of mechanotransduction leading to inflammatory protein expression and ultimately atherogenesis. While these cell culture-based studies have provided enormous insight into the effects of WSS on endothelial biology, the applicability to the normal, *in vivo* setting is questionable. We hypothesized that low magnitude oscillatory WSS acts through ROS to increase expression of inflammatory cell adhesion molecules leading to the development of atherosclerotic lesions. The overall objective for this thesis was to develop an *in vivo* flow model in the mouse that produces low magnitude oscillatory wall shear stress which could be used to investigate the *in vivo* molecular mechanisms of mechanotransduction.

We created a novel aortic coarctation model using a shape memory nitinol clip. The clip reproducibly constricts the aorta creating a narrowing of the lumen resulting in a stenosis. This mechanical constraint produces a region of flow separation downstream from the coarctation. We have characterized the coarctation in terms of the efficacy, pressure loss, and fluid dynamics. We then measured the endothelial response of shear sensitive redox and inflammatory markers. Lastly, we utilized genetically modified mice and mice treated with pharmacological inhibitors to investigate the mechanisms involved in the expression of WSS induced inflammatory and redox markers.

We found that inducing a coarctation of the aorta using a nitinol clip uniquely created a hemodynamic environment of low magnitude oscillatory WSS without a significant change in blood pressure. Using this model we found that the *in vivo* endothelial phenotype associated with acutely disturbed flow was characterized by increased production of superoxide and increased expression of select inflammatory proteins. In comparison, the phenotype associated with chronically disturbed flow was characterized by a more modest increase in superoxide and increased levels of multiple inflammatory proteins. We determined that in regions of acutely disturbed flow *in vivo*, VCAM-1 expression was not modulated by reactive oxygen species. Additionally, p47 phox-dependent NADPH Oxidase activity does not have a functional role in WSS induced superoxide generation in the endothelium.

In summary, we have created a novel murine model of low magnitude oscillatory WSS that can be used to investigate the *in vivo* molecular mechanisms associated with atherogenesis. While previous data obtained *in vitro* indicated that depletion of an individual ROS was sufficient to inhibit flow-induced inflammatory protein expression, our findings, to the contrary, showed that antioxidant treatment *in vivo* does not inhibit shear-dependent inflammatory protein expression. Our results suggest that atherogenesis in the *in vivo* environment is significantly more complicated than the *in vitro* environment and that parallel pathways and compensatory mechanisms are likely activated *in vivo* in response to WSS. These results could have significant implications in the efficacy of antioxidant treatment of atherosclerosis and could explain the complexity of results observed in clinical trials.

CHAPTER 1

SPECIFIC AIMS

Atherosclerosis is a multifactorial inflammatory disease of the vasculature that develops over many years. It is the underlying cause of numerous other cardiovascular diseases, notably myocardial infarction and stroke. These diseases are the leading cause of morbidity and mortality in the United States as well as a major financial burden on our society [1-3]. Significant resources, have therefore, gone into the research and understanding of the pathogenesis of atherosclerosis. Numerous risk factors for atherosclerosis have been identified such as age, smoking, obesity, genetics, diabetes, hypelipidemia, and hypertension. These risk factors are considered systemic risk factors; however, atherosclerosis is a focal disease that occurs in specific predisposed locations in the vasculature.

Specific hemodynamic conditions have been correlated to the localization of atherosclerotic lesion formation. These conditions uniquely occur in regions of disturbed blood flow where there is low magnitude oscillatory WSS. The majority of studies on the effects of WSS on endothelial biology have involved cell culture-based studies. The obvious and significant advantage of these systems is the ability to carefully regulate both the hemodynamic and biological environments. Research using these systems has generated a wealth of productive studies. These studies have shown that low and/or oscillatory WSS is associated with pro-atherogenic factors including oxidative stress, VCAM-1 expression, and uncoupled eNOS, among others. *In vitro* studies have specifically identified ROS as important mediators of pathologic WSS signaling. ROS have been shown to mediate the activation of the NFκB transcription factor and

subsequently inflammatory cell adhesion molecule expression. Conversely, physiologic, "high" shear stress has been associated with atheroprotective factors such as increased eNOS expression, increased expression of antioxidant enzymes and resultant increased concentrations of bioavailable NO.

While these cell culture-based studies have provided enormous insight into the effects of WSS on endothelial biology, the applicability to the normal, *in vivo* setting is questionable. Initial *in vivo* studies have shown correlations between pro-atherogenic factors and regions predisposed to atherosclerosis. However, the characterization of shear stress in the intact animal is extremely complex, and studies of these pro-atherogenic regions have been difficult and limited. It is imperative to develop more comprehensive *in vivo* shear stress models in order to definitively assess the applicability of these *in vitro* data to the *in vivo* setting. We hypothesized that low magnitude oscillatory WSS acts through ROS to increase expression of inflammatory cell adhesion molecules leading to the development of atherosclerotic lesions.

Specific Aim 1

Develop an acute mouse aortic coarctation model

Our first objective was to develop an *in vivo* coarctation model of controlled hemodynamic conditions in which we can quantitatively assess expression of pro-inflammatory gene products that have been linked to atherogenesis. Our model overcomes the limitations of previous flow models by inducing a precisely defined coarctation in the suprarenal region of the aorta using a shape memory nitinol clip. We used μCT and MRI techniques to obtain boundary conditions for a computational fluid

dynamic model. Using our CFD *in silico* model we characterized the hemodynamic environment associated with our *in vivo* coarctation model.

Specific Aim 2

Identify the expression of inflammatory markers in the mouse coarctation model

Our objective for specific aim 2 was to quantitatively measure the acute response of atherogenic markers in the region of low magnitude oscillatory WSS. We hypothesized that inflammatory proteins would increase in the region of low magnitude oscillatory WSS. We quantitatively measured expression of VCAM-1 and ICAM-1 using quantum dot nanoparticles with immunohistochemical techniques and also measured superoxide levels using the novel superoxide sensitive dye, hydro-Cy3. Additionally, we were able to compare differences between the acute response, on the order of days, and chronic response, on the order of months. The acute response was measured downstream from the coarctation while the chronic response was measured in the aortic arch.

Specific Aim 3

Investigate redox signaling mechanisms in the mouse coarctation model

Our final objective was to investigate the signaling mechanisms by which ROS mediate WSS transduction to induce inflammatory marker signaling using a combination of genetic models and pharmacological inhibitors. We hypothesized that atherogenic markers would increase in a ROS dependent manner in response to disturbed flow. To analyze this hypothesis we employed a combination of transgenic animals and pharmacological inhibitors to alter ROS signaling pathways with our coarctation model. We then measured VCAM-1 expression in these animal models. We found that inflammatory protein expression increased in response to acutely induced low magnitude

WSS and that decreased ROS levels were not sufficient to attenuate this response. This suggests that parallel pathways or compensatory mechanisms may be acting in this *in vivo* model.

Significance and Innovation

Research into the molecular mechanisms involved in the pathogenesis of atherosclerosis will lead to advancements in therapeutics to treat the leading cause of morbidity and mortality in the United States. Atherosclerosis develops at specific regions of the vasculature where the hemodynamics produce low magnitude oscillatory WSS. The endothelium transduces these stresses into biochemical signals leading to an endothelial phenotype that is susceptible to atherosclerosis development. Most research into the molecular mechanisms involving mechanotransduction pathways is limited to cell culture studies due to the lack of simple *in vivo* flow models. We present a novel *in vivo* flow model that makes significant advances over the complex and challenging *in vivo* flow models currently available.

The coarctation model presented in this thesis utilizes a novel shape memory clip to reliably induce a narrowing of the aorta. By utilizing the shape memory properties of nitinol we are able to obtain consistent recovery of the clip and thus induce a consistent coarctation. This technique minimizes variability due to human surgical error. We validate the efficacy of this technique using *in vivo*, *ex vivo*, and *in situ* imaging modalities. Current flow models are often poorly characterized and in particular tend to lack pressure measurements. We use innovative new techniques to validate morphology, flow, and pressure through direct measurements and then model the various mechanical forces that are applied to the endothelium.

We complement our novel *in vivo* flow model with novel histological imaging techniques. Quantum dot based immunohistochemistry quantitatively measures inflammatory protein expression. Quantum dots are highly stable fluorophores that do not photobleach. Additionally, they have a very narrow emission spectrum thus minimizing the signal to noise ratio. We apply these to an en face technique that uniquely allows for a highly quantitative analysis of regional expression levels of various inflammatory proteins. We also use novel superoxide sensitive fluorophore, hydro-Cy3, recently developed by our collaborators. Superoxide staining has been limited to the use of the highly unstable fluorophore, DHE. Hydrocyanines present a new class of superoxide sensitive fluorophores that are significantly more stable than DHE. This allows for improved quantitative measurements and staining in a wider variety of tissue preparations, including en face aorta preparations. We present a novel use for hydro-Cy3 in which we are able to measure regional endothelial superoxide levels.

Lastly, in our third aim, we analyze the *in vivo* contribution of WSS stimulated ROS to inflammatory protein expression. The role of ROS in various stages of lesion development is currently unclear. Using our aortic coarctation model with a combination of transgenic animals, knockout animals, and pharmacological inhibitors, we investigate the ROS dependent molecular mechanisms that mediate inflammatory protein expression. This study investigates the applicability of pathways already identified *in vitro* to the overall pathogenesis of atherosclerosis. The insight gained from this study will lead to improved knowledge about the timing of treatment of atherosclerosis, specifically with respect to antioxidants.

CHAPTER 2

BACKGROUND AND LITERATURE REVIEW

Cardiovascular Disease Epidemiology

CVD is the leading cause of morbidity and mortality in the United States. It has been estimated that CVD is present in 81 million Americans, slightly more than one third of the adult population [1, 2]. The top four presentations of CVD include: high blood pressure (74.5 million people), coronary heart disease (17.6 million people), heart failure (5.8 million people), and stroke (6.4 million people) [1, 2]. It is important to note that many people have two or more forms of CVD. Both coronary heart disease and stroke are products of atherosclerotic CVD and hypertension is a leading risk factor for the development of atherosclerotic lesions. The prevalence of CVD in males is at 37.1% of the population while prevalence in females is at 36.6%. CVD accounted for 871,517 deaths in 2006, 34.1% of all mortality [3]. There are large prevalence discrepancies in the racial distribution of disease. African American males have the highest CVD death rate of 422.8 (per 100,000), compared to 220.1 for white males and 136.3 for Asian males [3]. These diseases cost the country an estimated $431 billion in direct and indirect costs each year, presenting a significant burden on the country [2]. Though CVD is the leading cause of death, the age adjusted rate of death has been decreasing since the 1970s. Continued research into the pathogenesis of CVD will lead to novel therapeutics and help continue this trend.

Atherosclerosis Pathology

Atherosclerosis is an inflammatory disease of the cardiovascular system that is predisposed to specific locations in the vasculature [4-6]. Though the disease is

considered a systemic disease, advanced lesions develop in specific locations within the vasculature including: the coronary arteries, the carotid bifurcation, the abdominal aorta, and some peripheral arteries. Many systemic risk factors for atherosclerosis development have been identified; however, the focal development of plaque formation is most strongly correlated to disturbed flow and the resultant low and/or oscillatory WSS. Lesion formation is a multifactoral process that occurs through a combination of biochemical and biomechanical factors.

The AHA has characterized 6 stages of lesion development ranging from a healthy vessel to a complex lesion [7-9]. The initial stage is characterized by leukocyte recruitment leading to intimal thickening as well as intracellular lipid deposition and oxidation. It is this stage where the initial localization of the disease is initiated by disturbed blood flow. At the interface between the blood and the vascular wall, the endothelium acts as a sensor of WSS. The endothelium converts WSS into biochemical signals, which results in either a maintained state of vascular homeostasis under physiologic WSS levels or a shift toward endothelial dysfunction and atherogenesis under low and/or oscillatory WSS [10]. Mechano-sensitive pathways have been implicated as important mediators in regulating the inflammatory response of the endothelium, initially through modulation of genetic transcription factors, the redox state, and subsequent expression of inflammatory cell adhesion molecules. This process leading to lesion localization is highly dependent on complex *in vivo* flow behavior and the associated WSS, whereas the progression of the disease is believed to involve more systemic factors (figure 2.1).

The second stage is characterized by fatty streak formation. During this stage there is increased lipid deposition leading to foam cell formation. Additionally, there is adaptive intimal thickening. The next stage is an intermediate lesion with a fatty plaque or raised fatty streak. This is primarily characterized by lipid pools, though no lipid core is present. The fourth stage is an atheroma with the beginnings of a fibrous plaque. This stage is characterized by the development of a lipid core. Atheromas have high levels of connective tissue that develop in the intimal extracellular matrix; the ECM is largely composed of collagen, proteoglycan, fibronectin, and elastin fibers. The fifth stage is a fibroatheroma. In this stage there can be a variety of presentations including multiple lipid cores, a fibrotic cap, plaque vasscularization, or calcification. Histology has shown that plaques with thin fibrotic caps and proteoglycan rich erosion sites are vulnerable to rupture and therefore a cardiovascular event. The last stage is a complicated lesion which often presents as a ruptured or eroded plaque. These lesions can have the characteristics of a stage five fibroatheroma along with hemorrhage or thrombosis. Patients with complicated lesions often present with a cardiovascular event and therefore intervention is often recommended.

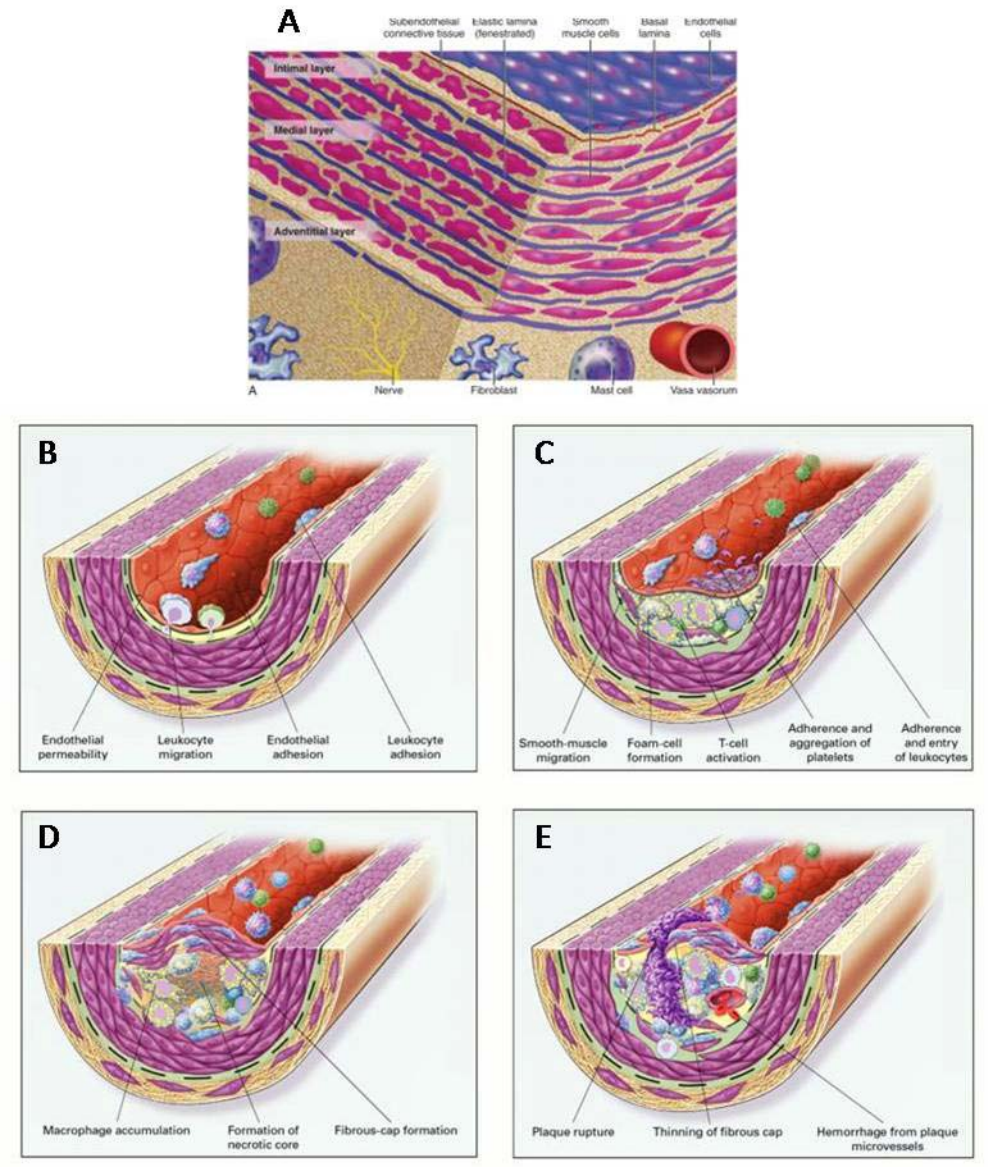

Figure 2.1 – Atherosclerotic Lesion Formation – A) healthy blood vessel. B) Endothelial dysfunction. Endothelium expresses adhesion molecules and becomes increasingly permeable. Leukocytes bind to the endothelium then migrate into the vessel wall. C) Neointima formation. Smooth muscle cells migrate into the intima, t cells become activated, and monocytes become foam cells. D) Advanced plaque formation. This stage can manifest itself in a variety of ways, shown in this figure: a fibrous cap forms over the lesion, a necrotic core forms, and macrophages accumulate. E) Plaque rupture. The fibrous cap thins eventually leading to plaque rupture. When this occurs, a thrombus can form leading to a myocardial infarction or stroke. Image adapted with permission from [6]

Flow in the Vasculature

Fluid Mechanics of Physiologic Flow

Atheroma formation is highly dependent on flow conditions in vivo that vary in different locations in the vasculature due to the boundary conditions imposed on the flow, namely inlet/outlet conditions and morphologic constraints. Flow conditions throughout most of the major arteries can be characterized as pulsatile and viscous and often fully developed. Two non-dimensional terms that are derived from an analysis of the Navier-Stokes equation are used to characterize these flow patterns: the Reynolds number and the Womersley number:

$$\mathrm{Re} = \frac{4\rho Q}{\pi \mu D}$$

$$\alpha = R\sqrt{\frac{\omega}{\upsilon}}$$

Where Re is the Reynolds number, μ is the viscosity, D is the diameter of the vessel, ρ is the density, υ is the kinematic viscosity, ω is the angular frequency, and R is the radius of the vessel. The Reynolds number is a measure of the stability of flow, relating inertial fluid momentum to the viscous frictional force. High Reynolds numbers correspond to flow dependent on momentum effects while low Reynolds numbers correspond to flow dependent on viscosity. The Reynolds number describes the stability of flow; laminar flow occurs at Reynolds numbers between 0 and approximately 2,300 at which point flow transitions to a turbulent state. In the vasculature, Reynolds numbers vary from 1 in small peripheral arteries to approximately 4000 in the aorta [12]. Therefore, flow can vary from laminar to turbulent and each artery must be examined individually to determine flow stability.

The Womersely number is a non-dimensional parameter of the pulsatility of flow. It relates the contributions of unsteady forces to viscous forces. At low Womersley numbers, viscous flows dominate, while high Womersley numbers correspond to flow dependent on inertial forces. The Womersley parameter characterizes the shape of the velocity profile where low Womersley numbers have a parabolic profile and high Womersley numbers have a flat, blocky, profile. Most Womersley numbers in the vasculature are in an intermediate range, between 1 and 10, and have flow profiles that vary depending on the location in the vasculature. Both the Reynolds number and the Womersley number will have large effects on the WSS acting on the endothelium [12]. The WSS acting on endothelial cells is governed by fluid dynamic principles, which under laminar flow in a straight rigid artery can be characterized by the equation:

$$\tau = \mu \frac{dU}{dr}$$

Variables are the same as above and U is the velocity. WSS under normal physiologic conditions is therefore dependent on dU/dr and the velocity profile. The velocity profile can vary between a blunt profile, where dU/dr at the wall will be relatively high, or a parabolic profile, where dU/dr at the wall will be moderate. The profile will be highly dependent on the location in the vasculature; however, on average, the vasculature in humans maintains a physiologic mean WSS around 15 dynes/cm^2 [12, 13]. Under physiologic flow conditions, WSS is relatively high, and the endothelial signaling is atheroprotective.

Disturbed Flow *In Vivo*

Blood flow can become disturbed by the pulsatility of blood flow as well as atypical geometric regions such as branch points, regions of high curvature, and stenoses. Disturbances of flow are commonly associated with secondary flow patterns and flow reversal resulting in non-physiologic flow. The WSS that is generated by disturbed flow is often low or even oscillatory. Regions of disturbed flow are predisposed to atherosclerosis formation. Atherosclerosis is commonly found in the coronary arteries, the carotid arteries and the infrarenal aorta [12]. Each region is characterized by disturbed flow that produces low magnitude oscillatory WSS. Though the principles behind the flow disturbances are the same the actual manifestation is unique to each region.

The carotid arteries are the simplest and most commonly characterized region of atherosclerostic lesion formation [5, 12, 14]. The carotid sinus is a unique anatomical region in the vasculature in which the artery has a normal out-pouching at a branching site. This results in a large expansion region where the distal vessel has a larger cross sectional area as compared to the proximal vessel. During the downstroke of systole, a negative pressure differential is created resulting in the separation of flow. This produces a reversal in flow at the outer wall, opposite the flow divider. Due to this unique anatomical feature, the carotid sinus is exposed to low magnitude oscillatory WSS resulting in a predisposition to atherosclerotic lesion formation.

The infrarenal aorta does not have an atypical geometric region, but is characterized by triphasic flow [12, 15]. The initial forward flow occurs from the heart beat which creates a positive pressure differential between the abdominal aorta and the

legs. During the middle stage of the cardiac cycle the aortic pressure begins to decline while the pressure in the legs increases creating a negative pressure differential and flow reversal. At the end of the cardiac cycle, the pressure in the legs drops below that of the abdominal aorta and flow becomes positive. There is some anterior skewing of the flow due to the curvature of the spine; however, the major determinant of oscillatory flow in the infrarenal aorta is due to to the pressure differential between the legs and abdominal aorta.

The coronary arteries are another location of atherosclerotic lesion formation [12, 16]. These arteries experience a very complex flow profile due to the contraction and movement of the heart. The outlet flow is reduced during systole as the heart contracts and increases during diastole when the heart is relaxed, though this can vary in the different coronary branches. The inlet on the other hand is at the aortic sinus resulting in flow that is not fully developed, a large Womersley number, and a blunt flow profile that is not well defined. Furthermore, as the vessels follow the morphology of the heart, there are regions of high curvature. The combination of these three features produces a complex flow profile with flow reversal.

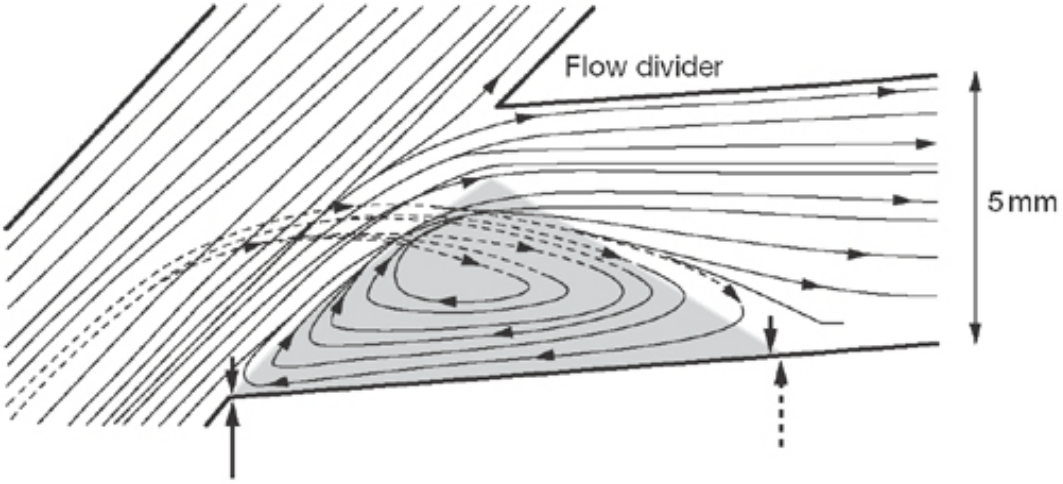

Figure 2.2 – Disturbed Flow Profile - Flow profiles showing streamlines at a representative branching location in the vasculature. Flow separation occurs in the shaded region opposite the flow divider. Image adapted with permission from [17]

Flow in a Stenosis

A stenosis is a narrowing of the vessel lumen, commonly occuring in vivo as complex atheromas that progressively grow into the lumen of an artery. However, induction of an artificial stenosis provides ideal conditions for WSS analysis. Stenoses are defined by the percentage of stenosis (either as a relative area or diameter). As atheromas progress there is a corresponding increase in percent stenosis as the lumen becomes smaller through the stenosis.

Stenotic flows have predictable flow patterns. Figure 2.3 shows streamlines through a stenosis. The continuity equation predicts that in the neck region of the stenosis there is an increase in velocity corresponding to the decrease in area, which results in an increase in WSS. Distal to the stenosis there is a jet stream in the middle of the lumen along with a recirculating region near the wall. Flow separation can occur due

to a positive downsteam pressure gradient which can occur due to pulsatility and expansion regions. A 1-D analysis of the unsteady Euler equation produces the equation:

$$\frac{dP}{dx} = -\frac{\rho}{A}\frac{dQ}{dt} + \frac{\rho Q^2}{A^3}\frac{dA}{dx}$$

When the pressure gradient (dP/dx) is positive, conditions are favorable for flow separation. This occurs during the downstroke of systole while dQ/dt is negative and in expansion regions where dA/dx is positive. The threshold for separation is dependent on the Reynolds number, yet this equation can still predict favorable conditions for flow separation in the distal region to the stenosis. The boundary layer between the jet stream and the recirculating region creates unstable shearing which can create turbulent conditions. Turbulence can be seen in a stenosis with a significantly reduced Reynolds numbers, ranging from 10 to 300 depending on the degree of stenosis. Depending on the degree of stenosis a wide variety of flow conditions can be obtained, including high WSS, low WSS, low and oscillatory WSS, and even random WSS from turbulent flows [12].

Differences between the Flow in Mice and Humans

Though both the mouse and the human have similar cardiovascular anatomy, there are some major differences that have profound effects on the blood flow. The first is the obvious discrepancy in the size of the vessel. The human aortic diameter is on the order of magnitude of 1 cm (usually about 2-3 cm) while the mouse aortic diameter is on the order of magnitude of 1 mm [18]. Considering that the velocity of the blood and the viscosity are the same in each animal, the equation for shear stress dictates that the wall shear stress imparted on the endothelium is approximately ten times higher in the mouse

than in the human. This matches reported observations in the literature [18-20]. The Reynolds number is about ten times smaller in a mouse than a human which would suggest a decreased likelihood of turbulent flow in the mouse. Additionally the Womersley number is about three times smaller in the mouse than the human resulting in a highly parabolic flow profile in the mouse. Both these parameters suggest increased stability of the flow in a mouse as compared to a human. The vessel wall is also dramatically different. The thickness of the wall and the composition result in a rather stiff human aorta and a very elastic mouse aorta. This results in higher dispensability in the mouse aorta which is believed to affect flow patterns. One particular observation was that the triphasic flow profile with flow reversal in the infrarenal aorta in humans is not observed in the mouse [19]. This could have implications in differential disease development a region where human develop atherosclerosis as well as aneurysms. An additional difference is that the cardiac cycle is about ten times longer in the human than the mouse, resulting in a human heart rate around 60 beats per minute and a mouse heart rate around 600 beats per minute.

Murine Flow Models

Mouse flow models of *in vivo* mechanotransduction tend to fall into two categories: chronic or device-based. Chronic models utilize regions where the innate morphology produces chronically disturbed flow [20, 21]. CFD models of the aortic arch have shown that there is low mean WSS at the inner curvature of the aortic arch (figure 2.4). The directionality of the WSS vectors further shows that the WSS oscillates throughout the cardiac cycle. These models have also identified the region opposite the flow divider of the brachiocephalic branch as a region of low magnitude oscillatory WSS.

As can be viewed in figure 2.4, the aortic arch has a very complex morphology and the location of disturbed flow occurs at a very precise and small region. This can make for challenging analysis when investigating the molecular mechanisms involved in mechanotransduction. Additionally, these regions experience a chronically disturbed flow environment which may allow for activation of compensatory mechanisms. Studies have recently described these chronically disturbed flow regions as "atherosusceptible." These studies have shown that various inflammatory markers are expressed in this region and that they are primed for the development of atherosclerotic lesions [20]. The aortic sinus, is also a plausible location for disturbed flow; however, it is a very challenging environment to model in the mouse due to the small diameter of the vessel, the undeveloped flow in this region, and the moving wall of the vessel and the valve. As of yet, it has not been characterized.

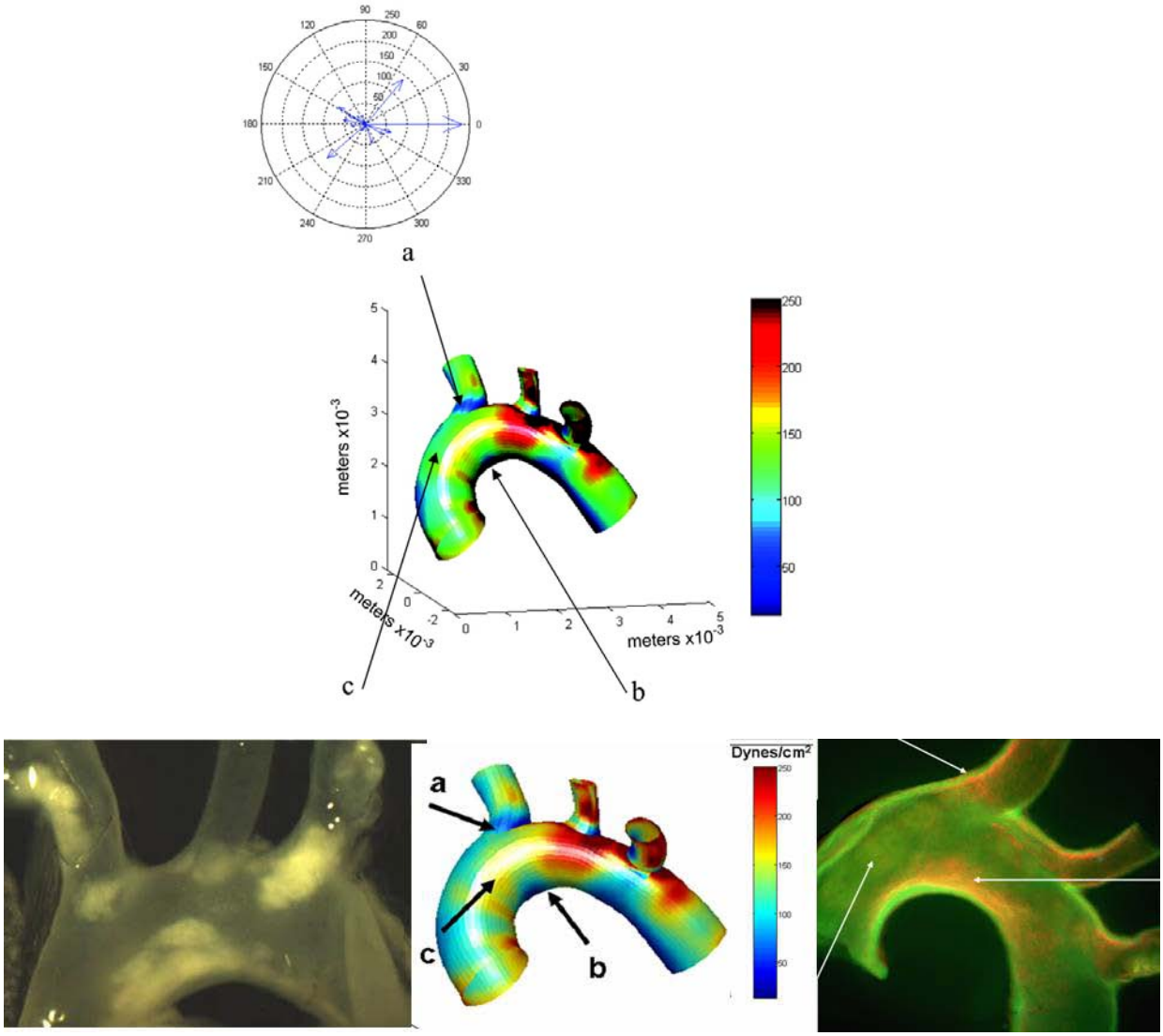

Figure 2.4 - CFD Model of the Aortic Arch of a Mouse - Low mean WSS was identified at regions a and b, while region c experiences high mean WSS. Polar plots of the WSS vectors show that there is oscillatory WSS at regions a and b while region c experiences unidirectional WSS. The lower panel shows lesion formation (left), in comparison to the CFD (middle), and VCAM-1 expression (right). Image Adapted with permission from [20]

Device-based models of disturbed flow allow for the investigation of mechanotransduction over an acute time course. This allows for the potential to separate the effect of compensatory mechanisms from pathways activated by direct mechanical transduction. These techniques are often complicated and not fully defined in terms of the precise hemodynamic conditions or create flow environments that do not experience low magnitude oscillatory WSS. Most device-based mouse models induce a coarctation using silver U-shaped clips, sutures tied around a needle, or polymer casts [22-24]. The initial coarctation models were used as models of upstream hypertension, utilizing first sutures, later refined to U shaped clips. These models induce a severe stenosis, thereby creating a large pressure drop and a systemic change in hemodynamics. These were not designed as models to investigate WSS based mechanotransduction and have not been characterized as such. Additionally, these methods have reported high mortality rates [23].

Recently a model utilizing a polymer cast to induce a coarctation was developed as a model of localized disturbed flow without systemic effects [25]. This model uses a polymer cast that is placed around the carotid artery to restrict flow and create a stenosis. This model reports a region of low unidirectional WSS upstream from the cast and a region of high magnitude oscillatory WSS downstream from the cast. It is important to note some limitations with this model. First, the region of low unidirectional WSS reports an average WSS of 100 dynes/cm^2. Mean WSS magnitudes in the carotid artery of mice have been reported to range from 31 dynes/cm^2 to 144 dynes/cm^2 with an average around 65 dynes/cm^2, thus the claim that 100 dynes/cm^2 as a region of low magnitude WSS is questionable [18]. It is plausible that another mechanical stimulus,

namely strain, could participate in this model; however, the study does not characterize the change in pressure or strain. Another limitation is that the oscillatory region reports high magnitude WSS levels with an average WSS of 140 dynes/cm^2 and a temporal range of 600 dynes/cm^2. There is no region in this model where low magnitude oscillatory WSS is produced.

A new type of device-based model was recently demonstrated using a partial carotid ligation. The partial carotid ligation significantly reduces the blood flow through the carotid artery and creates flow reversal during part of the cardiac cycle [26, 27]. Mean WSS in this model drops from 100 dynes/cm^2 to approximately 10 dynes/cm^2. The flow completely reverses and blood flows out of the carotid during diastole resulting in low magnitude oscillatory WSS. This is a very promising model as it creates low magnitude oscillatory WSS, but it is important to note that there is no characterization of any change in pressure and/or strain. Additionally, the pathologic response shows a significantly increased rate of atherosclerosis development resulting in complete occlusion of the vessel after three weeks. This disease development occurs much faster than in chronically disturbed flow regions such as the aortic arch. There is also significant adventitial remodeling and ROS production in the adventitia, suggesting that there may be an additional stimulus involved in this model.

Endothelial Mechanotransduction

The endothelium acts as a sensor for WSS by which changes in flow can affect biochemical signaling in the vascular wall. The current literature has identified four categories of potential mechanisms by which the endothelium transduces forces: cell-

ECM structures, cell-cell junctions, membrane structures, and the cytoskeleton of the cell which potentially links the former three mechanisms.

Membrane structures signal by activating mechanisms affecting the membrane potential or different phosphorylation cascades. Ion channels, in particular calcium and potassium channels, can be activated transiently by WSS to induce changes in the membrane potential and activate signaling molecules [28-30]. Additionally, signal transduction can occur through phosphorylation cascades activated by tyrosine kinase receptors, G proteins, or kinase rich caveolae domains [31, 32]. Tyrosine kinase receptors, particularly VEGF-R, have shown shear dependent activation independent of the presence of a ligand [32-34]. Similarly, G-proteins, such as Ras GTPase, have been shown to activate phosphorylation cascades in a shear dependent manner [35-37]. Shear stress can cause these proteins to aggregate in membrane domains rich in cholesterol known as caveolae [38]. Interactions between molecules in the domains can result in further activation of phosphorylation cascades. Recent studies have suggested that activation of the above mentioned membrane structures may involve signal transduction by the primary cilia which protrude into the lumen of the vessel [39-41].

Cell-cell junctions show two shear dependent mechanisms. The first acts through tyrosine phosphorylation of PECAM activating downstream signaling [42]. The second acts through adheren junctions, specifically VE Cadherin. VE cadherin is an adhesive protein that interacts through an anchoring molecule, Beta-Catenin, which is linked to the cytoskeleton. Forces transmitted through the cytoskeleton can therefore activate VE Cadherin dependent signaling.

Cell-ECM structures are largely composed of integrins that link the cell cytoskeleton to the basal lamina underneath the cell. Forces transmitted through the cytoskeleton can activate phosphorylation cascades and the binding of adaptor proteins. These events can act as modulators affecting the transcriptional profile of the cell. The cytoskeleton serves as the structural support that stabilizes the cell in a given mechanical environment. The cytoskeleton acts to connect the different mechanotransduction factors with one another. These interactions can allow communication between the membrane, the cell-cell junctions, and the cell-ECM junction all of which can have a direct affect on the cytoskeleton itself. Interactions between the cytoskeleton and integrins or focal adhesions have been shown to transduce stresses, resulting in cytoskeletal remodeling and conformational changes in the cell [43-45]. These transduction mechanisms likely interact to produce different temporal responses of molecular pathways, remodeling through adhesion complexes and integrin complexes, and changes in caveolae, gap junctions, and G-proteins[46]. Although many of these pathways have been identified as initial mediators in shear stress mechanotansduction, the exact mechanisms are not completely understood.

Mechanosensitive pathways directly affect the transcriptional profile of the endothelium. Under physiologic flow conditions, a baseline physiologic profile is expressed and an atheroprotective homeostasis is maintained. However, under disturbed flow conditions, atherogenic profiles are expressed, and, in particular, the transcription factor NFκB is activated and translocates to the cell nucleus. This process has an immediate effect on the redox state in the cell and inflammatory protein signaling.

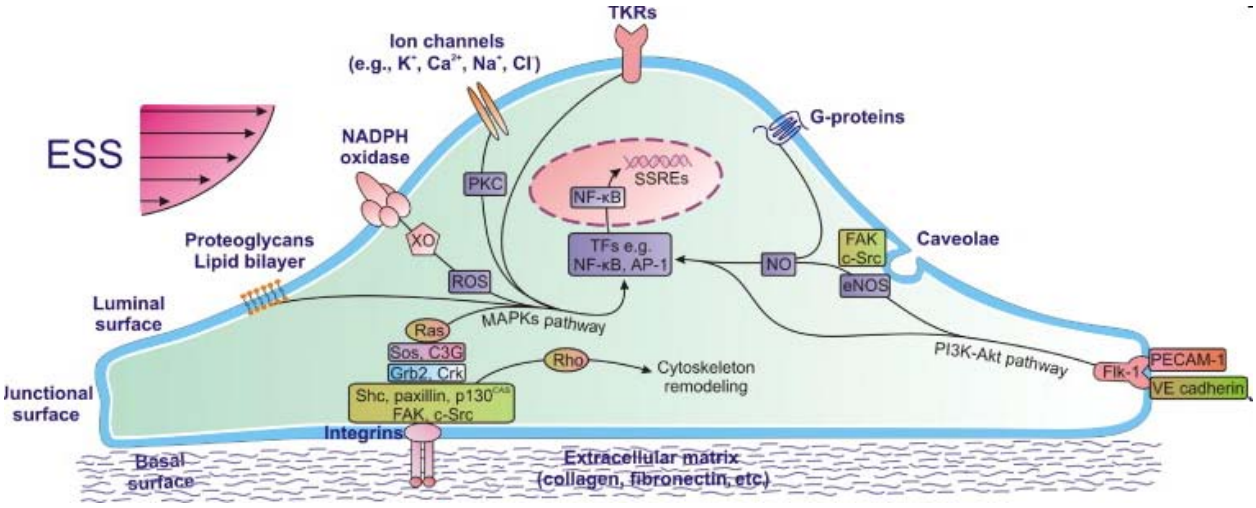

Figure 2.5 – Endothelial Mechanotransduction – Shear stress can be transduced by the endothelium through various structures as displayed in the figure. Membrane structures are on the luminal surface at the interface between the cell and the blood. These structures can include ion channels, caveolae, proteoglycans, and tyrosine kinase receptors, among others. Cell-ECM structures are at the basal surface and mainly mediated through integrins. At the junction between cells PECAM-1 and VE cadherin mediate signal transduction. The cytoskeleton serves as the mechanical scaffold for the cell and links the former three structures. Image adapted with permission from [47]

Endothelial Redox State

Redox State

The redox state within the cell is dependent on a balance between oxidants and anti-oxidants. This balance is critical to the homeostasis of the vasculature and physiologic processes particularly with relation to the molecule NO. NO is a potent vasodilator that is involved in regulating vascular tone. Changes in the oxidative state can alter the NO response leading to endothelial dysfunction and eventually hypertension. NO is a product of eNOS (NOS III) in the endothelium. For functional activity eNOS requires the cofactors tetrahydrobiopterin and substrates oxygen and L-argenine all of which can be regulated by the oxidative state. This process is subject to strict control to ensure appropriate vascular tone; however, a shift towards oxidative stress in vascular

cells can lead to the development and progression of numerous cardiovascular diseases including hypertension and atherosclerosis.

Oxidative stress is a principal feature of numerous cardiovascular diseases. Endothelial cells and smooth muscle cells both generate ROS. The primary ROS in the vascular wall are superoxide and hydrogen peroxide though others may be involved [48, 49]. The most potent sources of ROS in the endothelium are NADPH Oxidase (Nox), XO, uncoupled eNOS, and the mitochondrial electron transport chain. The balance in the redox state has been shown to be shear sensitive. Many important mediators of ROS generation and antioxidants are directly regulated through numerous mechanosensitive pathways. The shift to an oxidative state leads to increased inflammation within the cells thereby providing a feedback loop for further generation of ROS. NFκB, for example, can be activated by ROS and will then translocate to the cell nucleus resulting in increased transcription of numerous ROS sources. This series of events will eventually perpetuate the various stages involved in the pathogenesis of atherosclerosis.

Reactive Oxygen Species

Reactive oxygen species are molecules that have an unpaired free electron and contain an oxygen atom. The main ROS is superoxide, $O_2^{\cdot-}$. Superoxide is produced when molecular oxygen gains an additional electron from an oxidative source. Superoxide can act as an oxidant and extract an electron from a molecule leading to the formation of hydrogen peroxide or superoxide can donate an electron if the target has a higher electron potential. Superoxide is an unstable free radical with a short half life and is membrane impermeable. Superoxide has three primary effects *in vivo*. At basal levels, superoxide can serve as a signaling molecule mediating numerous physiologic functions.

As a signaling molecule it can alter the function of target proteins including phosphotases, kinases, small GTPases, transcription factors, ion channels, structural proteins, and metabolic enzymes [49]. Additionally, superoxide can act as a precursor to other ROS. In this manner superoxide can dismutate into the more stable hydrogen peroxide, or form the highly reactive ROS peroxynitrite. In the production of peroxynitrite, superoxide reacts with NO, decreasing NO levels and providing a mechanism to inhibit vasodilation, eventually leading to endothelial dysfunction [50]. Lastly, superoxide can serve as an oxidative compound reacting with the cell membrane, DNA, or other macromolecules. These processes often work in a feedback manner to perpetuate the oxidative state. Superoxide, for example, can react with BH_4 decreasing the BH_4 available for eNOS leading to eNOS uncoupling leading to the production of more superoxide [50].

Other ROS also dictate the redox state within the cell. Hydrogen peroxide is relatively stable for ROS and is membrane permeable making for a good signaling molecule [51]. Hydrogen peroxide can react with various targets. For example hydrogen peroxide can react with thiol residues to produce sulfur oxidation which can lead to changes in the cell state [52]. The functional contribution of hydrogen peroxide has been shown in the catalase overexpression transgenic mouse model. With increased catalase levels, hydrogen peroxide levels are kept low and atherosclerosis is inhibited under accelerated atherosclerotic conditions [Mendez and Taylor unpublished]. Hydrogen peroxide can also increase eNOS levels which at high levels of ROS serve to produce superoxide and peroxynitrite. Peroxynitrite on the other hand, is a highly reactive non-specific ROS. It can oxidize and nitrate numerous biomolecules including thiols and

metal-containing proteins [53]. Other ROS found *in vivo* include the hydroxyl radical, hypochlorous acid, lipid peroxide, lipid peroxy- radicals, and lipid alkoxyl radicals [49]. These additional ROS play a lesser role in the oxidative state, particularly with regards to the endothelium.

Techniques for ROS Measurement

ROS are challenging to measure due to their relatively short half life and low levels. Ideally, measurements will target an individual ROS, however current techniques make this very challenging. The most common techniques include cytochrome C reduction, chemiluminescence-based techniques, ESR, DHE, DCF-DA, and amplex red [54]. Many of the commonly used assays have limitations particularly with specificity and stability. It is often recommended to use multiple techniques or to use a scavenger to reduce the levels of the ROS of interest. In our model, we require that the technique we use allows for endothelial specific measurement of ROS and can differentiate the heterogeneous levels of ROS in small regions of tissue. We will discuss the applicability of current techniques to our requirements.

The cytochrome c assay is an indirect technique to measure superoxide levels. In this assay cytochrome c is reduced by superoxide (or other enzymes) changing its spectral absorption profile. It can be used in whole tissue, but tissue is at the lower limit of signal detection and the assay works best in the presence of large amounts of superoxide. This technique is good for measuring superoxide levels in cells that release large amounts of superoxide, such as neutrophils, however vessels generate much lower levels of superoxide that are below the limit of signal detection [54].

Chemiluminescence assays use probes which release a photon when in the presence of superoxide. This technique usually uses lucigenin to measure superoxide in 3mm lengths of vessel. There are some limitations due to specificity and redox cycling in which superoxide can be generated by lucigenin [55]. These limitations can result in an overextimation of the amount of superoxide in a piece of tissue. Additionally the technique requires a 3mm length of tissue and cannot distinguish regional changes in superoxide levels or determine endothelial specificity [54].

ESR uses a microwave radiation and an electromagnetic field to stimulate free radicals. Due to the short half life of most ROS, spin probes are often used creating an adduct or a more stable free radical, each of which has a unique ESR spectrum. This technique requires use with homogenized tissue, and therefore cannot distinguish the source of the superoxide or regional heterogeneity. Additionally there is a large overhead cost for the ESR spectrometer, which can limit the adoption of this technique as a common practice [54].

DHE is commonly used to measure the redox state of tissue. DHE can be visualized using fluorescence microscopy to look at the ethidium product that is formed upon reaction with ROS; however, there are concerns about the specificity in the formation of ethidium and it is believed that this is a measure of the redox state more so then a measure of superoxide [54]. When superoxide reacts with DHE it forms 2-hydroxyethidium [56]. 2-hydroxyethidium can be measured using HPLC, the peak from 2-hydroxyethidium can be used to estimate intracellular superoxide levels. The HPLC technique requires homogenization of the tissue during preparation. A clear limitation of DHE is that it is light sensitive and can react with oxygen in solution making it a

relatively unstable dye. This limitation makes DHE challenging to use for histology and in particular for *en face* mounting when the tissue must be mounted using a dissecting scope.

DCF-DA is cell permeable and can be cleaved into DCFH by intracellular esterases. DCFH can be oxidized by a variety of ROS but is primarily thought of as a measure of hydrogen peroxide since it does not react with superoxide. The various components of this cycle are not very specific and highly unstable. Additionally, the dye can itself generate ROS resulting in artifacts. DCF-DA is primarily analyzed under fluorescence microscope, though it photobleaches very quickly [54, 57].

The amplex red assay relies on horsereadish peroxidase to catalyze the reduction of amplex red by hydrogen peroxide. The product is the fluorophore, resorufin. This assay measures extracellular hydrogen peroxide only and requires diffusion of hydrogen peroxide from the tissue into the surrounding buffer. It is therefore not ideal for determining endothelial specificity or regional heterogeneity.

These common techniques for measuring ROS are not ideal for analysis of superoxide levels from endothelial cells *in vivo* (or *ex vivo*). We have recently worked with a collaborator to develop a novel superoxide sensitive dye, hydro-Cy3, which is significantly more stable than DHE for histological uses [58]. We will investigate the use of this dye to investigate endothelial specific production of superoxide.

Sources of Reactive Oxygen Species

The NADPH Oxidase family is a major source of ROS in the endothelium. This family is made up of complexes that contain a catalytic, membrane bound, Nox domain. This Nox domain catalyzes the transfer of an electron from NADPH to oxygen. There are four NADPH Oxidase isoforms that are expressed in the endothelium: Nox 1-, Nox2-, Nox4-, and Nox5-dependent NADPH oxidase. Measurements of endothelial mRNA levels have shown that Nox 4 mRNA and Nox 2 mRNA are expressed at high levels while Nox 5 and Nox 1 mRNA are expressed at relatively low levels [51, 59]. NADPH oxidase isoform activation requires translocation and assembly of Nox subunits. The subunit p22 phox is a subunit for Nox 1, 2, and 4 and can serve as a docking platform for p47 phox, though p47 phox is not needed for Nox 4 [49, 60]. mRNA levels of Nox isoforms and Nox complex subunits have been shown to be upregulated by proatherogenic stimuli.

Xanthine oxidase is another potent source of superoxide. Xanthine oxidase is a ROS-producing form of xanthine oxidoreductase in which XO uses oxygen as an electron acceptor. Xanthine oxidoreductase also exists in a non-ROS producing form, XDH [49, 60]. The ratio between XDH and XO is determinant of the oxidative state within the cell. The transition from XDH to XO can occur due to stimulation by inflammatory cytokines as well as through oxidation of cysteine residues by ROS, particularly peroxynitrite. This conversion has been shown to be stimulated by an increase in the activation of NADPH oxidase further perpetuating the oxidant state.

Endothelial nitric oxide synthase can become another source for ROS when the two subunits become uncoupled [49, 60, 61]. Under physiologic conditions, eNOS

expression is high, resulting in the production and bioavailability of the atheroprotective molecule nitric oxide. However, in the absence of BH_4, eNOS becomes uncoupled and electrons are transferred to oxygen instead of L-argenine, resulting in the formation of superoxide. As a cell shifts to an oxidative state, some eNOS remains coupled allowing for low levels of NO production that will further perpetuate formation of differing reactive oxygen species.

The final major contributor of ROS in the endothelium is the mitochondrial electron transport chain [49]. The mitochondrial electron transport chain acts through numerous complexes, I through IV, to pass an electron along from one complex to the next. The various complexes can then facilitate the transfer of the electron to oxygen producing superoxide depending on the electrochemical gradient. A proton is often transferred out of the mitochondria to maintain the electrochemical gradient. It is challenging to experimentally isolate the contribution of the mitochondrial electron transport chain to the production of ROS; however, it has been suggested that this may be a shear dependent process [62].

The ROS sources described thus far have focused on the production of superoxide, however, numerous other ROS forms exist. Two other principal forms of reactive oxygen species contributing to an oxidant state in the endothelium are peroxynitrite and hydrogen peroxide [49, 63]. Superoxide dismutase can scavenge superoxide to form hydrogen peroxide which can be converted to water and oxygen by catalase. Superoxide dismutase levels are increased in the presence of NO and can be increased by laminar flow [64]. Hydrogen peroxide can also form by spontaneous dismutation of oxygen or it can be generated directly by NADPH oxidases. The highly

reactive superoxide can also react directly with NO to form peroxynitrite. This balance between superoxide and NO is an important determinant of the redox state. These three forms of ROS appear to play key roles in the development of atherosclerosis; however, the specific contribution of the various sources and each individual ROS are still unknown.

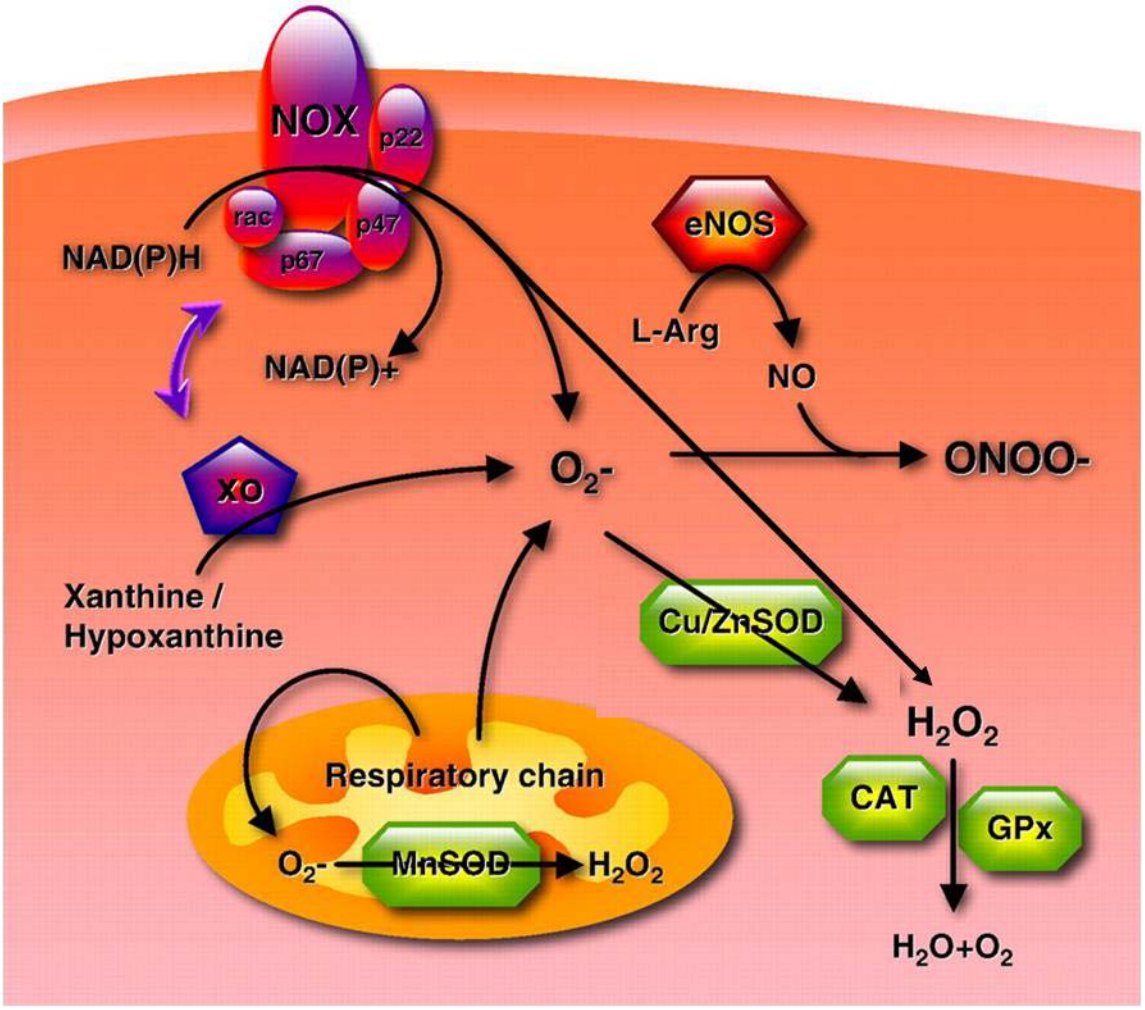

Figure 2.6 – Generation of Reactive Oxygen Species - ROS sources convert oxygen to superoxide. Superoxide can either be scavenged by SOD to form hydrogen peroxide or react with NO to form peroxynitrite. Hydrogen peroxide can be converted to water and oxygen by catalase. Image adapted with permission from [65]

Low Magnitude Oscillatory WSS and ROS

It is known that atherosclerotic lesions develop in regions of low magnitude oscillatory WSS, but the mechanism by which this process occurs is still unknown. ROS have been implicated as mediators in this process. Cell culture studies have shown that Nox expression changes in response to different flow patterns. Low magnitude oscillatory WSS increases expression of various NADPH oxidase subunits including Nox 2 and Nox 4 [66]. A corresponding increase in superoxide levels was also observed and could be attenuated by treatment with an NADPH inhibitor, 2-DOG, which blocks the pentose shunt pathway for NADPH production. Superoxide generated in response to oscillatory WSS has also been shown to be inhibited in cells from p47 $phox^{-/-}$ mice leading to inhibition of monocyte binding [67]. A separate study found similar, but slightly different results; oscillatory WSS increased expression of Nox 1 and Nox 2 but not Nox 4 [68]. This study showed oscillatory WSS increased monocyte adhesion which could be attenuated by knocking out p47phox, inhibiting BMP4, or through Nox1 siRNA treatment. There are some disparities between these studies, possibly due to differing cell types (MAECS vs BAECS), varying time courses (6 hours to 18 hours), differing flow patterns, or differing culture conditions. They all suggest however that superoxide is generated in response to oscillatory WSS through an NADPH oxidase mechanism, and in particular implicate the Nox 2-dependent NADPH oxidase. Additionally, monocyte binding and cell adhesion molecule expression increase in response to oscillatory WSS also mediated by NADPH oxidase. Indirect studies have shown that Nox can be activated through activation of tyrosine kinase c-Src,

transactivation of EGFR, and G-protein Rac-1 translocation, all of which have been shown to change activity in response to low, oscillatory shear [60].

Few studies have investigated shear dependent redox signaling *in vivo*, though the development of novel *in vivo* flow models is leading to increased research. A recent study showed that in low oscillatory WSS model of highly accelerated atherosclerosis, p47 phox$^{-/-}$ had attenuated superoxide generation and lesion development [27]. Additionally, the study showed increased superoxide levels in response to low oscillatory WSS and an attenuated response in p47 phox$^{-/-}$ mice. The majority of the superoxide generation in this model appeared to be in the adventitia and not the endothelium, and therefore, the source and stimulus of the superoxide generation requires further investigation. Some inferences can also be made from atherosclerosis models where lesions first form in the aortic sinus. Though the flow patterns in the aortic sinus have yet to be characterized, it is likely that the flow is disturbed in the surrounding region. Studies have shown that lesion formation throughout the whole aorta is attenuated in p47 phox$^{-/-}$ mice; however, when only analyzing the aortic sinus, there was no difference in lesion formation between the control and the p47 phox$^{-/-}$ mice [69]. This region of the aortic sinus may be involved in flow mediated lesion formation, while lesion formation in the whole aorta is primarily mediated by accelerated atherogenic conditions (i.e. atherogenic diet fed to apoE$^{-/-}$ mice) and not flow. These results suggest that p47 phox might not be involved in flow mediated lesion formation.

Studies have also shown that other ROS sources are regulated in response to shear stress potentially allowing for parallel mechanisms of ROS generation [70]. Low WSS has been shown to produce increased levels of xanthine oxidase in relation to xanthine

dehydrogenase resulting in increased superoxide generation. Additionally antioxidant enzymes have been shown to be down regulated by low magnitude oscillatory WSS [71, 72]. Low endothelial wall shear stress can decrease gene expression of superoxide dismutase or glutathione peroxidase [71, 73]. It is clear that these pathways are very complex and likely and involve numerous enzymes. Further research is needed to identify the molecular mechanisms by which low oscillatory WSS mediates redox signaling, especially *in vivo*.

Antioxidants

Oxidative stress has been shown to be a principal component to cardiovascular disease development. It has therefore been speculated that treatment with antioxidants might stabilize the oxidative state and prevent cardiovascular disease. Clinical studies have tested various antioxidants including ascorbate, vitamin-E, coenzyme Q_{10}, probucol, iron chelators (desferrioamine), or polyphenols [49]. Many of these treatments have shown some beneficaial effects, though results have been inconsistent. Further research is needed into the pharmacologic kinetics and molecular mechanisms by which these drugs act such that the dose of the antioxidant can be optimized as a treatment. Additionally, antioxidants treatment can be used in animal models to investigate the functional contribution of an ROS or ROS source to disease development; however, it is important to recognize the limitations and specificity of each inhibitor.

Selective inhibition of superoxide producing enzymes allows for investigation of individual pathways. Apocynin is an antioxidant, which inhibits the formation of the NADPH-oxidase complex. It is believed that apocynin inhibits the translocation of p47phox to the plasma membrane [74], though it is suspected that apocynin activation

requires MPO and hydrogen peroxide [75]. Studies have shown that treatment of endothelial cells with apocynin can inhibit NADPH oxidase activity and the generation of superoxide [76]. *In vivo* studies have shown that treatment with apocynin can decrease blood pressure and arterial superoxide levels [77, 78]. Apocynin has also been reported to increase ROS levels in some studies due to a suspected decrease in glutathione activity [79]. Additionally apocynin has been reported as a ROS scavenger [80]. Due to the many disparities in the literature about the function of apocynin further research is needed to determine the mode of action.

DPI is another antioxidant often used as an inhibitor of NADPH oxidase. DPI, inhibits other flavoproteins as well, and therefore is not a selective inhibitor [50]. Studies have shown that DPI can inhibit xanthine oxidase as well as NOS [81-83] both of which can generate superoxide. DPI has been shown in numerous studies to decrease superoxide levels [50]. Other inhibitors of Nox that are less frequently used include AEBSF, neopetrin, and gp91ds-tat; however reports have also questioned the specificity and potency of these inhibitors [84].

Other antioxidants that serve to decrease superoxide levels are of the form of SOD. Recombinant forms of Cu/Zn-SOD and Mn-SOD exist but have a very short half-life. PEG-SOD and other modified forms of SOD are also available and are significantly more stable than the recombinant SOD [85]. Tempol is an SOD mimetic that can scavenge superoxide but at high concentrations (on the order of 1 mM) can generate ROS [86]. Recent dose response studies have shown that a mid-level concentration (between 100uM and 1mM) is required to attenuate Ang-II induced superoxide generation in cell culture [87]. *In vivo* studies have shown tempol to be anti-hypertensive at various doses

[86, 88, 89]. Interestingly, in a hypertension model, tempol treatment did not lower superoxide levels [89]. Further work remains to characterize the bioavailability of tempol and proper dose *in vivo*.

Antioxidants that target other ROS also exist. Ebselen was commonly thought of as a glutathione peroxidase mimetic, however, recently ebselen has also been shown to use the thioredoxin system for antioxidant effects [90]. Ebselen has been shown to reduce hydrogen peroxide levels and peroxynitrite levels *in vitro* [91, 92]. *In vivo* models using ebselen treatment have shown antioxidant effects as well as protective effects from cardiovascular disease [93]. L-Arginine and tetrahydrobiopterin are cofactors of eNOS that may be thought of as antioxidants since they help increase NO production and prevent endothelial dysfunction [94-96]. Increased levels of these cofactors may also help prevent the uncoupling of eNOS which would then generate ROS. N(omega)-nitro-L-NAME is an inhibitor of NOS and at times used to investigate NOS as an oxidant. However, when L-NAME is given to apoE$^{-/-}$ mice, the NO mediated vascular response is inhibited and atherosclerotic lesion formation significantly increases [97]. Results can therefore be challenging to interpret.

Antioxidant treatment can provide useful information about redox mechanisms; however, care must be taken in the interpretation due to the lack of specificity of many of the antioxidants. Antioxidant treatment in vivo should be complemented with the use of knock out mice when available. Using these two methods in combination can help overcome limitations and validate results.

Endothelial Inflammatory State

One of the initial events in atherogenesis is the recruitment of inflammatory cells into the intima of the vessel wall at regions of disturbed flow. In these regions, inflammatory proteins have been shown to be upregulated, in particular cell adhesion molecules which mediate leukocyte rolling and migration. VCAM-1 and ICAM-1 have been shown to be shear responsive both *in vitro* and *in vivo*. Expression of inflammatory proteins is believed to be mediated by the activation of the transcription factor NFκB. Numerous studies have implicated ROS as mediators of NFκB activation and VCAM-1 expression thereby leading to atherogenesis.

NFκB

NFκB is a transcription factor involved in the control of many inflammatory genes including VCAM-1 and ICAM-1. It is a heterodimer composed of the p50 and p65 subunits. While inactive it is bound to the inhibitor I-κB in the cytoplasm. Activation occurs through the phosphorylation of I-κB, which is then marked for degradation. NFκB then translocates to the nucleus at which point it acts as a transcription factor. There are many regulatory steps in this pathway: production of an inhibitor, phosphorylation of an inhibitor, degradation of an inhibitor, translocation of NFκB, phosphorylation of NF-κB, modification of NF-κB binding sites, among others. NFκB has been described as the "Prototypical transcription factor subject to redox control [49]."

Reactive oxygen species generation leads to an oxidant state that is associated with changes in the transcription profile of a cell. Of particular importance are the effects from the transcription factor NFκB. NFκB can be upregulated directly by an acute

change in shear stress and activated in regions predisposed to lesion formation [98-101]. At low, oscillatory levels it has been shown that NFκB can increase ROS generation [98]. ROS also appear to act in a positive feedback manner to further perpetuate the increase in NFκB expression and activation [102]. It has been proposed that ROS act to degrade the NFκB inhibitor IκB allowing for activation and translocation of NFκB to the nucleus [98]. This has been shown using varying anti-oxidants to inhibit NFκB translocation. Additionally ROS have been shown to facilitate gene transcription in the nucleus by NFκB. NFκB has been shown to regulate gene transcription for numerous atherogenic proteins including TNF-alpha, IL-1, macrophage colony stimulating factor, VCAM-1, and ICAM-1, among others [98, 102-104]. As NFκB levels increase and the transcription factor translocates to the nucleus of the cell, there is a shift to an atherogenic transcription profile resulting in an increase in inflammatory protein signaling.

Cell Adhesion Molecules

One of the earliest identifiable atherogenic events is the expression of inflammatory cell adhesion molecules and subsequent monocyte adhesion. Cell adhesion molecules, in particular VCAM-1 and ICAM-1, facilitate tethering and firm adhesion of rolling leukocytes leading to extravasation into the intima. VCAM-1 is a member of the immunoglobulin superfamily that localizes to the surface of endothelial cells, allowing for exposure directly to the lumen of the vessel. It binds the integrin receptor VLA-4 to facilitate tethering and rolling of leukocytes. VCAM-1 expression can be upregulated by numerous cytokines but the promoter region of the VCAM-1 gene is known to have two NFκB binding sites [105]. Similar to VCAM-1, ICAM-1 is a member of the immunoglobulin superfamily that binds an integrin receptor, in this case LFA-1 or MAC-

1. ICAM-1 facilitates the firm arrest of leukocytes and the transmigration into the vessel wall. Both cell adhesion molecules are constituitively expressed at low levels but can be upregulated by numerous stimuli [106].

VCAM-1 and ICAM-1 have been shown to be WSS sensitive with ROS and NFκB implicated as mediators [66, 68, 107]. The VCAM-1 gene in particular has two NFκB binding sites in its promoter region resulting in increased VCAM-1 expression in response to increased NFκB levels and activation [98, 99]. ICAM-1 expression on the other hand has been shown to be regulated by numerous inflammatory cytokines that are regulated by NFκB such as IL-1 and TNF-alpha. Studies have shown that ROS inhibition through antioxidants profoundly attenuates inflammatory protein expression likely through diminished NFκB levels [98, 102, 108]. While there is general agreement that VCAM-1 and ICAM-1 are upregulated by low magnitude and/or oscillatory WSS, some in vitro studies have shown differing data [66, 68, 71, 98, 107, 109, 110]. The varying cell types, culture conditions, and environmental factors *in vitro* make an *in vivo* study essential for determining the shear induced expression of cell adhesion molecules. I*n vivo* studies have correlated increased expression to areas predisposed to atherosclerotic lesions [20-22, 27, 111-113]. Knockout mice deficient in either VCAM-1 or ICAM-1 show significantly attenuated lesion formation [111, 114]. Though VCAM-1 ko is embryonic lethal, the VCAM-1 mice are domain 4-deficient (D4D) and have decreased VCAM-1 expression. ICAM-1 deficiency attenuates lesion formation in an accelerated atherosclerosis model where lesions form in a non-flow dependent manner throughout the whole aorta [114]. In a model investigating flow dependent lesion formation in the aortic arch and aortic sinus, VCAM-1 deficiency attenuated lesion

formation but ICAM-1 deficiency resulted in normal lesion formation, comparable to the control [111]. These results suggest that although both adhesion molecules are important for lesion formation and are regulated by flow, VCAM-1 may play a more critical role in flow-dependent atherogenesis than ICAM-1.

Background Summary

Atherosclerosis is a major burden on the American population. It is a multifactoral inflammatory disease of the vasculature that is predisposed to localization in regions of disturbed flow. Endothelial cells act as mechanotransducers to respond to differeing flow patterns which can lead to a healthy physiologic state or a pathologic state. Cell culture studies have shown that endothelial cells exposed to disturbed flow have an atherogenic phenotype with increased oxidative stress and inflammation. These data primarily come from cell culture studies and have provided a wealth of insight into the molecular mechanisms leading to lesion localization; however, there are clear differences between the *in vitro* and *in vivo* environments. Mice provide an ideal *in vivo* animal model in which to investigate *in vivo* molecular mechanisms of mechanotransduction. There are currently only a few *in vivo* flow models that provide environments of disturbed flow. Improved *in vivo* models of disturbed flow along with the wealth of transgenic and knock out animals will allow for further investigation of mechnotransduction pathways as they relate to atherosclerosis formation.

CHAPTER 3

MURINE AORTIC COARCTATION MODEL

Specific Aim I - Develop an acute mouse aortic coarctation model

Introduction

Our first objective was to develop a simple *in vivo* coarctation model and characterize the associated hemodynamic environment. Most flow studies currently utilize *in vitro* flow setups with simplified WSS profiles. *In vitro* experiments provide insight into the behavior of endothelial cells; however, they lack the complex biochemical environment in which the endothelial cells live *in vivo*. *In vivo* flow models fall into two categories: chronic or device-based. The chronic *in vivo* flow models provide a pathologic environment, but the complex hemodynamics are difficult to model and chronic adaptive changes may have occurred. Alternatively device-based models allow for the investigation of mechanotransduction pathways in response to acutely disturbed flow. These models can potentially separate the effects of compensatory mechanisms from pathways activated by direct mechanical transduction. Currently, these models are limited by complex procedures that do not have fully characterized hemodynamic environments and often do not produce low magnitude oscillatory WSS. Therefore, there is a lack of adequate in vivo models that can be used to analyze the molecular mechanisms involved in pathologic mechanotransduction.

Our objective for aim 1 was to develop an *in vivo* coarctation model of controlled hemodynamic conditions. The coarctation model was designed with the criteria that a region of low magnitude oscillatory WSS was created downstream from the stenosis and that there was no significant loss in blood pressure or change in strain. Our model

overcomes the limitations of previous flow models by inducing a precisely defined coarctation in the suprarenal region of the aorta using a shape memory nitinol clip. We used μCT and MRI techniques to obtain boundary conditions for a computational fluid dynamic model. Using our CFD *in silico* model we characterized the hemodynamic environment associated with our *in vivo* coarctation model. This *in vivo* model with a controlled mechanical environment provides a powerful tool for the analysis of shear stress sensitive molecules.

Methods

Animals

C57/BL6 mice were purchased from Jackson Laboratories. Male mice aged 11-13 weeks were used for this study. The animals were housed and cared for according to the guidelines proposed by the National Institute of Health and the experimental protocol was approved by the Emory University Institutional Animal Care and Use Committee.

Clip Design - SMP Clip Manufacturing

We used a SMP clip surgically implanted around the suprarenal aorta of twelve week old wild type mice (C57 Bl/6) to induce a coarctation. The SMP was first polymerized into thin sheets by photopolymerization of t-butyl acrylate cross linked with polyethyleneglycol dimethacrylate using a photo initiator [115]. Circular clips were then cut out of the sheets using a CO_2 laser cutter. We manufactured clips with varying inner diameters and thicknesses to optimize the conditions for the coarctations. The resolution limitations of the laser cutter allowed for manufacturing of clips with inner diameters as small as 0.3 mm and increasing diameters by 0.05mm. We used a range of coarctations with different inner diameters between 0.6 mm and 1.0 mm. As a control we used a non-coarcted model and a non-obstructive sham model where the internal diameter of the clip is larger than the aorta. These clips uniquely exhibited a shape memory effect in which they can recover to a preset shape due to a thermal activation (similar to figure 3.1) .

The circular clips were heated to a deformation temperature in boiling water and deformed to a linear shape. The polymer was then cooled and set in a temporary linear shape. The clip could then be implanted underneath the aorta of a mouse. Upon

implantation the body temperature of the mouse thermally activated the recovery of the clip to return to its original shape, thereby inducing a coarctation. External heat was applied by warmed saline to increase the rate of recovery as necessary. All clips were sterilized in 90% ethanol prior to implantation.

Nitinol Clips

Superelastic nitinol tubing was purchased from Memry (Menlo Park, CA – Tube-BB-32X39.5 and Tube-BB-54.4X70.8) in various sizes. The tubing was cut into 1 mm lengths using a diamond saw (Struers Accutom-2 with a Struers 805861 blade,). Each 1mm segment of tubing was then cut axially using an infrared laser cutter (Impressario Q-switched Nd:YLF - Resonetics, Nashua, NH) producing C-shaped clips 1 mm in length (figure 3.1). The clips were then heat treated to transition them from a superelastic state to a shape memory state in which the recovery temperature was optimized for in vivo conditions at 36 deg C. Clips were heated in an oven at 450˚ C for 2.5 hours then quickly quenched in ice water [116].

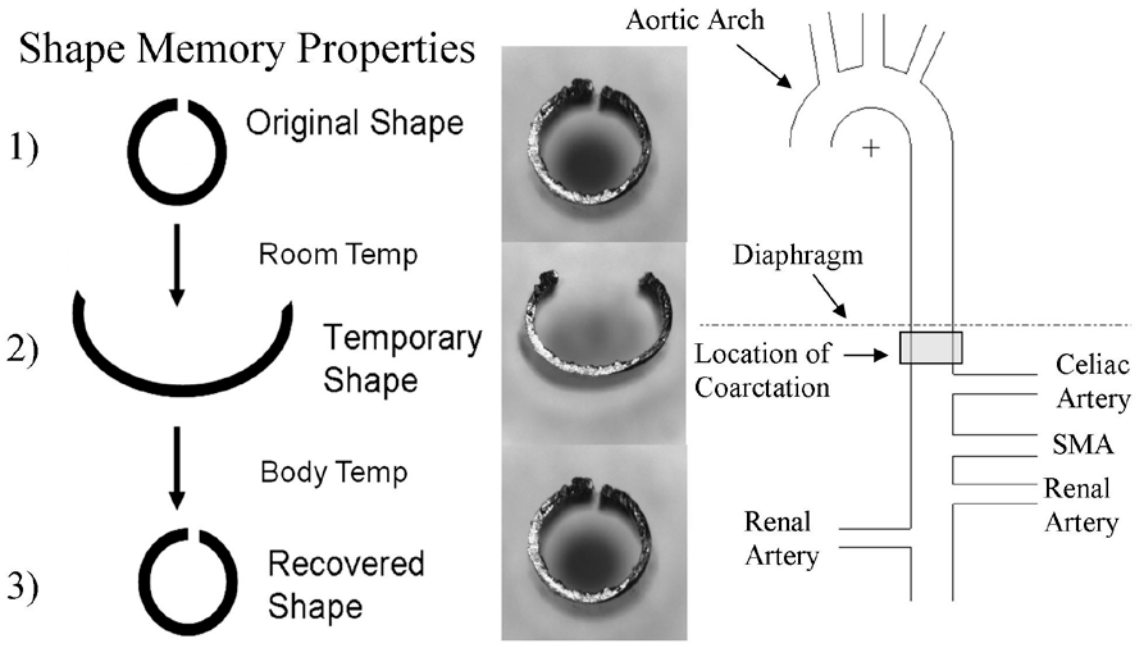

Figure 3.1 – Shape Memory Properties of a Nitinol Clip - The left panel shows the stages of the shape memory response of the nitinol clip. At room temperature the clip can be readily deformed by an applied force and hold the temporary shape. In the temporary shape the clip can be inserted underneath the aorta of the mouse. The body temperature of the mouse then thermally activates the recovery of the clip and the clip returns to its original shape inducing a coarctation. The right figure shows the location of the coarctation. The clips were placed proximal to the celiac branch and distal to the diaphragm.

Coarctation Surgery

Male C57/Bl6 mice were anesthesized using isoflurane (oxygen was delivered through inhalation at a flow rate of 0.5L/min mixed with isoflurane at 3% for induction and 1.5% for maintenance). All hair was removed from the surgical field by first shaving using clippers then applying a depilatory (Nair). The skin was then sterilized using a betadine wipe to maintain an aseptic surgical area. An incision was made along the midline of the skin and peritoneum of the abdomen. The abdominal cavity was exposed using a self-retaining retractor (World Precision Instruments, Inc.) to push open the skin and peritoneum. The intestines were displaced from the abdominal cavity and placed

between two sterile pledglets of gauze soaked in saline. The abdominal aorta was then located using a dissecting microscope (Olympus). Periadventitial fat was removed by performing a blunt dissection with micro-forceps. The clip, either nitinol or SMP, was then deformed to an open state and placed underneath the aorta. The body temperature from the mouse thermally activated the recovery response of the clip inducing a coarctation of the aorta. The thermal recovery was assisted as needed by applying warmed saline locally to the clip to increase the rate of recovery. The intestines were then returned to the abdominal cavity and the peritoneum and skin were sewn together with absorbable sutures. Finally surgical staples were applied along the incision line to ensure proper healing. The animals were then kept on heating pads during recovery and given buprenorphine (0.01 mg/kg intraperitoneal) as necessary.

Magnetic Resonance Velocimetry

Male C57/Bl6 mice were anesthesized using oxygen delivered through inhalation at a flow rate of 0.5L/min mixed with isolflurane at 3% for induction and 1.5% for maintenance. Imaging was performed using a 4.7 Tesla Varian INOVA MRI scanner (Varian, Palo Alto, CA). The suprarenal region of the aorta was located and cine images were acquired taking ten frames, equally spaced over the cardiac cycle [19]. Image J (NIH, Bethesda, MD) was then used to obtain average cross sectional velocity values.

Catheter Based Pressure Measurements

Mice were anesthetized with isoflurane as described above. A Millar pressure catheter (Millar Instruments SPR-671 Pressure Transducer, AD Instruments, Colorado Springs, CO) was inserted into the right carotid artery and right iliac artery to measure

blood pressure above and below the abdominal aorta [117]. Baseline blood pressure was measured for 10 minutes. The abdomen was then opened and a nitinol clip was placed around the aorta as described earlier. The abdomen was then closed and the blood pressure was allowed to equilibrate before the upstream and downstream blood pressures were recorded for 10 minutes. Data were acquired and analyzed using a Powerlab system and Chart software (AD Instruments, Colorado Springs, CO).

Ex-vivo Pressure Inflation

Mice were euthanized using CO_2 inhalation. Aortas were dissected, cleaned, and branches were tied off with suture. Prepared aortas were cannulated in a vessel isolation chamber (Living Systems (LSI), Burlington, VT) that was mounted on a Nikon DIAPHOT 200 inverted microscope. The aortas were stretched to the in vivo length, bathed with 37°C DMEM (Sigma-Aldrich, St. Louis, MO) with HEPES buffer at pH 7.4 containing 10 μM sodium nitroprusside, and allowed to equilibrate for 30 minutes. Transmural pressure was ramped from 0 to 130 mmHg at 0.5 mmHg/sec using a peristaltic pump and pressure controller (LSI). A video dimension analyzer (LSI) was used to optically measure the outer diameter of the vessel during the transmural pressure ramp to obtain compliance measurements.

μCT Imaging Specimen Preparation

Tissues were prepared in accordance with previously described methods [20, 118]. Animals were euthanized using CO_2 inhalation. The thoracic cavity was opened and the inferior vena cava was cut. A needle was placed in the left ventricle and the vasculature was perfused at a pressure of 100 mmHg with 0.9% normal saline for five minutes followed by 10% neutral buffered formalin for five minutes. The formalin was flushed from the vasculature with saline. Microfil (Flow Tech, Carver Ma) was prepared per the manufacture's guidelines and then injected into the vasculature. Tissue was then decalcified in Cal-Ex II for 48 hours.

μCT Imaging

The abdominal aorta was imaged using a high resolution (20um isotropic voxel size) μCT imaging system (μCT 40 Scanco Medical, Basserdorf, Switzerland). The parameters were set to a voltage of 55kVp, current of 145 uA, and resolution set to medium. The raw data was reconstructed into serial tomograms using a cone beam filtered back projection algorithm [118]. A global threshold was applied to the tomograms which were then exported as a 3-D reconstruction in the .stl format.

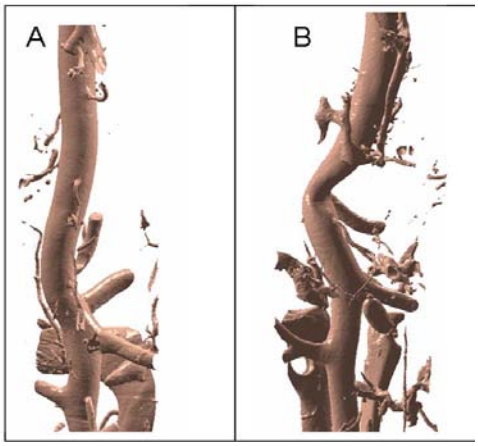

Figure 3.2 – Representative μCT Reconstructions - Panel A shows the morphology from a control aorta. Panel B shows the morphology from an aorta with a coarctation from a SMP clip.

Computational Fluid Dynamic Modeling

Abdominal aortic morphology was imported into Geomagic software (Geomagic Inc., Research Triangle Park, NC). Small branches were removed and the aortic surface was smoothed. The aortic diameters were then scaled outward by an expansion factor as determined by in situ pressure inflation measurements. The pathlines were created along the aortic surface which was then converted into NURBS format and exported as an .iges file. Files were imported into GAMBIT (Ansys, Canonsburg, PA) where mesh and boudary layers were applied. The files were exported as .msh and imported into FLUENT (Ansys). Blunt, cross sectional averaged, inlet velocity profiles over the time course of a cardiac cycle were obtained from MR phase contrast velocimetry. Outlet conditions were set to 80 mmHg as an approximate mean arterial pressure. Maps of WSS were then generated in Fluent while velocity profiles were generated using Paraview (Kitware, Inc,, Clifton park, NY).

Statistical Analysis

Quantitative results were analyzed with a one-way ANOVA using GraphPad Prism software (GraphPad Software, La Jolla, CA). Results are shown as mean ± SEM. A p-value of <0.05 was considered statistically significant.

Results

Aortic Coarctation Using SMP Clips

We found that the SMP clip was able to induce a coarctation of the mouse aorta. Figure 3.3 shows WSS maps from a control aorta and an aorta with a SMP clip induced coartation. The map shows the WSS during the downstroke of systole, when flow separation is most likely to occur. WSS levels in the upstream aorta had levels near 400 dynes/cm^2 for both the control and coarctation aortas. There is some flow skewing due to the curvature of the spine resulting in a heterogeneous distribution of WSS in the renal area. Additionally, the branch sites of the celiac artery, the superior mesenteric artery, and the renal arteries create areas of increased WSS at the flow divider and decreased WSS opposite the flow divider. The WSS within the coarctation increases significantly compared to the comparable area in the control. There is a large region of low magnitude WSS just downstream from the coarctation. This WSS distribution matches the predicted WSS profiles from the theoretical stenosis models (figure 2.3).

The velocity vectors also match the predicted flow profile. Figure 3.4 shows the velocity vectors in an aorta with a coarctation at various points in the cardiac cycle. During the upstroke of systole and during diastole flow is unidirectional through the region downstream from the coarctation. During the downstroke of systole flow separation is observed downstream from the coarctation resulting in an oscillation in the flow. This oscillation in flow is representative of the directionality of the associated WSS. The WSS in this downstream region is therefore low magnitude and oscillatory and mimics the hemodynamic environment associated with atherogenesis. However, it is important to note that the stenosis is non-concentric.

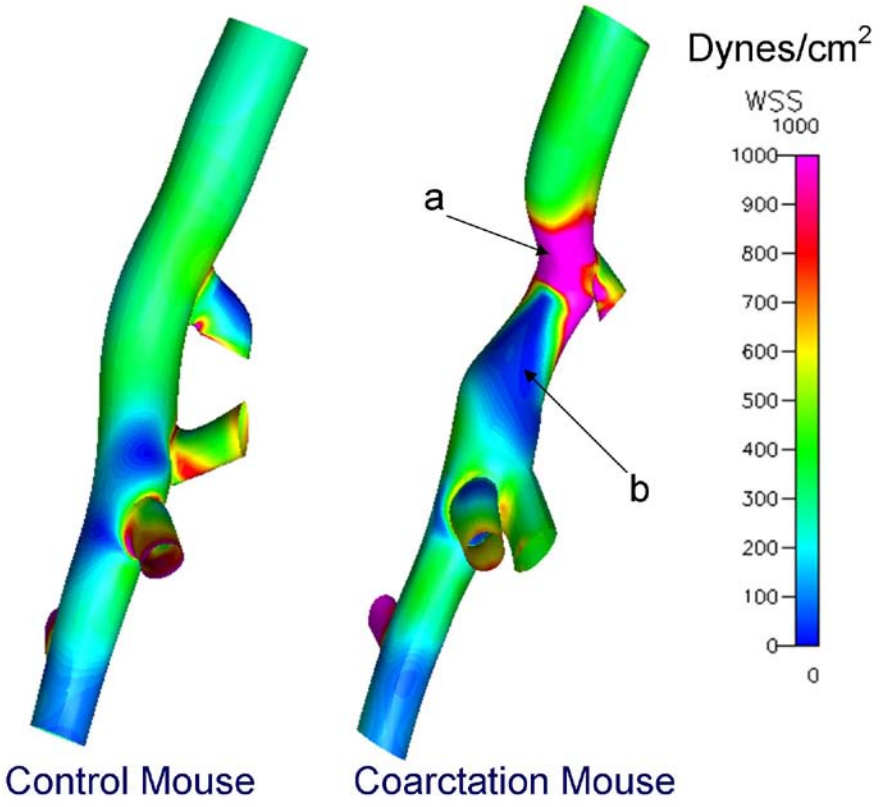

Figure 3.3 – WSS map generated from a CFD model in a control mouse and a mouse with an SMP clip coarctation - The control mouse shows relatively high levels of WSS with some low magnitude regions near branch points. The coarctation mouse shows a large region of low magnitude WSS downstream from the coarctation and a region of increased WSS in the stenotic region.

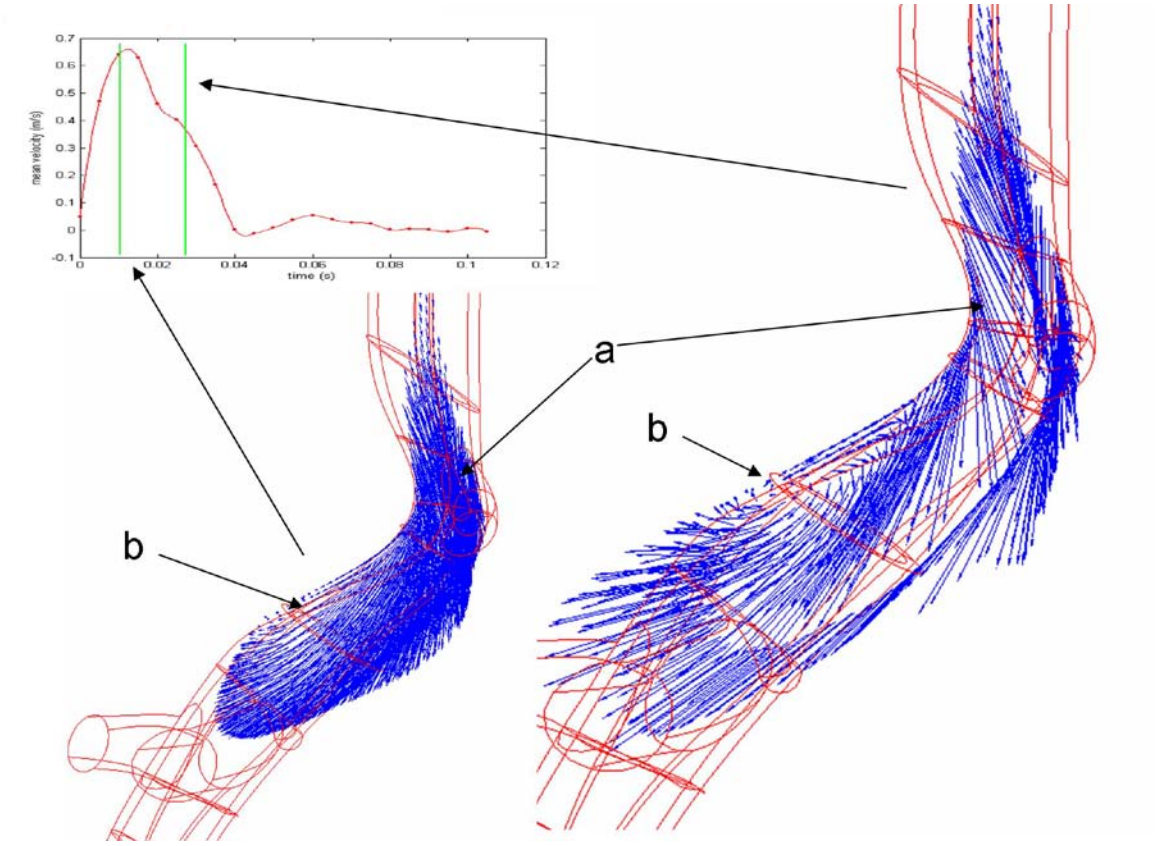

Figure 3.4 – Velocity Vectors in a Coarctation Mouse Model - During the upstroke of systole flow is unidirectional through the coarctation and in the downstream region. During the downstroke of systole flow separation occurs in the downstream region (b) resulting in oscillatory WSS.

Efficacy of the SMP Clip

Though the SMP clip was able to produce a region of low magnitude oscillatory WSS, there were issues with the reproducibility of the stenosis. Figure 3.5 shows the percent stenosis using various size clips. Even when the clip had an inner diameter of 1.0 mm, near the size of the aorta, a significant stenosis was induced. Furthermore, there was no significant difference between the stenosis induced by four different sized clips. This was likely due to the large kink that is produced in the aorta due to the thickness of the clip. As the clip was placed underneath the aorta, it pressed against the spine and the thickness displaced the aorta. Since the thickness was 0.5 mm, about half the aortic diameter, a large kink was created. The cross sectional view showed that the aorta did not maintain its circular morphology through the stenosis. The aorta was flattened on the posterior side, where the kink was located, while the anterior side of the aorta remained circular. Additionally there were significant issues in the reproducibility of the shape of the degree of stenosis and the cross section. We therefore, decided to investigate using clips made from a different material.

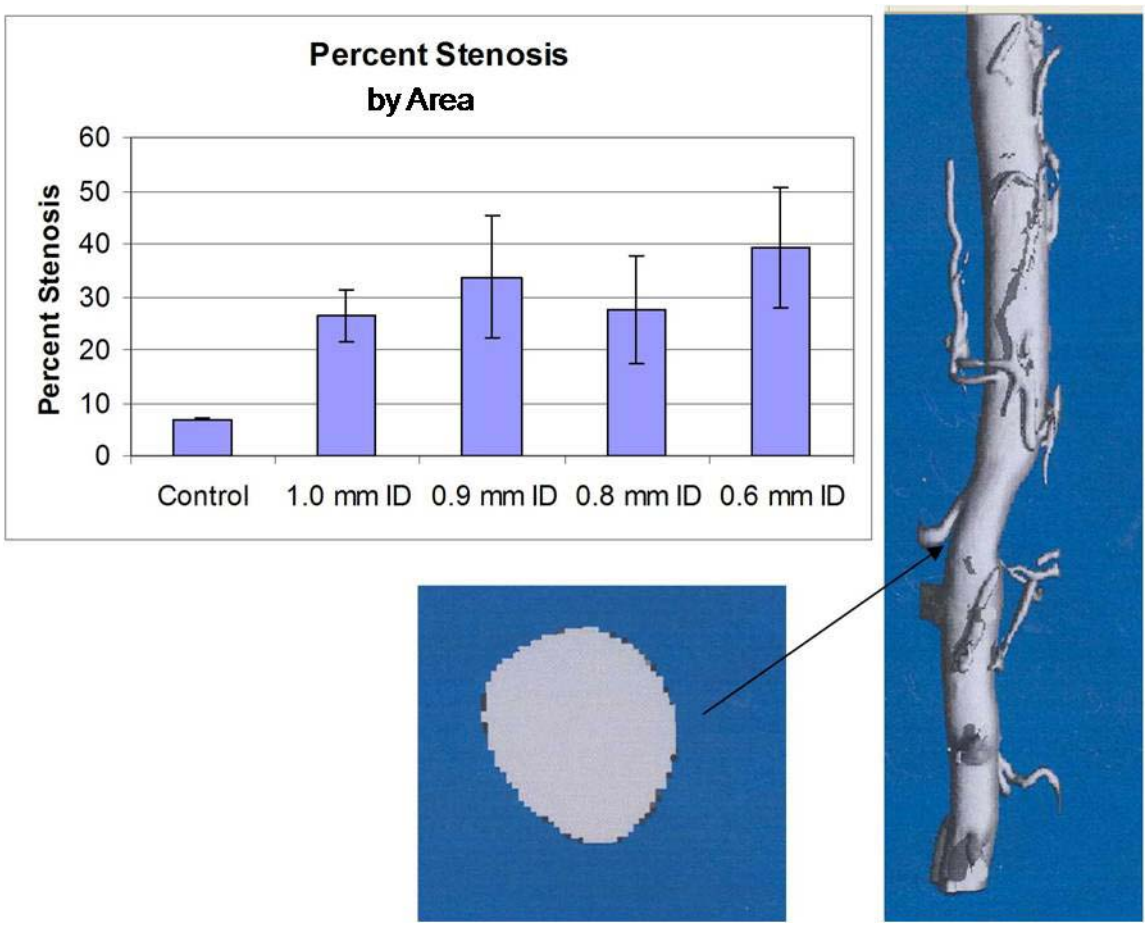

Figure 3.5 – Comparison of Degree of Stenosis Induced by SMP Clips – We used μCT to obtain the morphology of aortas with coarctations produced by SMP clips. The upper plot shows the percent stenosis by area that was induced by clips with varying inner diameters. No significant difference in the percent of stenosis was observed between the groups. There was large variability within individual groups primarily due to the variable shape of the aortic cross section at the site of stenosis. The lower image shows a representative cross section from the middle of the coarctation. The cross section had more of an oval shape than the normal round shape, likely from the kink in the aorta produced by the SMP clip.

Development of Nitinol Clip Coarctation Model

We found that nitinol clips could be used to induce an aortic coarctation. The clips uniquely exhibited a shape memory effect at body temperature (figure 3.1). At room temperature the clips were deformed under an applied force and maintain a temporary, open state. In this open state they were inserted underneath the aorta of the mouse. The body temperature of the mouse then thermally activated the recovery of the clips returning them to their original shape thereby inducing a coarctation. Additionally, the clip had a minimal thickness, 0.01 mm, allowing for the induction of a near ideal, concentric, stenosis. In performing these experiments we report a mortality rate of less than 10%. The mortalities were most often the result of human error from puncturing a local branching artery or caused by an overdose of anesthesia.

Characterization of the Nitinol Clip Coarctation

The hemodynamic environment of our coarctation model is highly dependent on the morphology of the aorta at the coarctation, thus it is critical to establish the efficacy of this coarctation technique. The induced stenosis was characterized as the difference between the diameter within the coarctation and the diameter proximal to the coarctation. We measured the proximal diameter and the stenotic diameter using two different techniques, *ex vivo* pressure inflation and μCT. *Ex vivo* pressure inflation was used to increase the luminal pressure of excised aortas from 10 mmHg to 130 mmHg. The proximal aortic diameter showed a sigmoidal compliance response ranging from 0.780 ± 0.005 mm to 1.247 ± 0.032 mm, similar to previous reports (figure 3.6) (personal communication, Dr. Kathryn Rafferty). We could not make direct measurements of the

aortic wall within the coarctation since we were unable to image through the nitinol. Therefore, measurements of the external diameter of the clip were obtained and the thickness of the clip subtracted to obtain the approximate diameter of the aorta within the coarctation. These measurements showed an aortic diameter of 0.748 ± 0.003 mm, with no significant change over the pressure cycle. From these measurements we calculate that the degree of stenosis (by diameter) induced by the clip, ranged from 29.4 ± 3.1 % at 60 mmHg to 38.4 ± 1.9 % at 100 mmHg These *ex vivo* results demonstrate the efficacy of the coarctation under physiologic blood pressure.

μCT measurements were used to validate the *ex vivo* coarctation efficacy measurements. The results show a proximal diameter of 0.80 ± 0.04 mm, and a diameter within the coarctation of 0.69 ± 0.02 mm. The upstream measurements as determined by μCT correspond to a pressure of approximately 20 mmHg as measured by *ex vivo* inflation suggesting a fixation artifact in the μCT preparation technique. The difference in the coarctation diameter between the two techniques appears to be attributable to the vessel wall thickness which is included in the inflation measurements but not the μCT measurements. Both techniques demonstrate the efficacy of the coarctation technique using nitinol clips and show small variability between mice (standard error was less than 0.05mm).

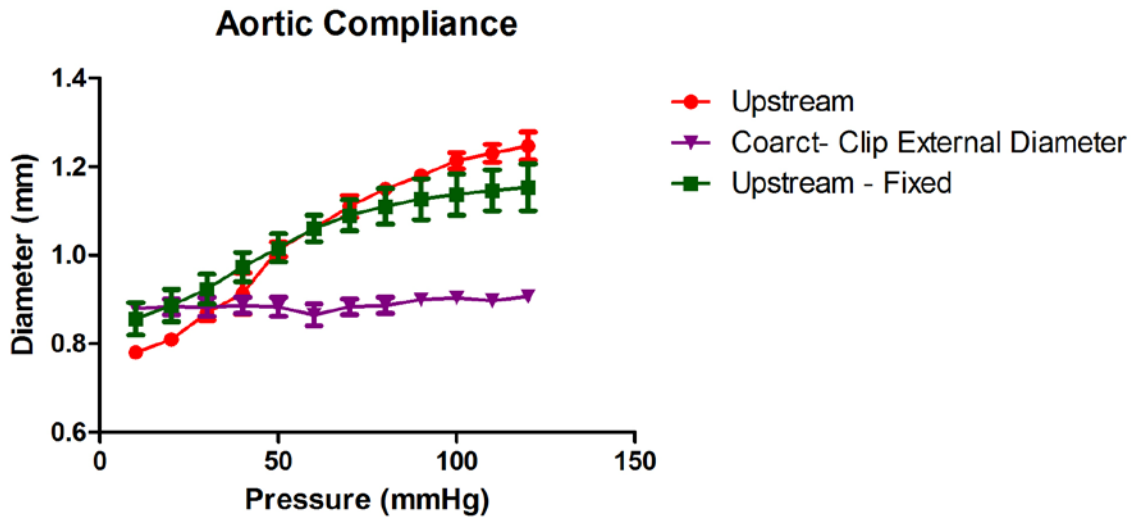

Figure 3.6 – Fixation Effects on the Aortic Pressure Diameter Curve - Aortas were inflated by increasing the luminal pressure. The diameter from the upstream region of the aorta was recorded. Aortas were then fixed with formalin at 80 mmHg for 5 minutes and the recordings were repeated. There was a trend for a slight decrease in compliance, yet there was still a significant diameter change over the pressure ramp. This shows that even with pressure fixation the mouse aorta remained compliant and did not fix the morphology to the comparable morphology at 80 mmHg *in vivo*.

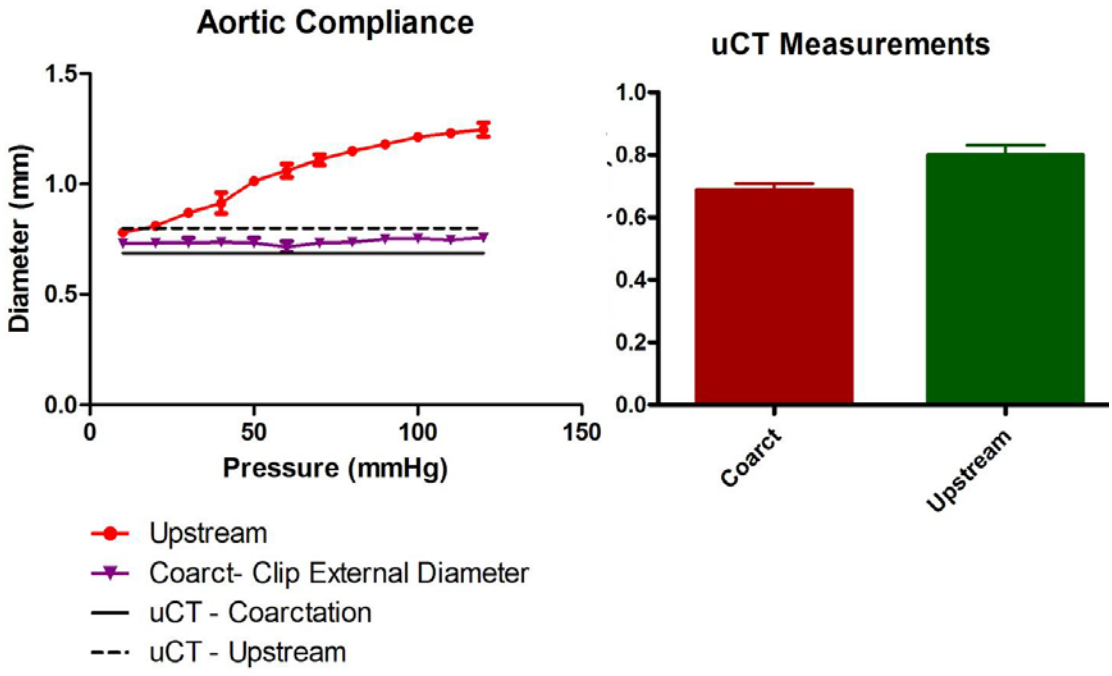

Figure 3.7 – Coarctation Efficacy – Measurements were taken to show the reproducibility of the degree of stenosis induced by the coarctation surgery. In situ pressure inflation (left) shows the diameter of the aorta as the luminal pressure is increased from 10 mmHg to 100 mmHg. The red line shows the diameter of the aorta upstream from the coarctation while the purple line shows the measurements of the outside diameter from the nitinol clip. The outside diameter measurements are indicative of the aortic diameter within in the clip and the thickness of the clip. The black lines show the aortic diameter measurements obtained from μCT as reference. The right figure shows diameter measurements from *ex vivo* μCT of aortas pressure fixed at 100mmHg. The measurements were taken upstream from the coarctation and at the coarctation.

Boundary Acquisition

Measurements of the thoracic aortic diameter yielded disparities between values determined by μCT and by pressure inflation (figure 3.7). This was likely due to the fixation artifact characterized in figure 3.6. To correct for this artifact, we performed an *in silico* diameter expansion based on in situ pressure inflation measurements. The expansion factor for the regions upstream and downstream from the coarctation was derived from the upstream *ex vivo* inflation measurements while the expansion factor for the coarcted region was derived from the inflation measurements at the clip. An upstream expansion factor of 30% correlated to a blood pressure of approximately 60 mmHg. Additionally we used an expansion factor of 10% and 20% to look at the sensitivity of the CFD model to this *in silico* expansion. The resultant morphology was then used as the boundary conditions for the morphologic input into the CFD model. A representative image of the resultant morphology is shown in figure 3.8.

The inlet aortic velocity was obtained from *in vivo* MR phase contrast velocimetry. The cross sectional velocity was averaged to obtain a blunt, time dependent, velocity at ten incremental time points throughout the cardiac cycle. Measurements were obtained in the upstream (suprarenal) and downstream (infrarenal) regions of control mice (figure 3.9). No significant difference was observed in mice with a coarctation.

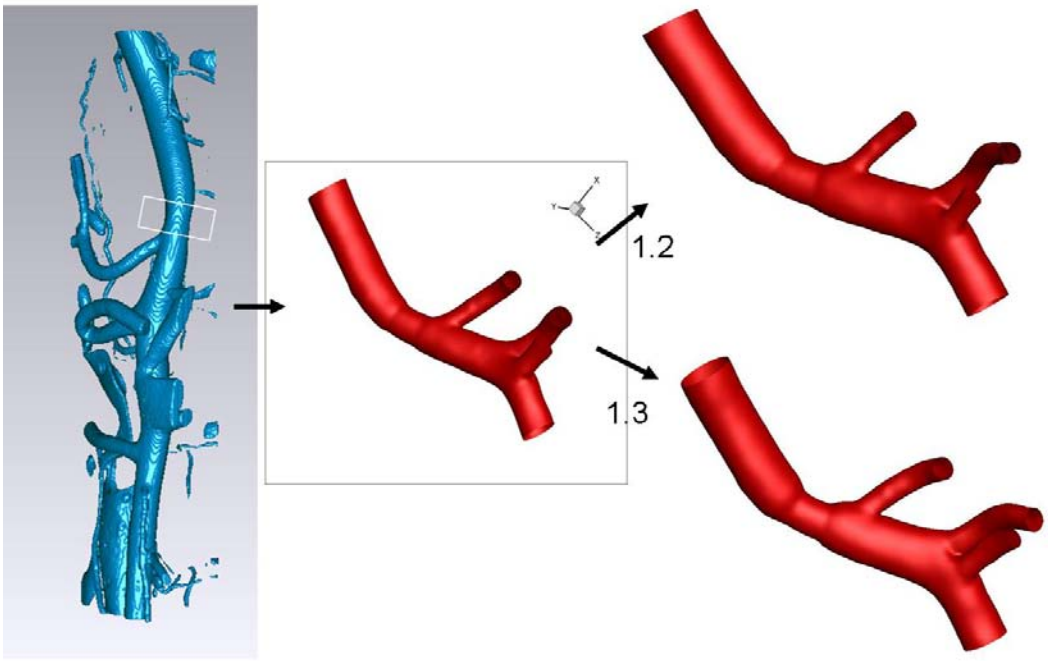

Figure 3.8 – Boundary Conditions and Expansion Factor - Boundary conditions were obtained from μCT imaging. The figure on the left shows representative raw data from a reconstructed aorta. The central figure shows the aorta after *in silico* processing with Geomagic software. The two figures on the right show the *in silico* expansion of the aorta based on calculations from the aortic compliance measurements in figure 3.7.

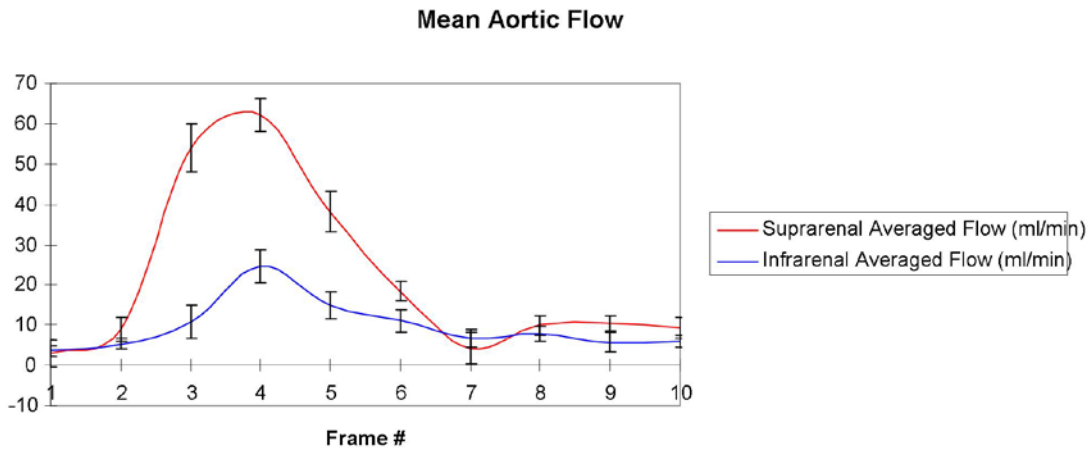

Figure 3.9 – Aortic Flow Profiles - Flow profiles in the suprarenal and infrarenal aorta of control C57 Bl/6 mice. These profiles were generated using MR phase contrast. There was a significant decrease in flow in the infrarenal aorta as a large portion of the mouse flow is diverted to the kidneys and the gut and little to the legs. These results are consistent with previous findings [19]. These flow profiles were used to obtain velocity profiles for the input and output boundary conditions for the CFD model.

Aortic Blood Pressure

Catheter-based blood pressure measurements proximal and distal to the coarctation region were obtained. During the course of the insertion of the catheter into the femoral artery, there was a significant drop in arterial pressure, approximately 40 mmHg. Pressure stabilized around 50 mmHg and maintained good waveforms. Pressure measurements obtained prior to the coarctation surgery showed a mean arterial pressure differential of 3.6 ± 10.3 mmHg while post-coarctation measurements show a mean arterial pressure differential of 2.1 ± 7.7 mmHg, thus showing minimal change in pressure differential.

Due to the significant drop in systemic blood pressure, we also modeled the pressure drop across the coarctation using CFD. The physiologic pressure drop across the renal arteries for a control (non-coarctation) aorta was found to be approximately 7.5 mmHg during systole and about 1 mmHg during diastole. The pressure drop across the

coarctation, on the other hand, was found to be approximately 13 mmHg during systole and 1 mmHg during diastole. The pressure loss produced by the stenosis during systole can be estimated to be approximately 6.5 mmHg. From our previous *ex vivo* inflation measurements of aortic compliance (figure 3.7), we predict that a pressure loss of 6.5 mmHg would produce a change of less than 0.05 mm to the aortic diameter and therefore would have a small effect on the strain at physiologic blood pressures. This effect is less than the natural variability in diameter and blood pressure between mice.

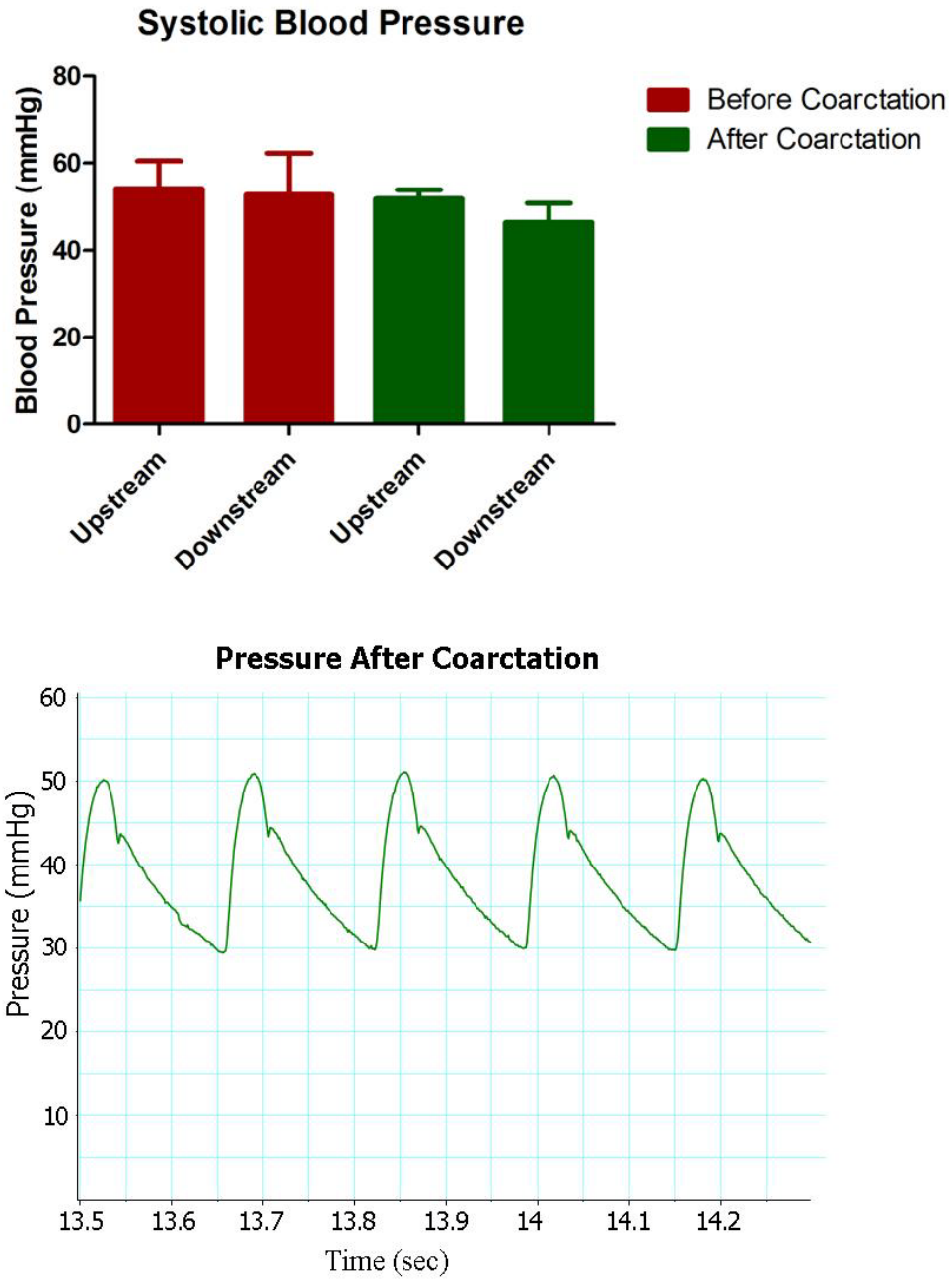

Figure 3.10 – Blood Pressure Measurements – The upper panel shows the blood pressure during systole before and after coarctation. No significant pressure drop was observed across the coarctation. The bottom panel shows a representative blood pressure waveform.

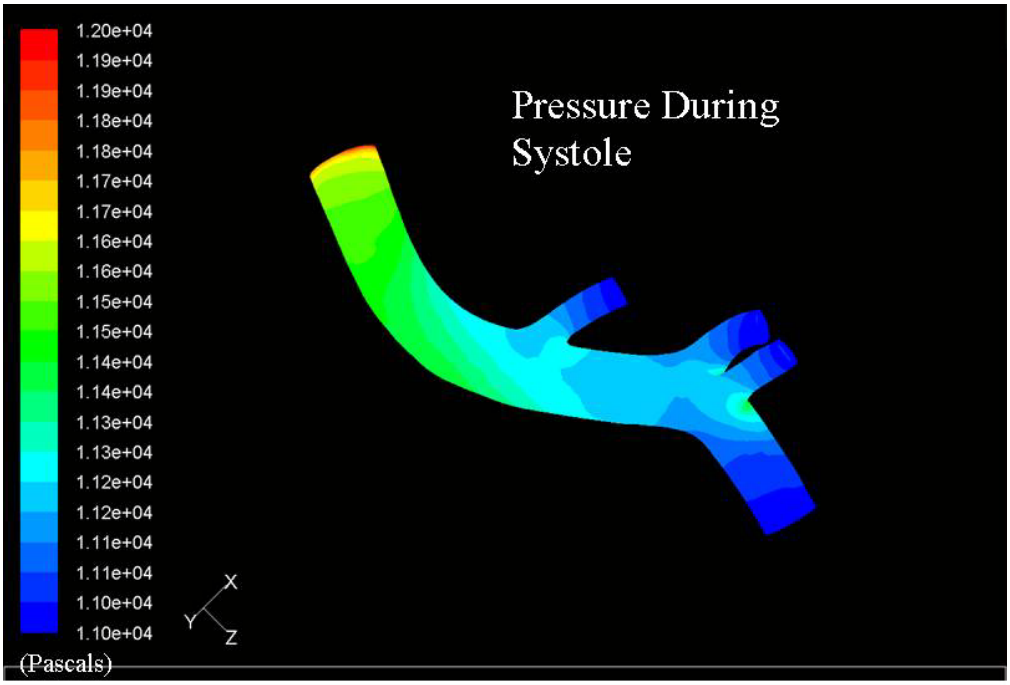

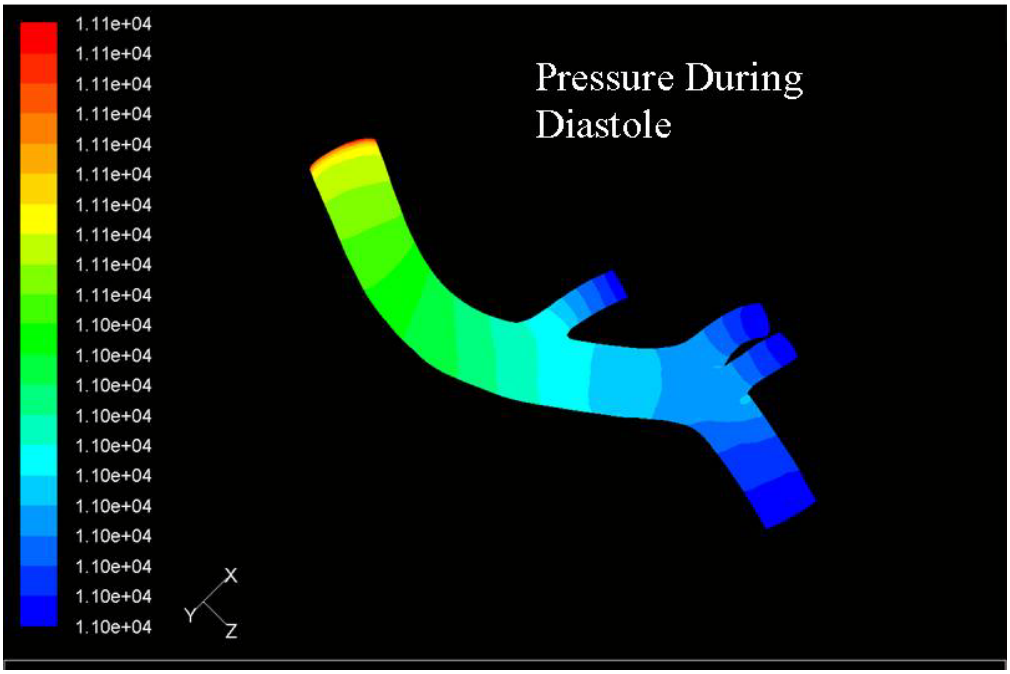

Figure 3.11 – Pressure Drop Across the Renal Arteries in a Control Mouse – The computational fluid dynamic model was used to model the pressure drop in a control mouse. During systole the pressure drop across the coarctation was approximately 1000 Pascals (~7.5 mmHg) while the pressure drop during diastole was approximately 100 Pascals (~1 mmHg).

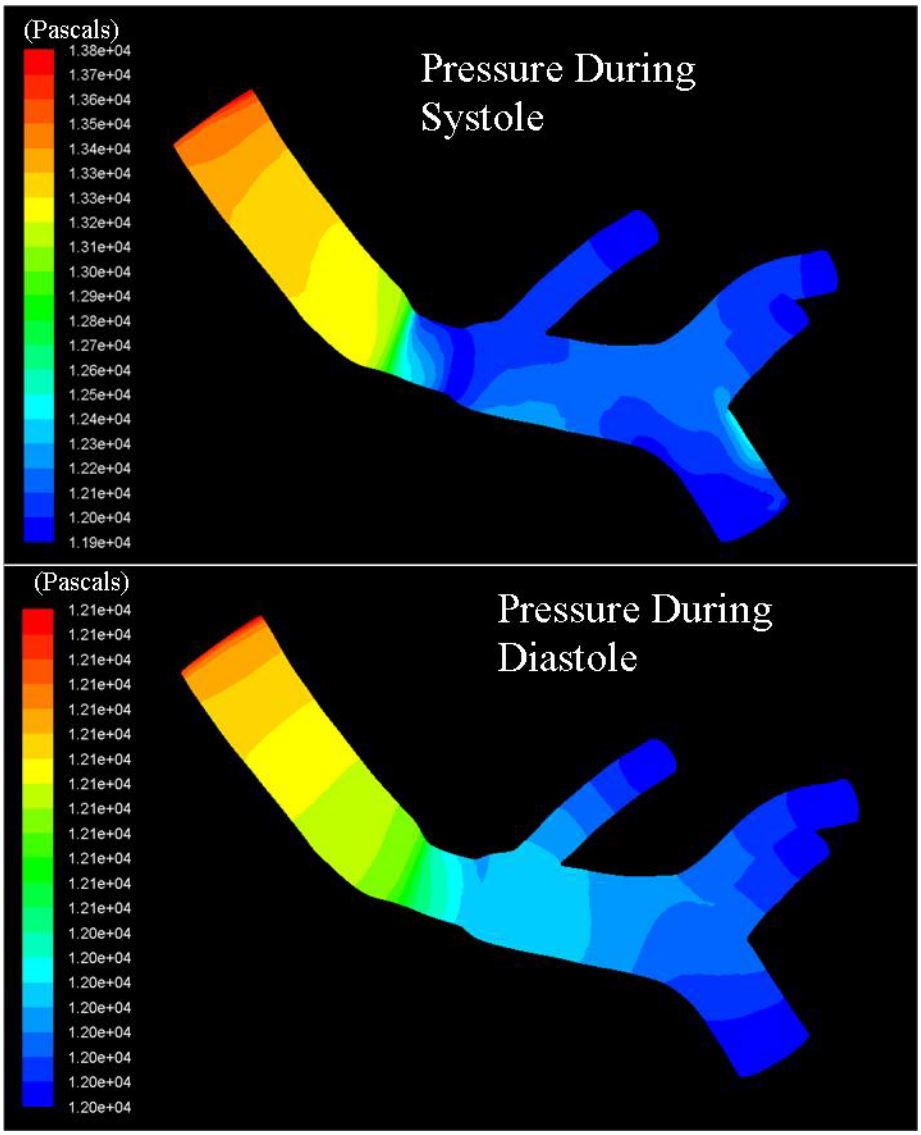

Figure 3.12 – Pressure Drop Across the Coarctation – The computational fluid dynamic model was used to model the pressure drop across the coarctation. During systole the pressure drop across the coarctation was approximately 1700 Pascals (~13 mmHg) while the pressure drop during diastole was approximately 100 Pascals (~1 mmHg).

Computational Fluid Dynamics

The morphology and velocity profiles obtained as described earlier were used as boundary conditions to generate a computational fluid dynamic model using FLUENT software. WSS maps and cross sectional velocity vectors were generated using a CFD model for control, non-coarctation aortas and coarctation aortas (Figures 3.13-3.21). Figures are presented from the early upstroke of systole, peak systole, the downstroke of systole, and during diastole. The control aorta shows unidirectional velocity through the aorta at all four time points. The WSS is relatively low during the early upstroke of systole and during diastole. During peak systole and the downstroke of systole the control aorta shows high WSS throughout the aorta with a further elevated WSS region on the posterior side produced by velocity skewing as well as at the flow divider of branching vessels. Mean WSS in the control is relatively homogenous between 10 pascals (100 dynes/cm^2) and 15 pascals (150 dynes/cm^2).

The hemodynamic environment is significantly altered in the coarctation aorta. During early systole and diastole, flow is unidirectional and there is a slight increase in WSS in the throat of the stenosis. During peak systole, there is a significant increase in WSS in the throat and hotspots of high WSS on the posterior side of the aorta and at the flow divider of branching vessels. Flow is mostly unidirectional, however, flow separation may occur in a small region immediately downstream from the coarctation on the anterior side of the aorta. This region of flow separation becomes very large during the downstroke of systole, still on the anterior side of the aorta. Additionally a large region of low magnitude WSS can be observed on the anterior side of the aorta, downstream from the coarctation. This clearly creates a region of low magnitude

oscillatory WSS downstream from the coarctation on the anterior side of the aorta. The mean WSS map for the coarctation aorta shows low mean WSS in this downstream, anterior, region. These models showed unidirectional and relatively high magnitude WSS in the upstream, thoracic, region of control and coarcted mice. The spatial heterogeneity of the WSS was relatively minimal with some skewing towards the posterior side due to the curvature of the spine. Downstream from the site of the aortic coarctation the model showed low magnitude oscillatory WSS on the anterior side of the aorta, while the control animals showed unidirectional flow with high magnitude WSS.

From these results we identified three regions of interest: the thoracic aorta, the low magnitude oscillatory WSS region in the abdominal aorta of mice from the coarctation group, and the comparable abdominal region near the celiac branch in control animals. We included the aortic arch as an additional region of interest based on previous studies showing chronic induction of low oscillatory WSS in this region [20]. This animal model can therefore compare regions of high magnitude unidirectional WSS with regions of both acutely and chronically disturbed flow producing low magnitude oscillatory WSS.

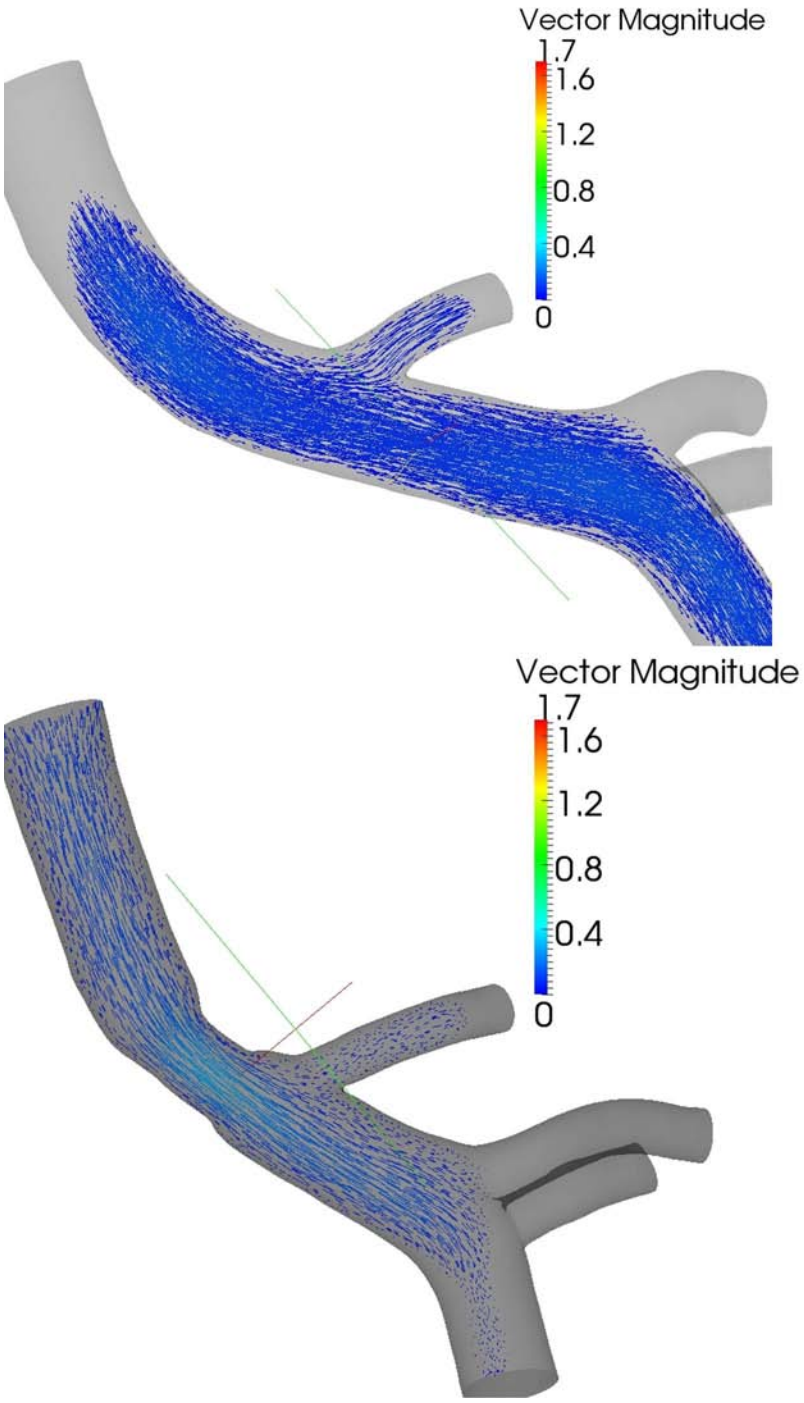

Figure 3.13– Velocity Vectors During Early Systole - Velocity vectors (m/s) from control and coarctation aortas during early systole. Flow is unidirectional throughout the aorta in both control and coarctation aortas.

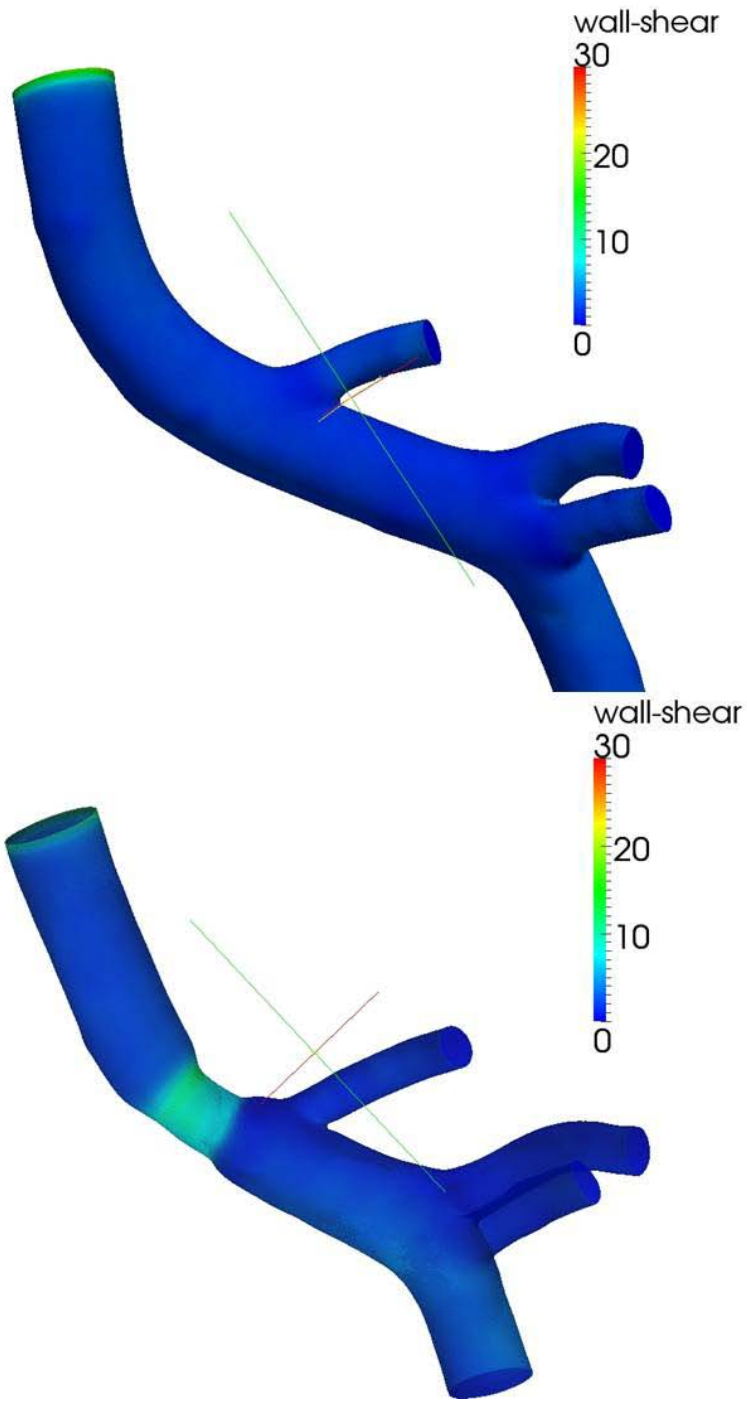

Figure 3.14 – WSS Map During Early Systole - WSS map (Pascals) from control and coarctation aortas during the initiation of systole. WSS is relatively low in both control and coarctation aortas. A slight increase in WSS is observed in the throat of the coarctation.

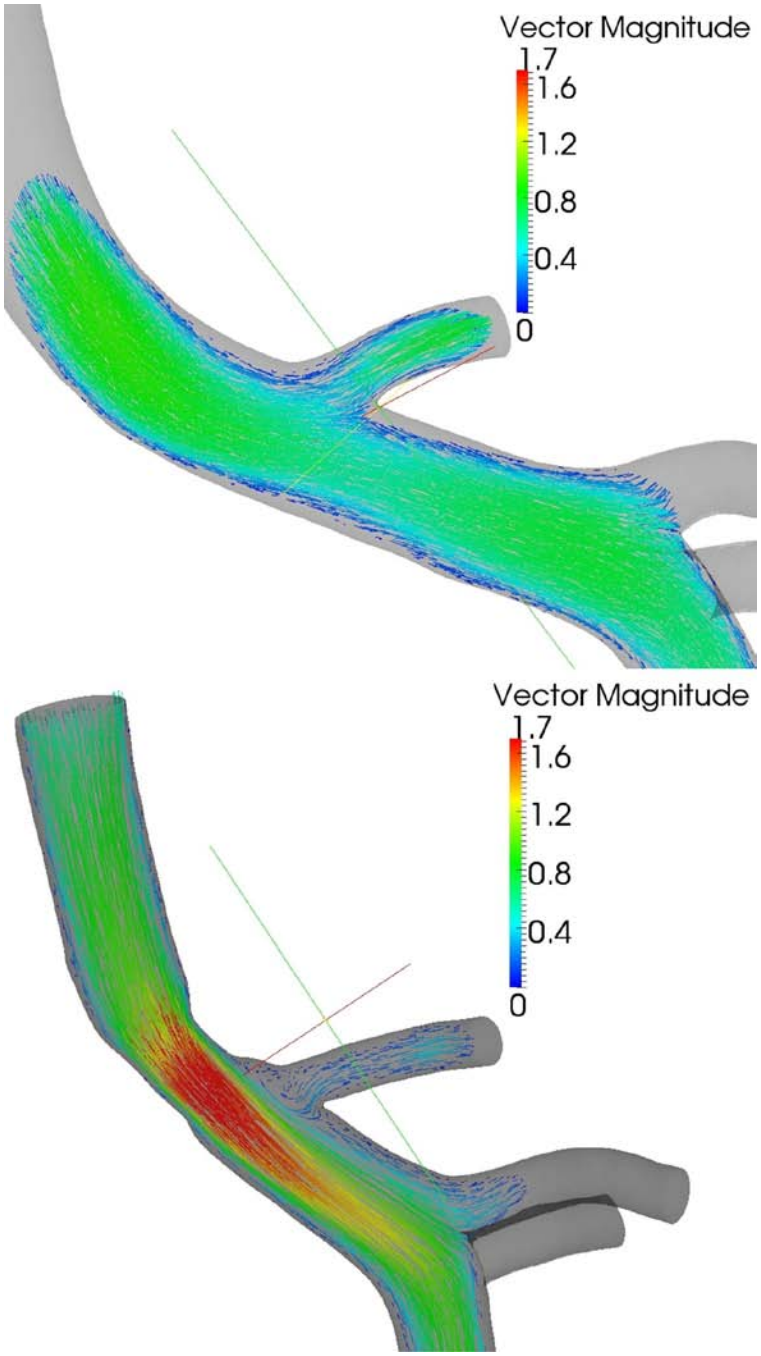

Figure 3.15 – Velocity Vectors During Peak Systole - Velocity vectors (m/s) from control and coarctation aortas during peak systole. Flow is high and unidirectional in the control aorta. The velocity in the throat of the coarctation increases significantly while the initiation of flow separation is observed in the region immediately downstream from the coarctation.

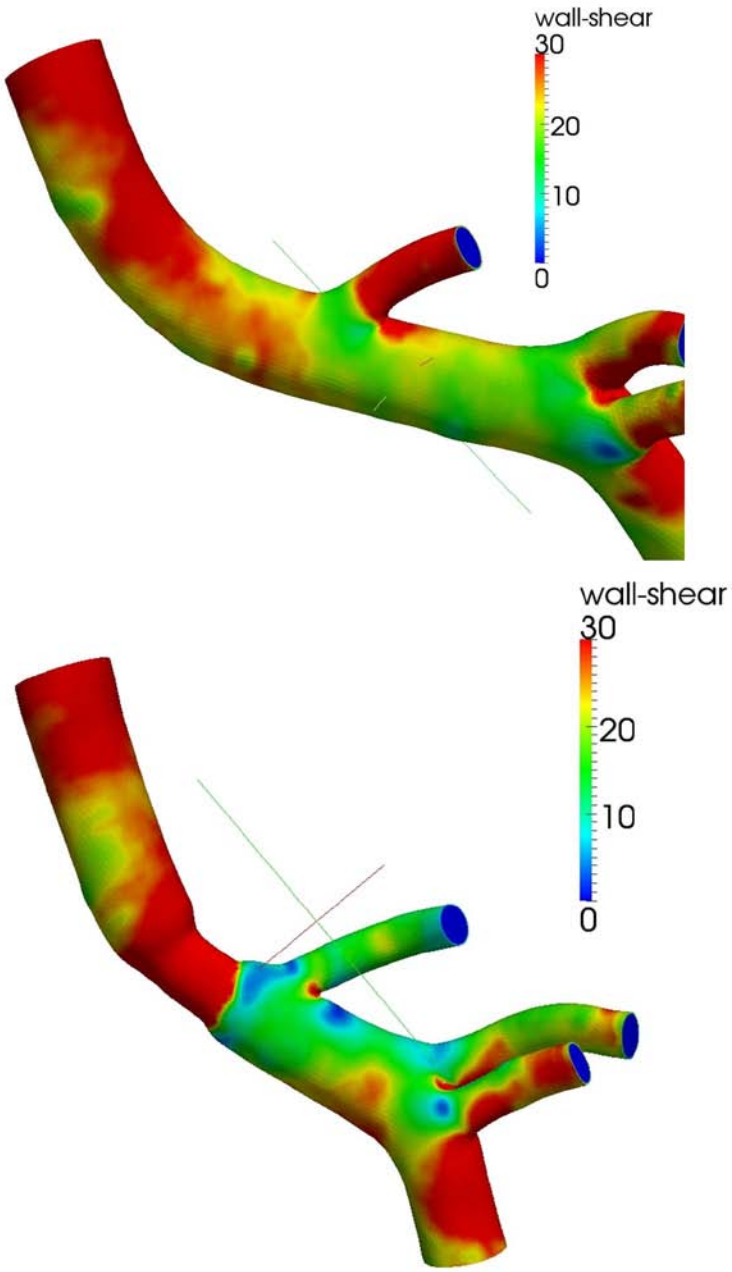

Figure 3.16 - WSS Map During Peak Systole – WSS map (pascals) from control and coarctation aortas during peak systole – WSS is relatively high in posth the control and coarctation aortas with hotspots at the flow divider of branching vessels. Additionally WSS increases within the throat of the coarctation.

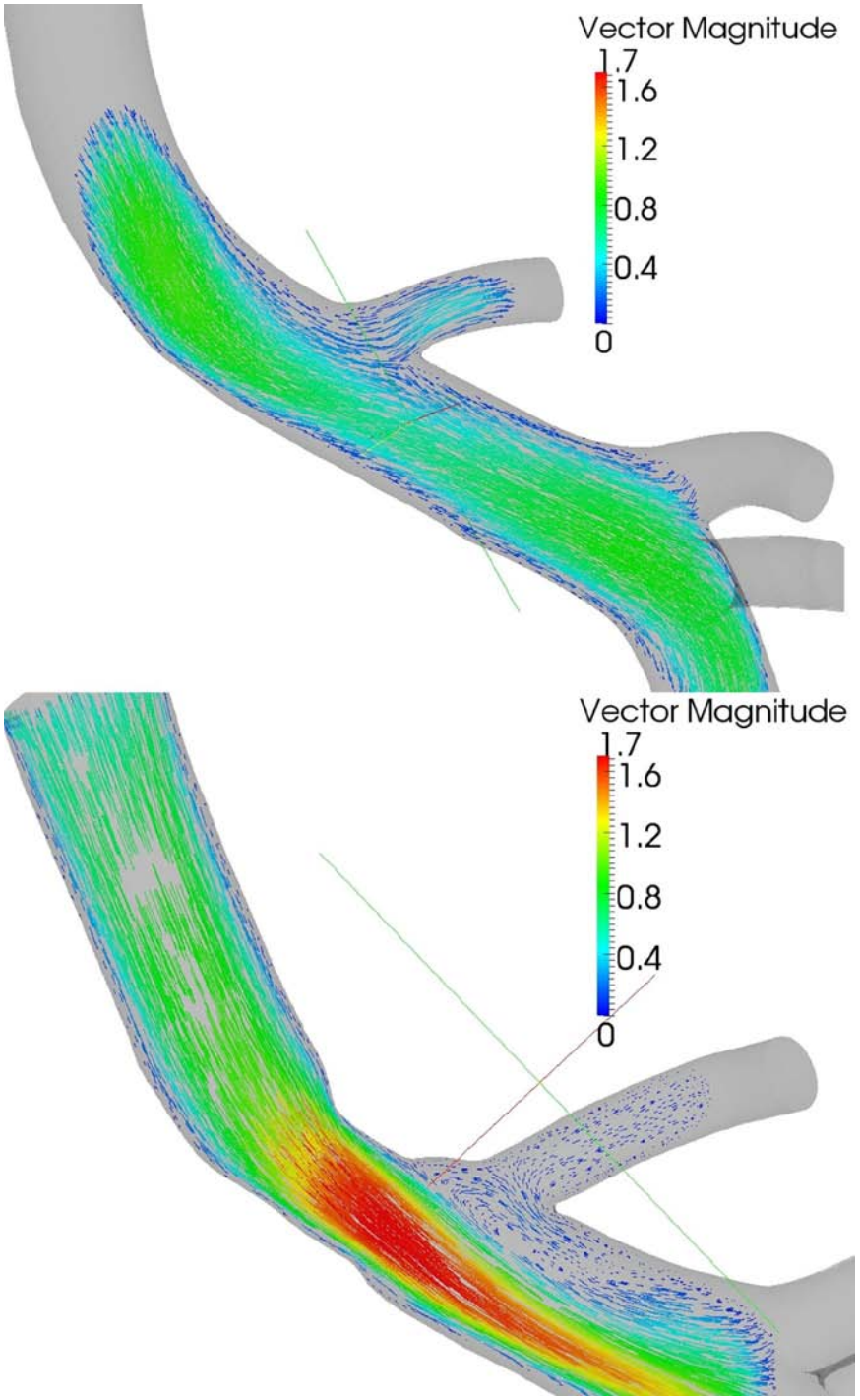

Figure 3.17 – Velocity Vectors During the Downstroke of Systole - Velocity vectors (m/s) from control and coarctation aortas during the downstroke of systole. Flow is unidirectional in the control aorta. There is a large region of flow separation downstream from the coarctation on the anterior side of the aorta.

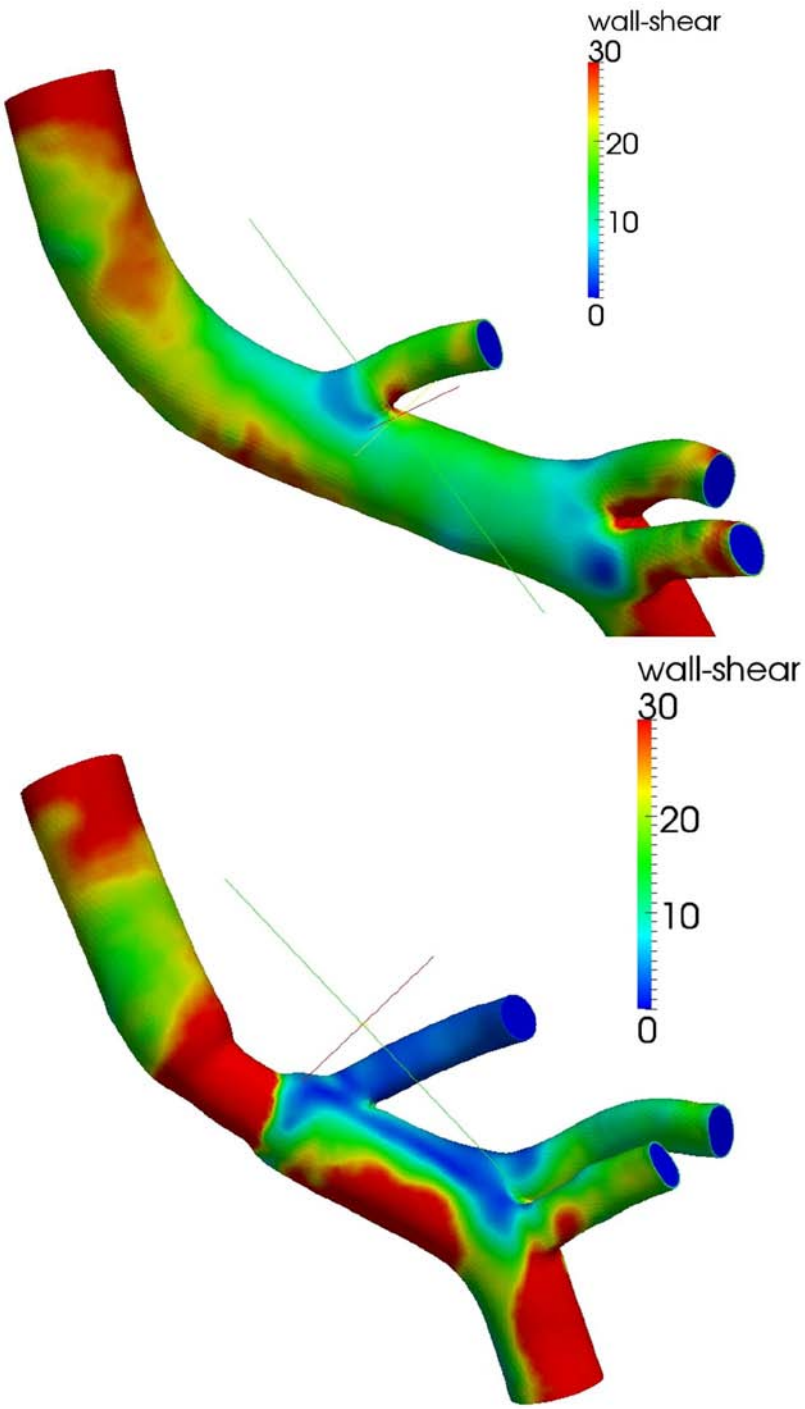

Figure 3.18 – WSS Map During the Downstroke of Systole - WSS maps (pascals) from control and coarctation aortas during the downstroke of systole. WSS is still relatively high in the control aorta. There is a significant decrease in WSS in the region downstream from the coarctation on the anterior side of the aorta.

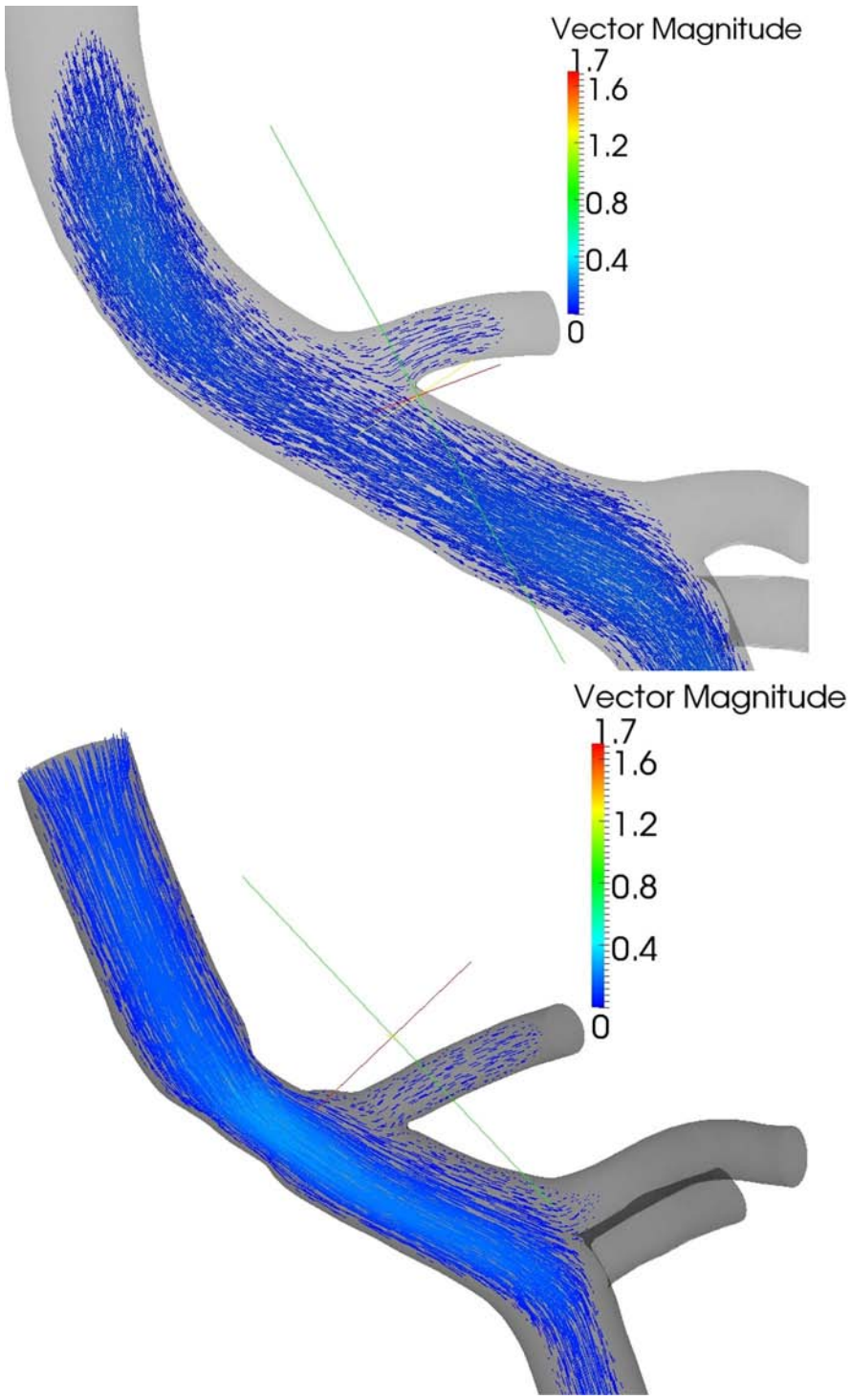

Figure 3.19 – Velocity Vectors During Diastole - Velocity vectors (m/s) from control and coarctation aortas during the diastole. Flow is unidirectional throughout the aorta in both models.

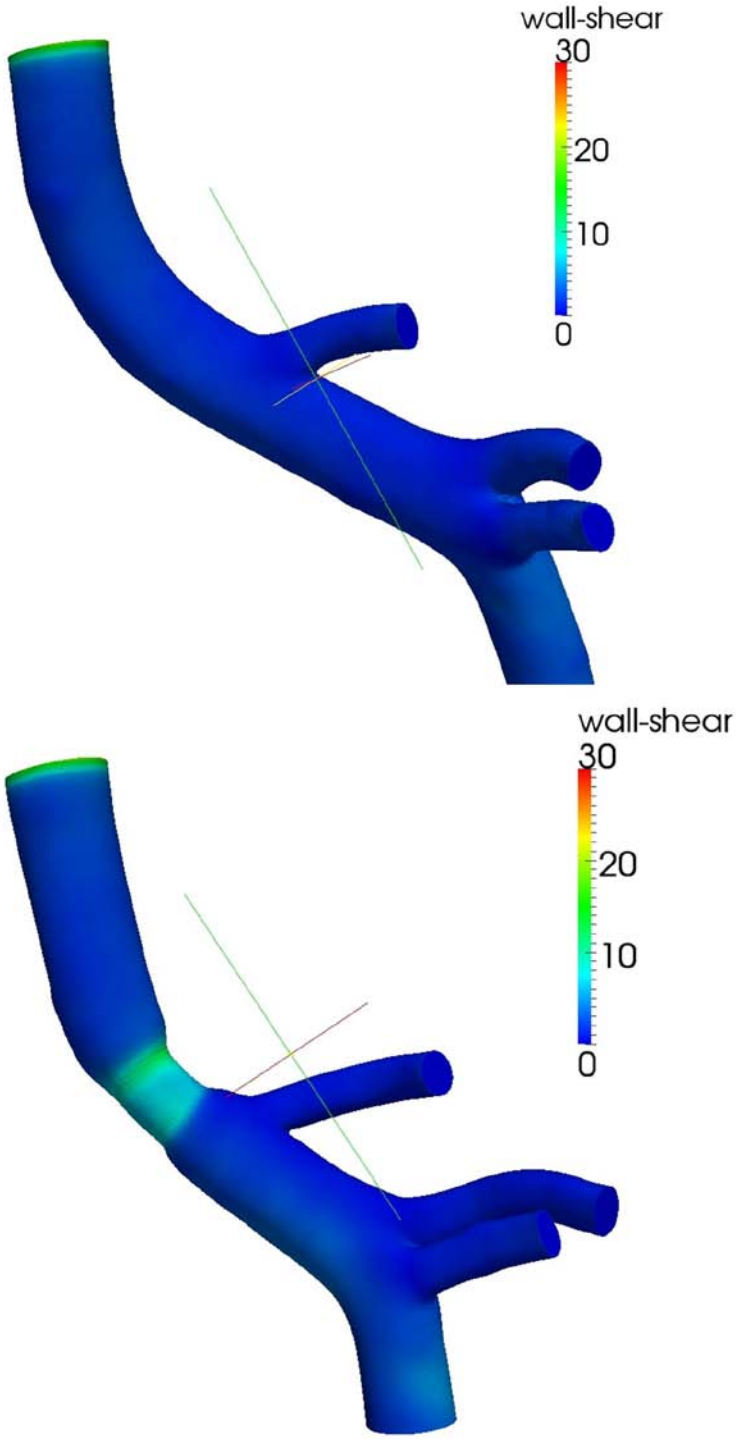

Figure 3.20 – WSS Map During Diastole - WSS (pascals) from control and coarctation aortas during diastole. WSS is relatively low in both models.

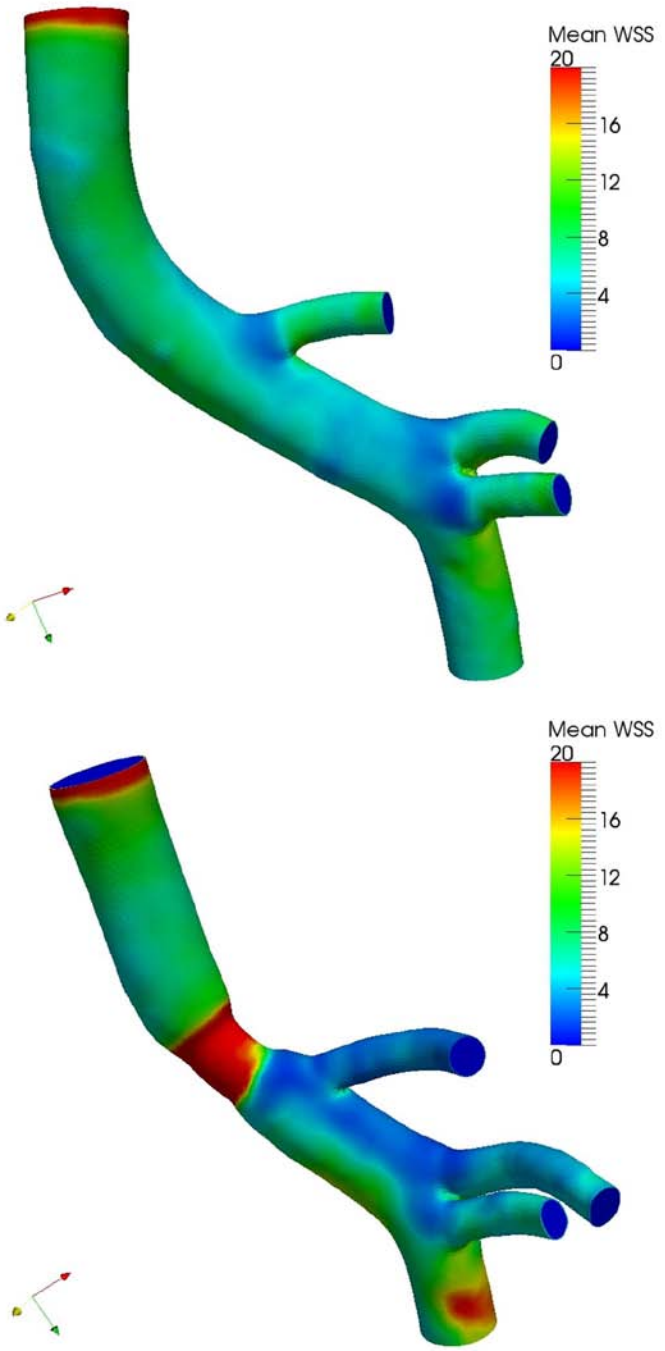

Figure 3.21 - Mean WSS Maps - Representative mean WSS (Pascals) maps. Maps were generated from CFD models of a control mouse aorta (upper image) and a coarctation mouse aortic (lower image). Mean WSS is significantly reduced downstream from the coarctation on the anterior side of the aorta.

Sensitivity Analysis

We performed a sensitivity analysis to investigate the sensitivity of flow reversal and WSS magnitude to the in silico expansion. Figure shows an aorta with no expansion factor, a 10% expansion factor, a 20% expansion factor and a 30% expansion factor. From our ex vivo inflation measurements, we determined that the 10% expansion factor (upstream diameter ~ 0.90mm) corresponds to a pressure of 30 mmHg, a 20% expansion factor (upstream diameter ~ 0.96 mm) corresponds to a pressure of 40mmHg, and a 30% expansion factor (upstream diameter ~ 1.03 mm) corresponds to a pressure of 60 mmHg. With either a 10% expansion factor or no expansion factor flow reversal was not observed in the downstream region and WSS was not significantly decreased. Using a 20% or 30% expansion factor, a region of low magnitude WSS along with flow reversal can be observed in the downstream region. The use of a 30% expansion factor correlates to a blood pressure of 60 mmHg, which is expected to be a conservative estimate since the mean physiologic blood pressure averages around 100 mmHg in the mouse [119].

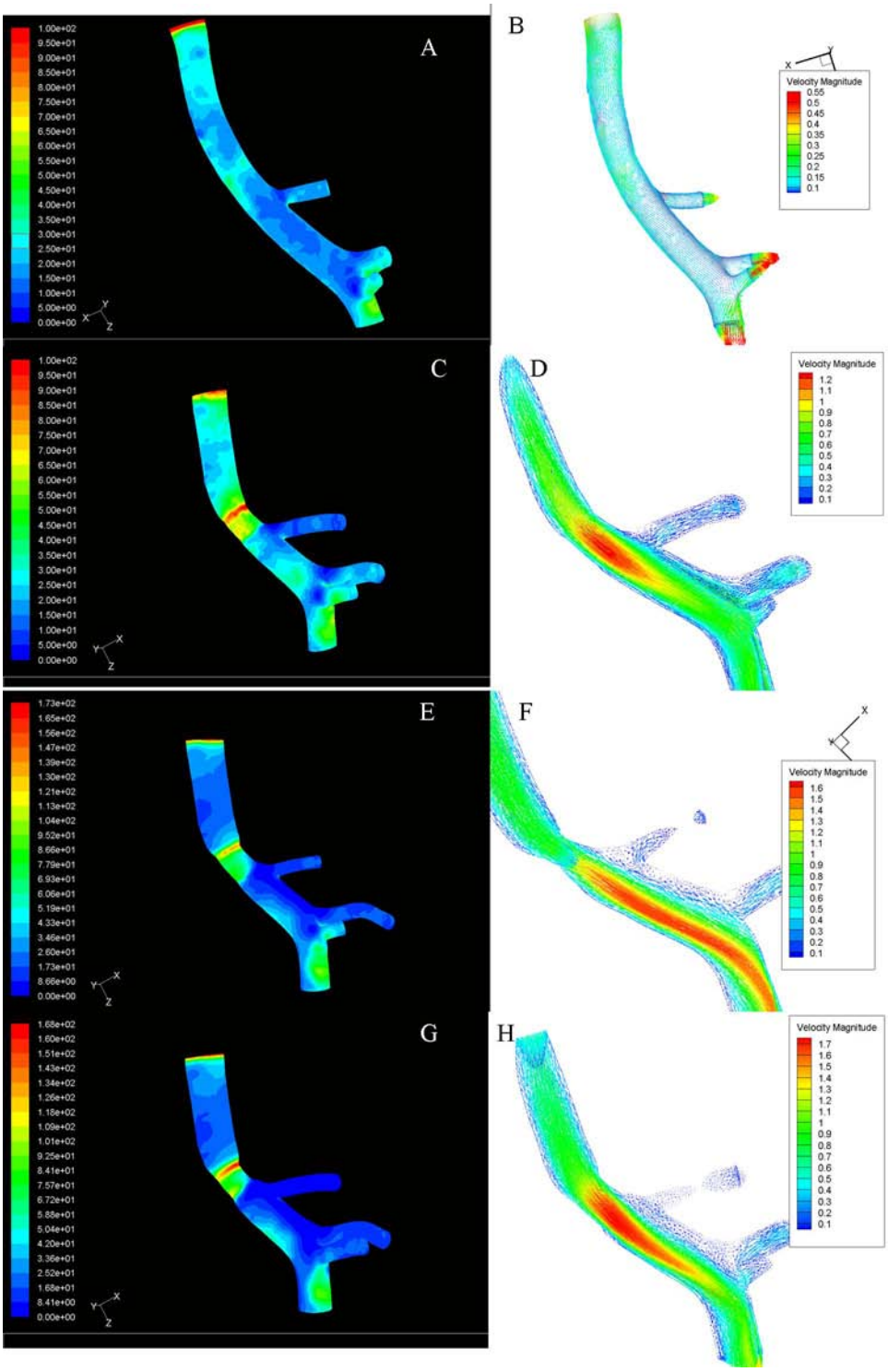

Figure 3.22 – Sensitivity Analysis of the Expansion Factor - Panels A, C, E, and F show representative WSS maps (Pascals) while panels B, D, F, and H show velocity vectors all from the downstroke of systole. Panels A and B show the aorta with no expansion factor. WSS is relatively low and flow is unidirectional. Panels C and D show an aorta after the application of a 10% expansion factor, which correlates to an *in vivo*

pressure of 30 mmHg. At a 10 % expansion factor, flow is unidirectional and WSS is starting to show lower relative levels immediately downstream. Panels E and F show an aorta that has had a 20% expansion factor applied to it, correlating to an in vivo pressure of approximately 40 mmHg. There is a large region of low magnitude WSS and flow reversal can be observed on the anterior side. The panels G and H show an aorta with a 30 % expansion factor correlating to a pressure of 60 mmHg. These panels show a large region of low magnitude WSS and flow reversal.

Discussion

Our objective for this aim was to develop a novel mouse model of acutely disturbed flow. We present two different methods to induce an aortic coarctation. The first method uses a shape memory polymer clip. Using the SMP clip we were able to create an environment of low magnitude oscillatory WSS. However, this technique produced a large kink in the aorta due to the thickness of the clip. We therefore, progressed to a model using a nitinol clip. The nitinol clip is significantly thinner than the polymer clip and did not produce the large kink observed with the SMP clip. In addition, the material properties of the clip were such that there was no significant effect of pressure changes on a physiological range on the diameter of the clip. We thoroughly characterized the hemodynamic environment associated with the coarctation induced by the nitinol clip. Using a combination of techniques, *in situ* μCT and *ex vivo* pressure inflation, we showed that we can effectively constrict the aortic diameter at the clip with minimal variability. We further showed that this constriction produced a minor stenosis with no significant pressure loss. The CFD model showed that the coarctation produced low magnitude oscillatory WSS in the distal region.

Our main *conclusion* for this aim is that the nitinol clip coarctation model uniquely creates a hemodynamic environment of low magnitude oscillatory WSS without a significant effect on blood pressure.

The initial method using the SMP clip produced a unique hemodynamic environment that created a region of low magnitude oscillatory WSS. However, we had problems with consistency of the morphology through the coarctation and the degree of stenosis. The morphology was non-uniform creating an elliptical shape with a flat

posterior side and a circular anterior side. The aorta was non-concentric and was shifted towards the anterior aspect of the body. These morphological features were the product of the thickness of the clip. The clip was 0.5 mm thick due to manufacturing limitations as a result of the resolution of the laser cutter. When the clip was placed underneath the aorta the clip pressed against the spine and shifted the coarctation away from the normal aortic pathline creating a kink in the aorta. The result of this kink was that even the control, non-constricting, clip still created the same degree of stenosis as the constricting clip. We therefore would not have been able to have an appropriate control to test the non-specific effects of the material and isolate that from any hemodynamic effects. We then investigated the use of a shape memory alloy, to see if we could improve the morphological features associated with our coarctation model.

The nitinol clip model produced a significantly improved and idealized stenosis. We used uCT and *ex vivo* pressure inflation to demonstrate the efficacy of the nitnol clip. The pressure inflation showed that we were able to induce an ideal stenosis under *ex vivo* conditions without interference from surrounding tissue. An unintended observation from this experiment was that we noticed that our fixation technique did not fix the tissue to the morphology associated with the fixation pressure. After fixation for 5 minutes at 100 mmHg the aorta remained largely compliant and did not fix to the physiologic morphology at 100 mmHg. We determined that when we removed the fixed tissue from pressure, the tissue returned to a diameter comparable to the diameter of unfixed tissue at 30 mmHg. When pressure was reapplied to the tissue, the diameter increased in a sigmoidal manner very similar to the unfixed tissue. We then fixed the tissue for an

additional 45 minutes under pressure and again ran the compliance test. Again, the fixed tissue remained compliant.

We were very surprised to find that fixation under pressure did not maintain the morphology when pressure was released. We speculate that this is likely due to the thickness of the tissue and the composition of the tissue. The vessel wall of the mouse is very thin in comparison to a human tissue. Additionally, the composition of the mouse vessel makes for a significantly more compliant vessel. There is likely much less ECM to be fixed in the mouse vessel and the ECM that is in the vessel wall is composed of more elastin in comparison to collagen. The fixative might therefore have less ECM available to cross link. This is a very interesting observation and could be a point for further research. With respect to this project, though, it is important to compensate for this lack of fixation when acquiring boundary conditions for CFD.

The μCT measurements demonstrated that the coarctation produced an idealized, concentric, stenosis. The cross sectional morphology showed that the aorta was circular upstream of the coarctation, in the middle of the coarctation, and downstream from the coarctation. There was only a slight measureable stenosis, however, this was likely due to the fixation artifact described above. Using the compliance measurements upstream from the coarctation, at the coarctation, and downstream from the coarctation we were able to determine an expansion factor. We applied these expansion factors *in silico* to the aortic diameter of the μCT reconstruction. When the expansion factor was applied to expand the tissue to an aortic diameter comparable to the diameter during diastole, about 60 mmHg, a significant stenosis can be observed. We used the *in silico* expanded aorta for the CFD modeling.

The CFD model showed results as predicted by the idealized stenosis model. Flow was unidirectional during the upstroke of systole, flow separation occurred during the downstroke of systole, and then was again unidirectional during diastole. WSS was high upstream from the coarctation, increased further in the stenotic region, then decreased significantly downstream from the coarctation. Additionally we showed that there was no significant pressure loss produced by the coarctation. These results demonstrate a model with significant advantages over current *in vivo* murine models of WSS.

The comparable murine flow models are the carotid coarctation reported by Cheng et al. and the carotid partial ligation reported by Nam et al. [25, 27]. Our model produces a unique model of low oscillatory WSS with minimal disturbances to pressure and therefore strain. The carotid coarctation model reports a region of low magnitude unidirectional WSS and a region of high magnitude oscillatory WSS [25]. Furthermore, this model does not characterize any alterations to pressure and/or strain. The partial ligation model reports low magnitude oscillatory WSS, but does not characterize pressure and/or strain. The low flow in this model likely produces a moderate change in strain which could modulate the biological response. These distinct differences in the mechanical environments of the three models and the limitations of each model provide unique *in vivo* models to investigate different biological responses.

Though this model makes improvements over current *in vivo* WSS models, there are still limitations. One limitation is that the aortic morphology near the clip can not be directly imaged *in vivo*. *In vivo* intravascular μCT is very challenging in mice, particularly when imaging the aorta, because it is difficult to obtain significant contrast

between the aorta and the spine due to the high density of the bone and low radiodensity of the vasculature [120]. MR measurements on the other hand have high errors due to temporal acceleration and irregular flow through the stenosis and downstream region as well as signal interference around the clip [121, 122].

We used a combination of μCT and *ex vivo* inflation to obtain and validate the morphologic boundary conditions. Our validation requires application of an expansion factor *in silico* to best approximate the *in vivo* morphology. The expansion was based on ex vivo pressure inflation measurements. We performed a sensitivity analysis to determine the sensitivity of our model to the in silico expansion. We determined that an expansion correlating to a blood pressure of 40 mmHg or greater (20% expansion factor) produced low magnitude oscillatory WSS while an expansion factor correlating to a blood pressure of 30 mmHg or less (10% expansion factor) did not produce low magnitude oscillatory WSS. We conclude that the sensitivity of the model to the expansion factor does not effect the observation of low magnitude oscillatory WSS even for a conservative estimate of blood pressure at 60 mmHg.

Another limitation is the assumption that the change in WSS is the primary stimulus of any response. The coarctation creates an altered strain on the nearby aortic wall. These could contribute to any response, and since we can not feasibly remove this variability from the model, we must make the assumption that the primary stimulus to the endothelium is the change in WSS. The model is also limited in molecular analysis techniques due to the small region of interest. This model is ideal for use with quantitative staining methods utilizing quantum dots since other techniques would likely require the pooling of mice [123].

We conclude that this study presents a novel model of acutely disturbed flow. The model utilizes the shape memory response of a nitinol clip to induce an aortic coarctation with high reproducibility. We showed low magnitude oscillatory WSS in the region distal to the coarctation. This model can be used in future studies without the need for further validation of the flow environment and will significantly increase the accessibility of *in vivo* experiments addressing mechanical transduction. This model provides a number of advantages over existing *in vivo* mouse models of disturbed flow including: ease of use, high reproducibility, low mortality rate, an acute time course, and a fully defined hemodynamic environment exhibiting low magnitude oscillatory WSS. With many mechanosensitive pathways already identified *in vitro*, it is important to analyze the *in vivo* contribution of these various mechanisms to atherogenesis. Taking advantage of the wealth of transgenics and knockout mice in combination with this flow model could provide significant insight into the mechanisms involved in mechanotransduction *in vivo*.

CHAPTER 4

ATHEROGENIC MARKERS IN A MURINE AORTIC COARCTATION MODEL

Identify the expression of inflammatory markers in the mouse coarctation model

Introduction

Our objective for aim 2 was to compare inflammatory marker signaling in response to both acute and chronic, low magnitude oscillatory WSS. Inflammatory cell adhesion molecules are the earliest identifiable markers associated with atherosclerosis. Expression of these molecules has been associated with disturbed flow over time courses usually ranging from 6 hours to 72 hours [107, 124]. Even within these highly controlled environments there is a notable change in cell adhesion molecule expression at various points in the time course. *In vivo* studies have correlated increased inflammatory protein expression to regions predisposed to atherosclerosis development. In murine models, this has specifically been shown in the inner curvature of the aortic arch and opposite the flow divider at the brachiocephalic branch [20]. These chronically disturbed flow regions are believed to be atherosusceptible; however, the atherosusceptible endothelial phenotype appears to have increased oxidative stress and inflammation, yet is able to reach a stable equilibrium that does not progress to lesion formation without an additional stimulus [125, 126]. This stimulus can include knocking out the apoE gene, feeding a high fat diet or treatment with Ang II among others [119, 125]. Compensatory mechanisms are suspected to be activated in these chronically disturbed flow regions resulting in a stable yet atherosuscpetible phenotype. This phenotype may well be different than the inflammatory phenotype observed *in vitro* where the time course is 72 hours or less.

Our objective for specific aim 2 was to quantitatively measure the acute and chronic response of atherogenic markers in regions of low magnitude oscillatory WSS.

We hypothesized that the acute model would produce an endothelial phenotype that experiences increased oxidative stress and inflammation. Additionally, we hypothesized that there would be distinct differences between the acute and chronic models, such that there would be an increases in NFκB and superoxide that would be present in the acute model, but not in the chronic model. We quantitatively measured expression of VCAM-1, ICAM-1, NFκB, and superoxide, using quantum dot nanoparticles with immunohistochemistry techniques as well as the novel superoxide sensitive dye, hydro-Cy3 [58]. Figure 4.1 shows the proposed pathway which we investigated. Additionally we were able to compare differences between the acute and chronic atherogenic response by analyzing the acute response downstream from the coarctation and the chronic response in the aortic arch.

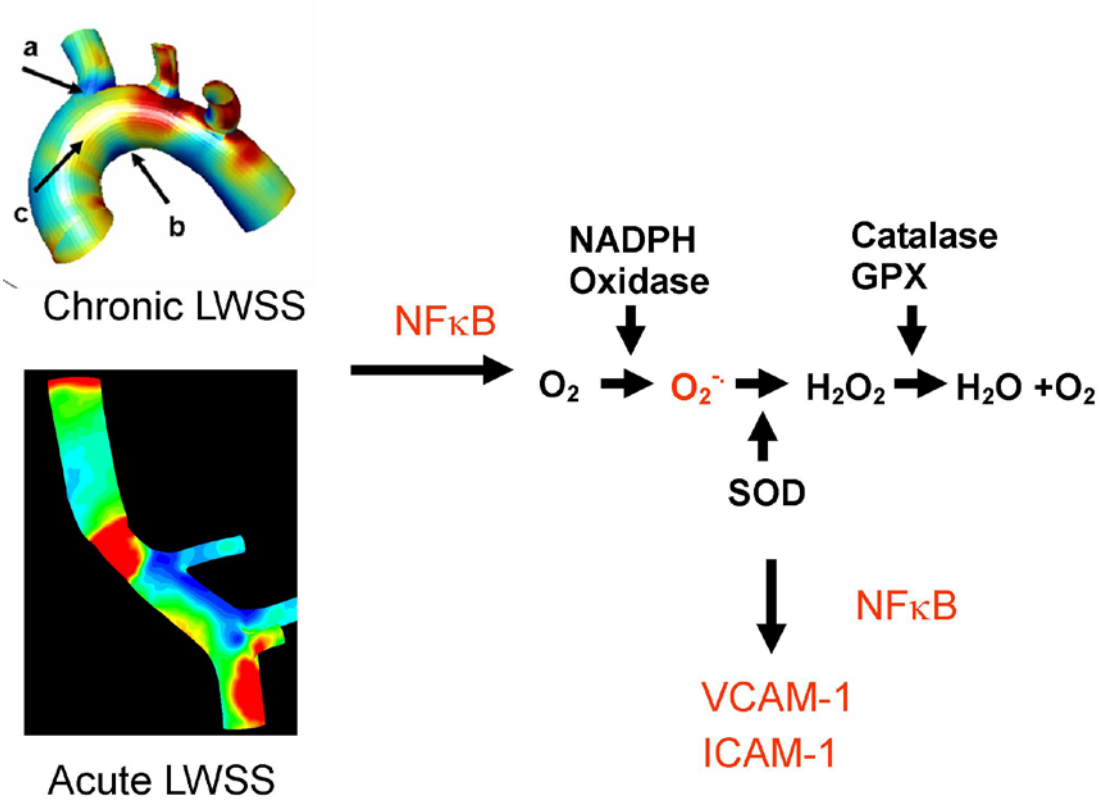

Figure 4.1 - Proposed Mechanisms of Redox Signaling – Proposed mechanisms of redox signaling in response to low magnitude oscillatory WSS. Each animal can be used as a chronic (aortic arch) and acute (aortic coarctation) model of low magnitude oscillatory WSS. We propose that these models of low magnitude oscillatory WSS will induce activation and increased expression of NFκB, superoxide generation, and increased expression of VCAM-1 and ICAM-1. We will directly measure the markers in red: NFκB, superoxide, VCAM-1, ICAM-1.

Methods

Animals

C57/BL6 and apoE$^{-/-}$ mice were purchased from Jackson Laboratories. Male mice aged 11-13 weeks were used for this study. The animals were housed and cared for according to the guidelines proposed by the National Institute of Health and approved by the Emory University Institutional Animal Care and Use Committee.

Coarctation Surgery

Coarctation surgery was performed with SMP clips and nitinol clips as described in specific aim I.

Immunohistochemistry

Tissues were prepared in accordance with previously described methods [123]. Animals were euthanized using CO_2 inhalation. The thoracic cavity was opened and the inferior vena cava was cut. A needle was placed in the left ventricle and the vasculature was perfused at a pressure of 100 mmHg with 0.9% normal saline for five minutes followed by 10% neutral buffered formalin for five minutes and then rinsed again with saline. Aortas were excised then washed in PBS before being permeabilized in 0.2% Triton X-100 (Sigma Aldrich). Aortas were then washed overnight in a humid chamber at 4 degrees C with the primary antibody. For VCAM-1 staining anti-VCAM1 antibody (BD Pharminogen) was diluted at 1:100 in blocking buffer (PBS, 2% BSA, 5% goat serum). For ICAM-1 staining anti-ICAM-1 antibody (Southern Biotech) was diluted at 1:100 in blocking buffer. For NFκB staining anti-p65 antibody (eBioscience) was diluted at 1:250 in blocking buffer. The following morning aortas were rinsed with PBS then

washed with secondary antibodies conjugated to 655 quantum dots (Invitrogen) at a dilution of 1:100 in blocking buffer (PBS, 2% BSA). Aortas were then mounted *en face* on glass slides using Vectashield with DAPI (Vector Labs).

Hydro-Cy3 Staining

Animals were euthanized using CO_2 inhalation. The thoracic cavity was opened and the inferior vena cava was cut. A needle was placed in the left ventricle and the vasculature was perfused at a pressure of 100 mmHg with 0.9% normal saline for five minutes. The perfusion was continued with a hydro-Cy3 dilution (stock solution - 2 mg hydro-Cy3 dissolved in 2 ml methanol, working solution – 500 μL stock solution in 100 ml 0.9% normal saline – final concentration 2.5 μM) for five minutes. This was followed by pressure perfusion with 10% neutral buffered formalin for five minutes and then a rinse with normal saline. Aortas were excised and washed in phosphate buffered saline (PBS). Samples were then mounted *en face* on glass slides using Vectashield with DAPI (Vector Labs).

Microscopy and Quantification of Fluorescence Intensity

Procedures were described previously [123]. *En face* images were collected using a Zeiss LSM 510 META single-photon microscope with a 63x (Plan-Neofluor, NA 1.3) oil immersion objective connected to an inverted Zeiss Axiovert 100 microscope. Separation of the emission signals was performed using the META detector with a 40 nm window for samples stained with quantum dots and a long pass filter for samples stained with the hydro-Cy3. Region of interest was determined using an external registration with a notched slide. Measurements were made prior to the *en face* mounting using the

dissecting microscope with the attached digital camera (Q Capture, Micropublisher 3.3) to determine the distance from the proximal end of the aorta to the region downstream from the clip (approximately 1mm, the length of the clip). Using the confocal microscope, the stage location was registered at to the proximal end of the aorta. The slide was switched to a notched slide and the stage was moved the distance determined by the dissecting scope measurements. The slide with the *en face* mounted aorta was then returned to the stage. Three replicate images from each region of interest were obtained. A series of images, a z-stack, was taken through the intimal layer at each location. Each series of images was then projected into a single image by using a maximum intensity projection algorithm that was built into the ZEN software. The resultant projected image gives a single image representation of the endothelium which can then be quantified. The mean fluorescence intensity was quantified from each projected image using the frequency histogram function of the ZEN examiner software.

Epiflourescence images were obtained to produce low magnification regional expression profiles. These images were obtained using an upright Zeiss microscope that excites the Qdots at 405 nm and detects their emission at 655 nm using a long pass filter. Epifluorescent images were obtained using intact aortas or *en face* mounted aortas. The intact aortas have a lower signal to noise ratio but regional features are more easily distinguished.

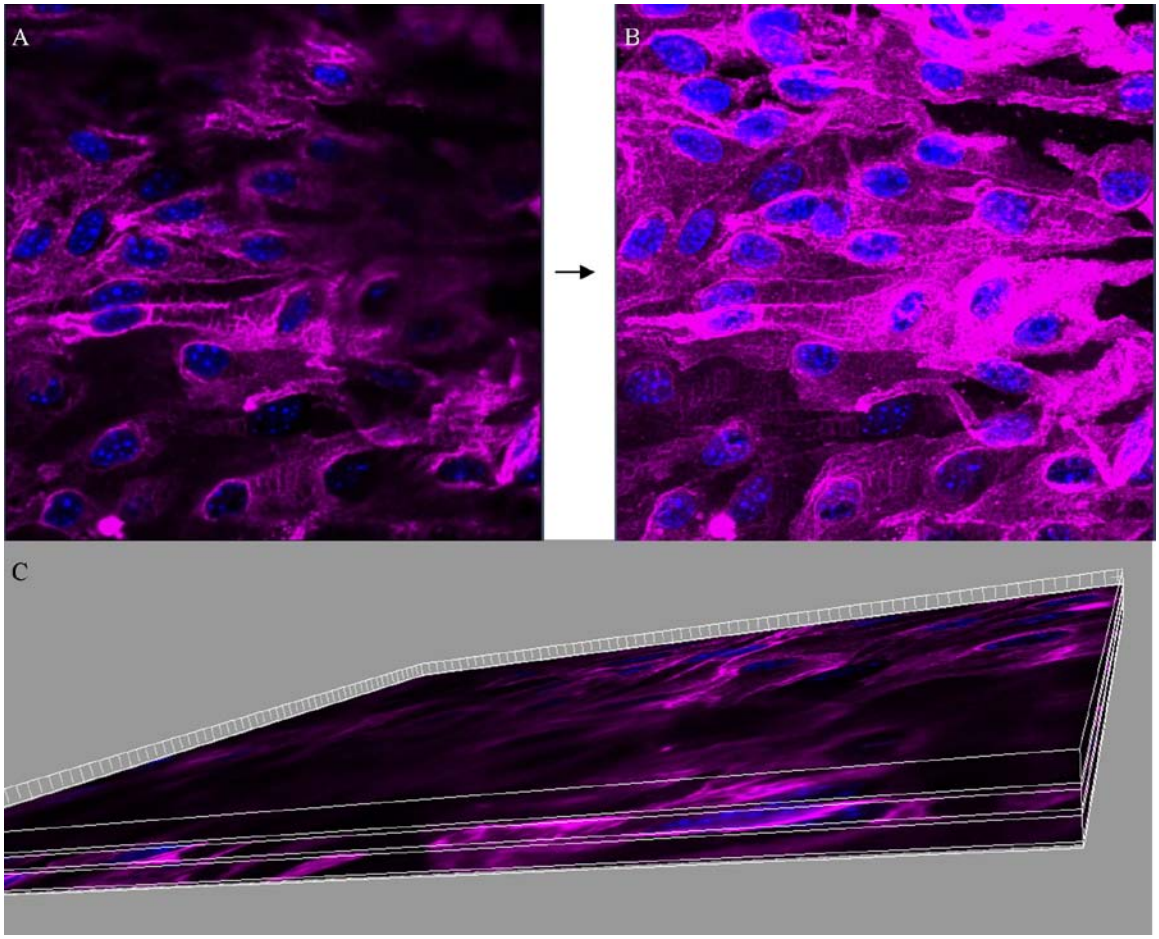

Figure 4.2 – Projection of a Confocal Z-stack – Panel A shows a single slice through the center of the intima. The slice is out of plane from much of the endothelial cells and does not give an accurate image of the mean fluorescent intensity of the quantum dot staining at this location. Panel B shows the projected image. All nuclei are in plane and the mean fluorescent intensity of the quantum dots can be accurately measured. Panel C shows an isometric view of the series of slices through the endothelium.

Oil Red O

apoE$^{-/-}$ mice on a normal chow diet were used for this portion of the study. Three experimental groups were used: control mice with no coarctation, mice with a sham, non-constricting clip, and mice with a coartation inducing clip. Mice were euthanized 2 months after the coarctation surgery and the vasculature was pressure perfused with saline followed by formalin. The aortas were excised and mounted in a black wax based dish and preserved in formalin. 0.7g oil red o was dissolved in100 ml propylene glycol

and heated to 100 deg C. The solution was then filtered through a #2 Whatman filter on top of a medium porosity fritted glass filter. Aortas were then rinsed with water to remove formalin followed by a 15 min wash with the oil red o solution. The aortas were then destained using 70% ethanol for 5 min then finally washed again with water. The aortas were then imaged using a digital camera (Q Capture, Micropublisher 3.3) attached to a dissecting microscope (Olympus SZ61). Oil Red O stain was then quantified using Image J.

Statistical Analysis

Quantitative results were analyzed with a one-way ANOVA using GraphPad Prism software (GraphPad Software, La Jolla, CA). Results are shown as mean ± SEM. A p-value of <0.05 was considered statistically significant.

Results

Aortic VCAM-1 Expression from a Shape Memory Polymer Clip Coarctation

We used an SMP clip to induce a coarctation of the aorta producing low magnitude oscillatory WSS downstream from the stenosis. VCAM-1 expression was quantitatively measured using quatum dots for *en face* immunohistochemmistry. The staining showed relatively low levels of VCAM-1 expression throughout the aorta in the control, non-coarctation, mice. VCAM-1 expression was similarly low in the upstream region of a mouse with an aortic coarctation. Downstream from the coarctation VCAM-1 expression increased significantly. Figure 4.3 shows representative confocal images from various locations in the aorta, while figure 4.4 shows regional VCAM-1 expression from epifluorescent images. There is some increase in VCAM-1 expression in the coarctation region and even just upstream from the coarctation as observed in the epifluorescent images. Though we were able to observe the expected biological response by observing VCAM-1 expression in the downstream region, aim I showed that the SMP produced variable morphology and likely an inconsistent hemodynamic environment.

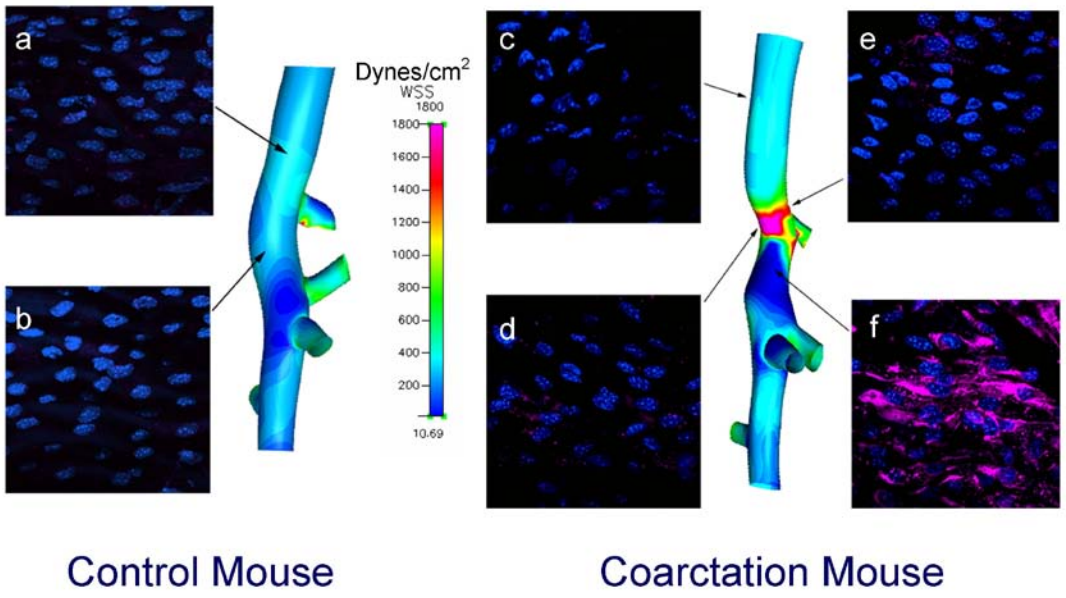

Figure 4.3 – VCAM-1 Expression Coarctation Aorta with a SMP Clip - A WSS map from a control animal is presented in the left panel. Images a and b are representative confocal images of VCAM-1 staining in the upstream (a) and downstream (b) regions from control mice. The right panel shows a WSS map from a mouse with a coarctation. Figures c, d, e, and f are representative confocal images of VCAM-1 staining from the upstream region (c), stenotic region (d and e), and the downstream region (f).

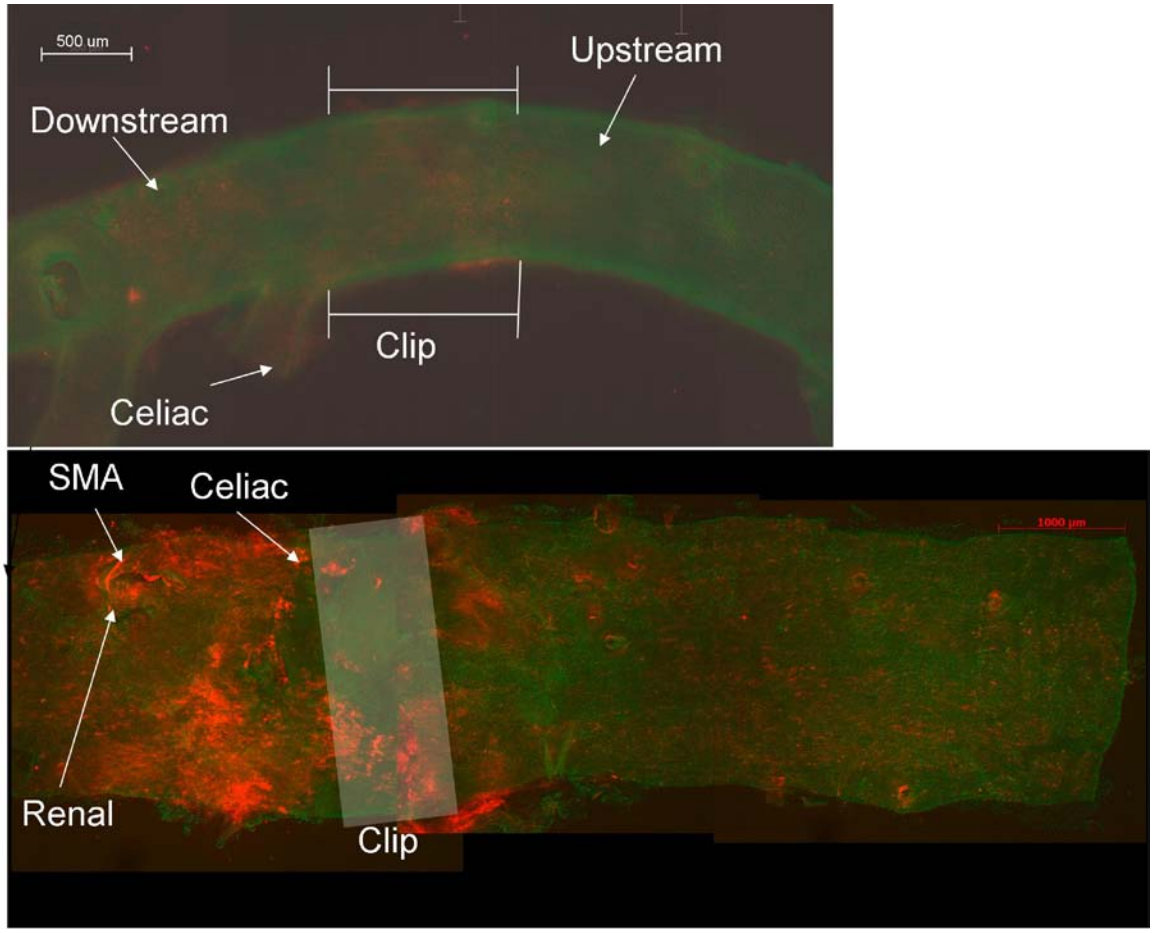

Figure 4.4 – Epifluorescence Images of VCAM-1 Expression a Coarctation Aorta with a SMP Clip - The top panel shows an intact aorta. The bottom shows an aorta which has been mounted *en face* (the signal is clearer when mounted *en face*). VCAM-1 expression is increased in the region downstream from the coarctation, though there is some increase in expression within the coarctation. The clip location is approximate.

Nitinol Clip Coarctation

Aim I showed that using a nitinol clip instead of an SMP clip to produce an aortic coarctation resulted in a more ideal and reproducible coarctation. We sought to characterize the inflammatory marker response using a nitinol induced coarctation in comparison to the SMP induced coarctation. Similar to the SMP induced coarctation, the nitinol induced coarctation showed a significant increase in expression of specific atherogenic markers in the region downstream from the coarctation. Figure 4.5 shows low VCAM-1 expression and superoxide expression in the upstream region and an increase in both markers in the downstream region.

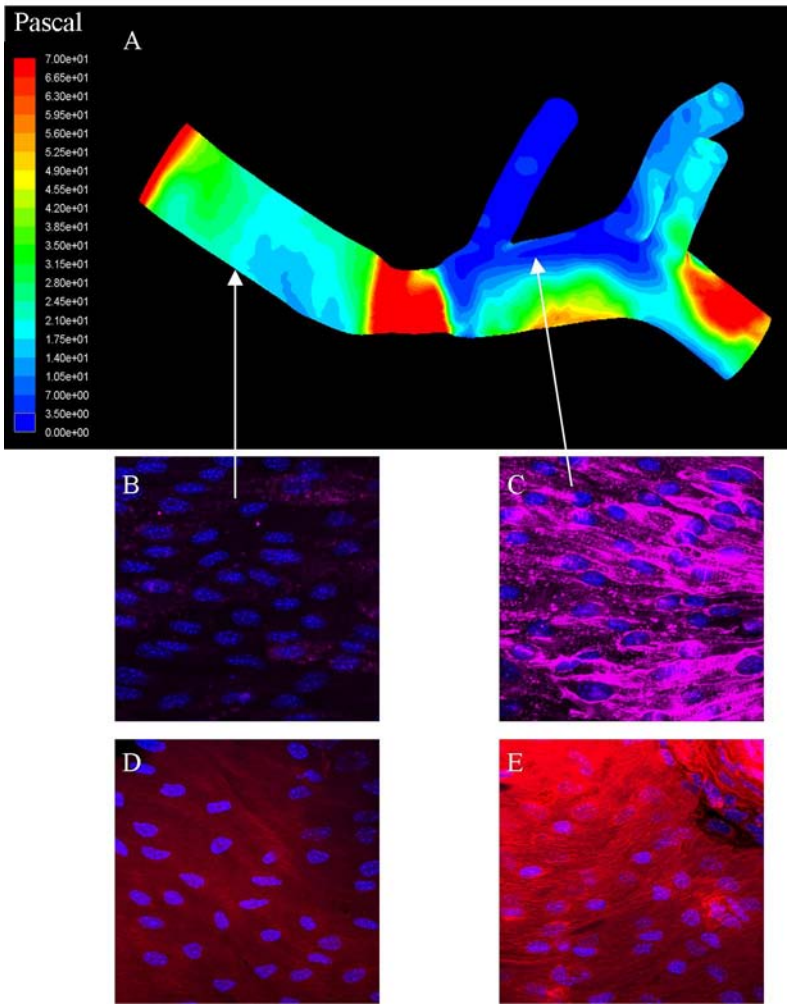

Figure 4.5 – VCAM-1 and Superoxide Expression in an Aorta with a Nitinol clip Induced Coarctation - The upper panel shows a representative WSS Map during systole from an aorta with a coartation (A). There is low magnitude oscillatory WSS in the downstream region and physiologic unidirectional WSS in the upstream region. The lower images show representative confocal images (63x) from *en face* mounted aortas stained for either VCAM-1 (B and C) or superoxide (D and E). The images on the left (B and D) were taken from the upstream region while the images on the right (C and E) were taken from the downstream region.

We compared VCAM-1 expression in the downstream region from control animals, SMP coarctation animals and nitinol coarctation animals. A significant increase in VCAM-1 expression was observed downstream from the SMP clip and the nitinol clip with a slight attenuation of the response from animals with a nitinol clip. Though both

clips produced an increase in VCAM-1 expression correlating to low magnitude oscillatory WSS, the nitinol clip produced a more desirable hemodynamic environment. Our study therefore proceeded with nitinol clips only to further investigate the molecular mechanisms involved in mechanotransduction of low magnitude oscillatory WSS.

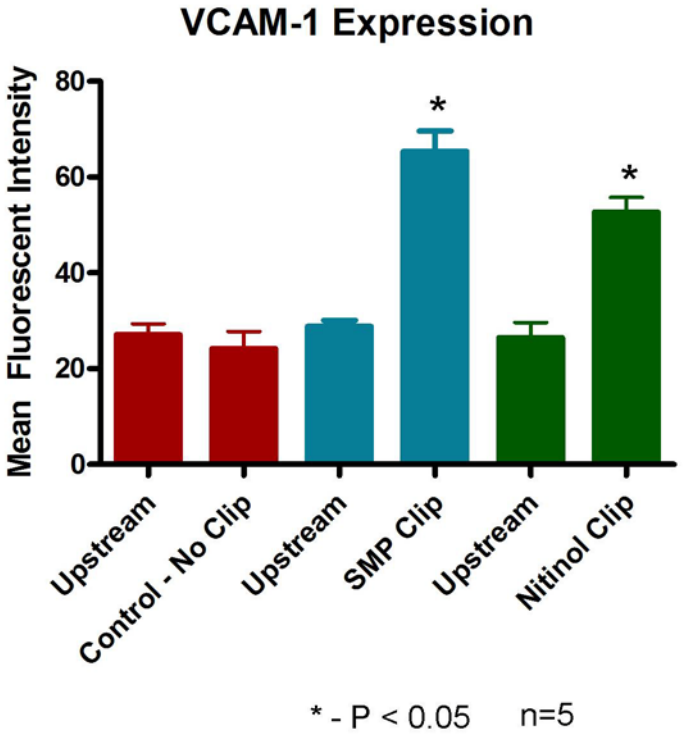

Figure 4.6 – Comparison of VCAM-1 expression using SMP clips and Nitinol Clips - VCAM-1 expression increases in the downstream region from coarctations induced by either nitinol clips or SMP clips. n=5 *=p<0.05

Cellular Adhesion Molecule Expression

Cellular adhesion molecules are inflammatory proteins that mediate the migration of leukocytes into the vessel wall and are an early marker of atherosclerosis. We used quantum dot based immunohistochemistry to quantify the expression of two cellular adhesion molecules, VCAM-1 and ICAM-1. Control non-coarcted aortas and control

aortas with a sham, non-constricting clip, showed low levels of VCAM-1 expression in the comparable downstream regions (figure 4.7). Coarctation aortas with a nitinol clip showed a significant increase in VCAM-1 expression in the disturbed flow region downstream from the coarctation. This increase in VCAM-1 expression was comparable to VCAM-1 expression in regions of chronically disturbed flow and significantly higher than regions of unidirectional laminar flow (figure 4.8).

We further investigated the correlation of ICAM-1 expression to regions of disturbed flow (figure 4.9). We found that similar to previously published results, ICAM-1 expression increased in regions of chronically disturbed flow, specifically opposite the flow divider at the brachiocephalic branch [20]. Unexpectedly, we found that ICAM-1 expression did not increase in response to acutely induced low magnitude oscillatory WSS downstream from the coarctation. This was a notable difference from the expression pattern of VCAM-1.

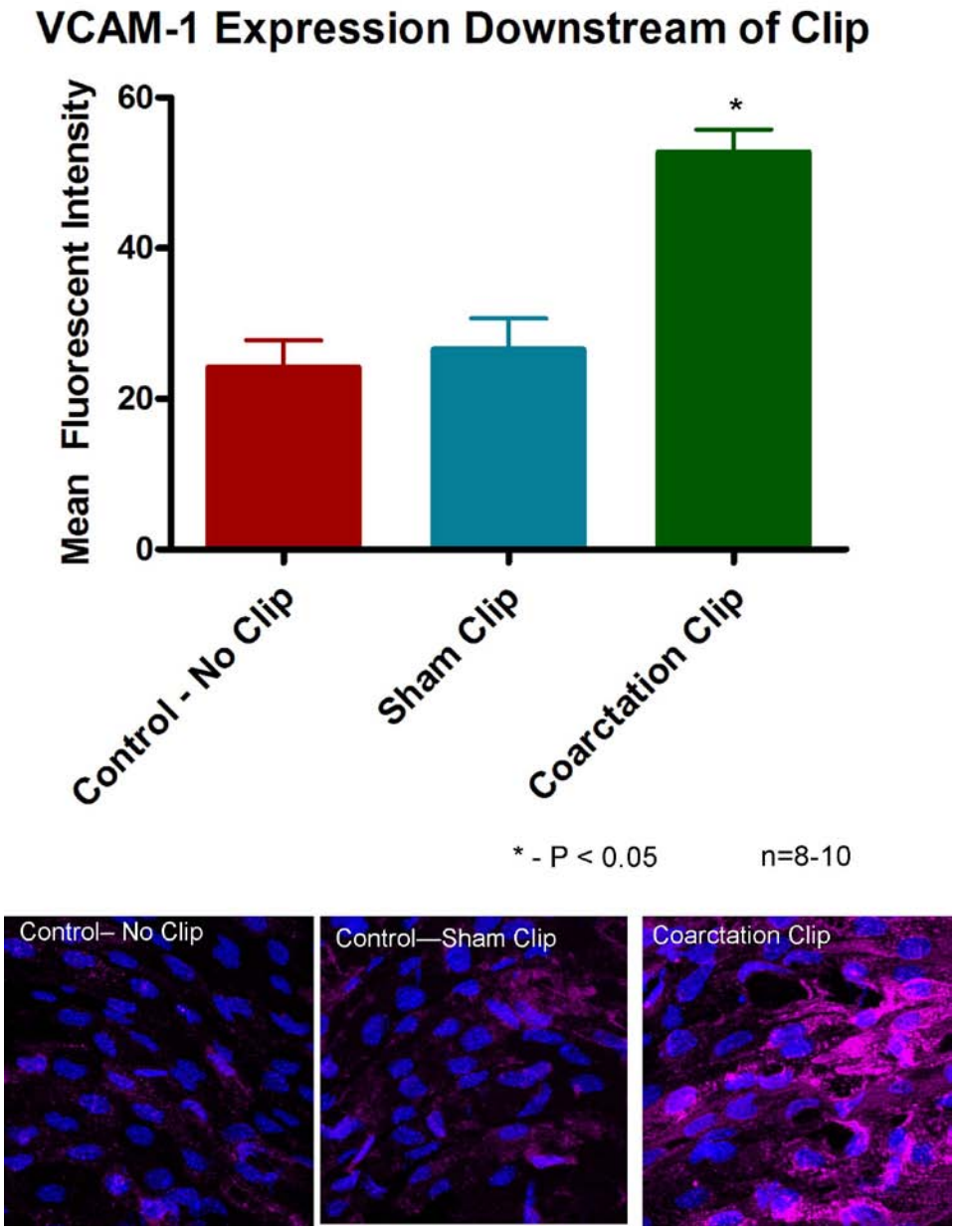

Figure 4.7 – VCAM-1 Expression in Coarctation Mice – VCAM-1 expression in control animals and animals treated with a sham, non-constricting clip, had low levels of VCAM-1 expression in the downstream region. VCAM-1 expression increased significantly in the downstream region in an animal with a coarctation inducing clip. n=8-10 *=p<0.05

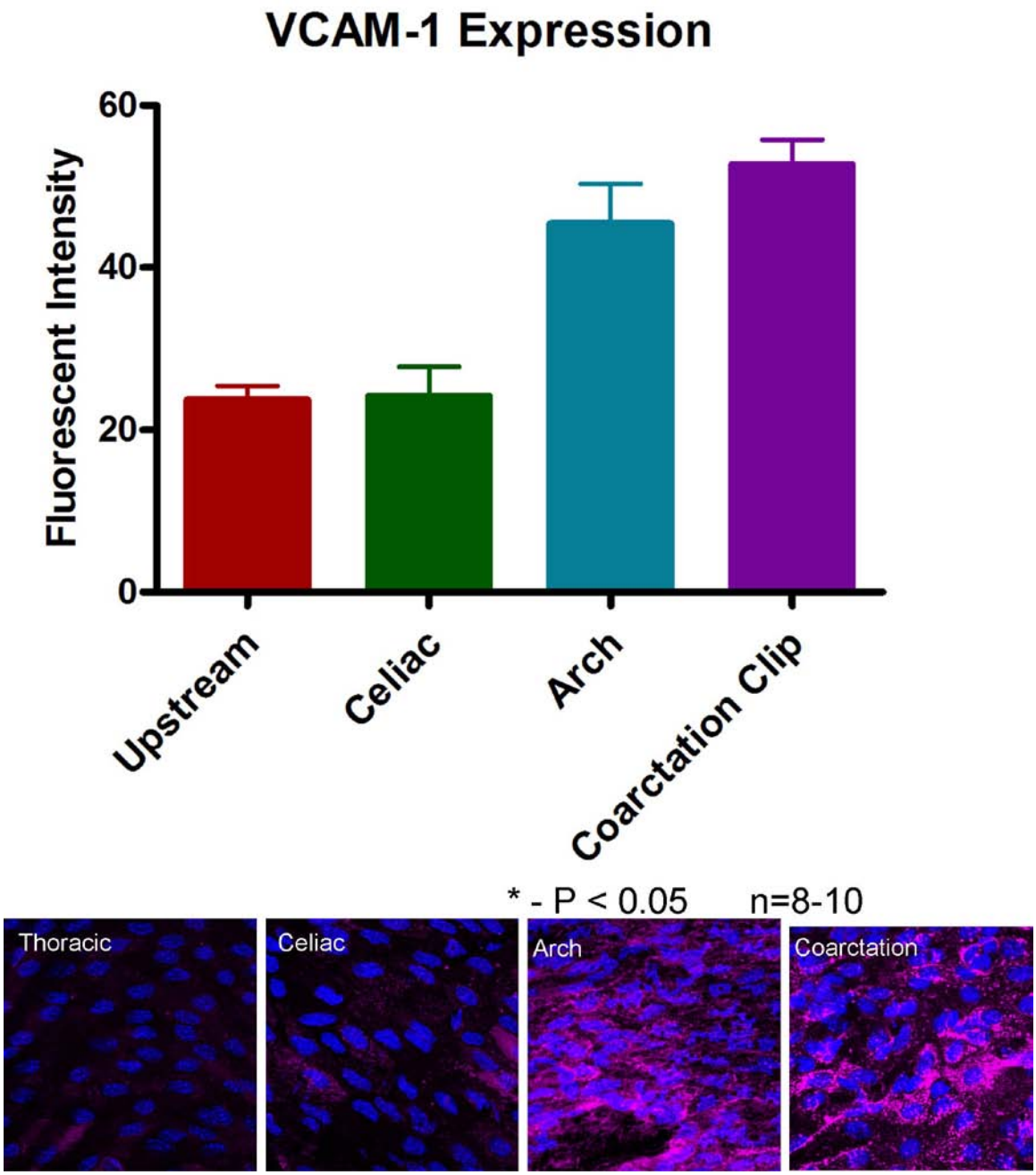

Figure 4.8 – Regional VCAM-1 Expression in Coarctation Mice - VCAM-1 expression increased in the inner curvature of the aortic arch and downstream from the nitinol clip induced coarctation. Low basal levels of VCAM-1 expression were observed in the upstream, thoracic aorta, and in the downstream, celiac region, of control mice. n=8-10 *=p<0.05

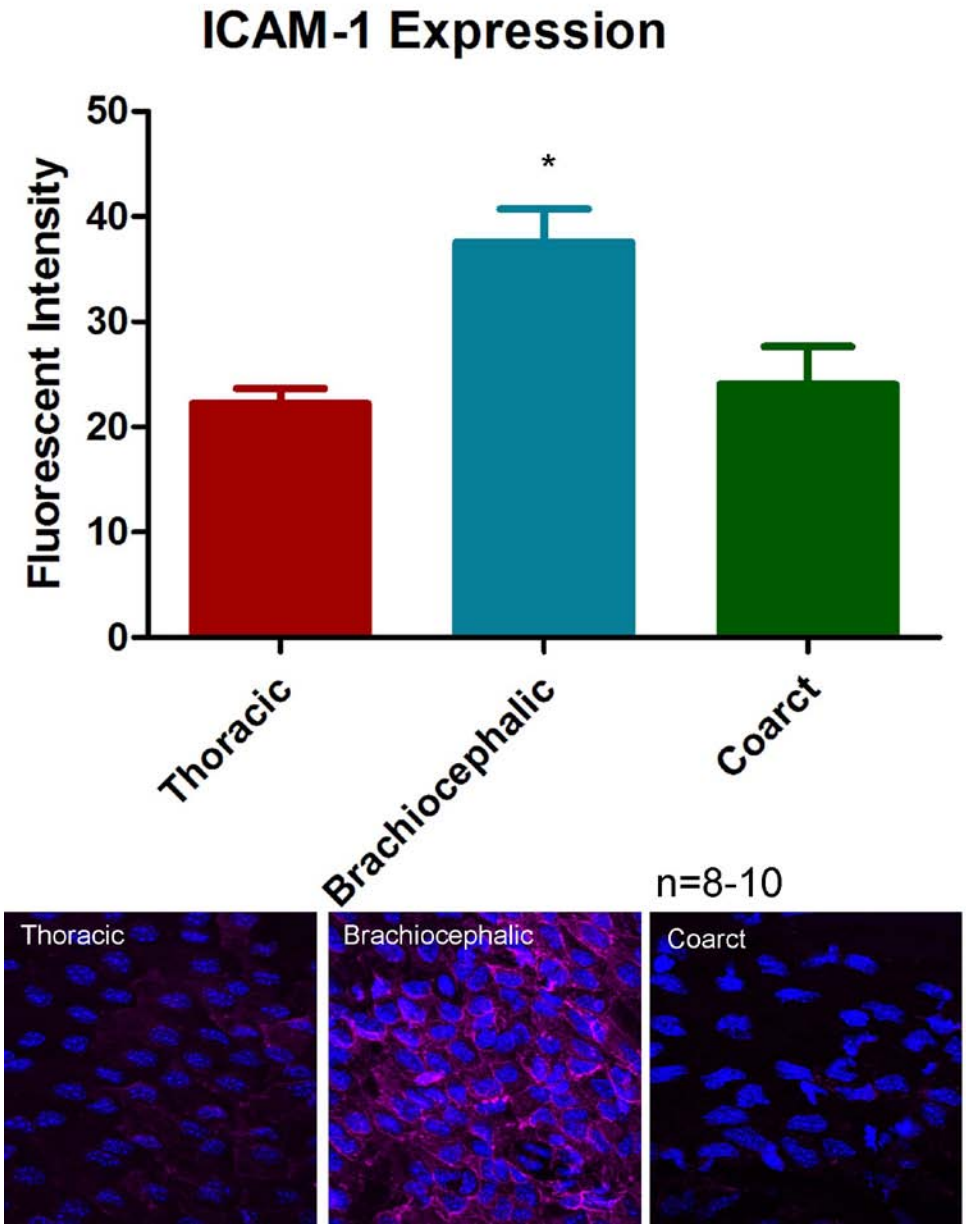

Figure 4.9 – Regional ICAM-1 Expression in Coarctation Mice – ICAM-1 expression is relatively low in the thoracic aorta and downstream from the coarctation. A significant increase in ICAM-1 expression is apparent in the brachiocephalic branch opposite the flow divider. The bottom panels show representative confocal images from each location. n=8-10 *=$p<0.05$

Transcription Factor Expression and Activation

Previous *in vitro* studies have found that the transcription factor, NFκB, increases expression and activation in response to low magnitude oscillatory WSS [98, 127]. We measured expression of the NFκB subunit, p65, in our coarctation model (figure 4.10). Low levels of expression were measured in the upstream region and in regions of chronically disturbed flow. We found that there was no significant change in p65 expression downstream from the coarctation though there was a slight trend for an increase in expression. Qualitatively, in the downstream region, there appeared to be increased localization of p65 expression in the nucleus representative of NFκB activation.

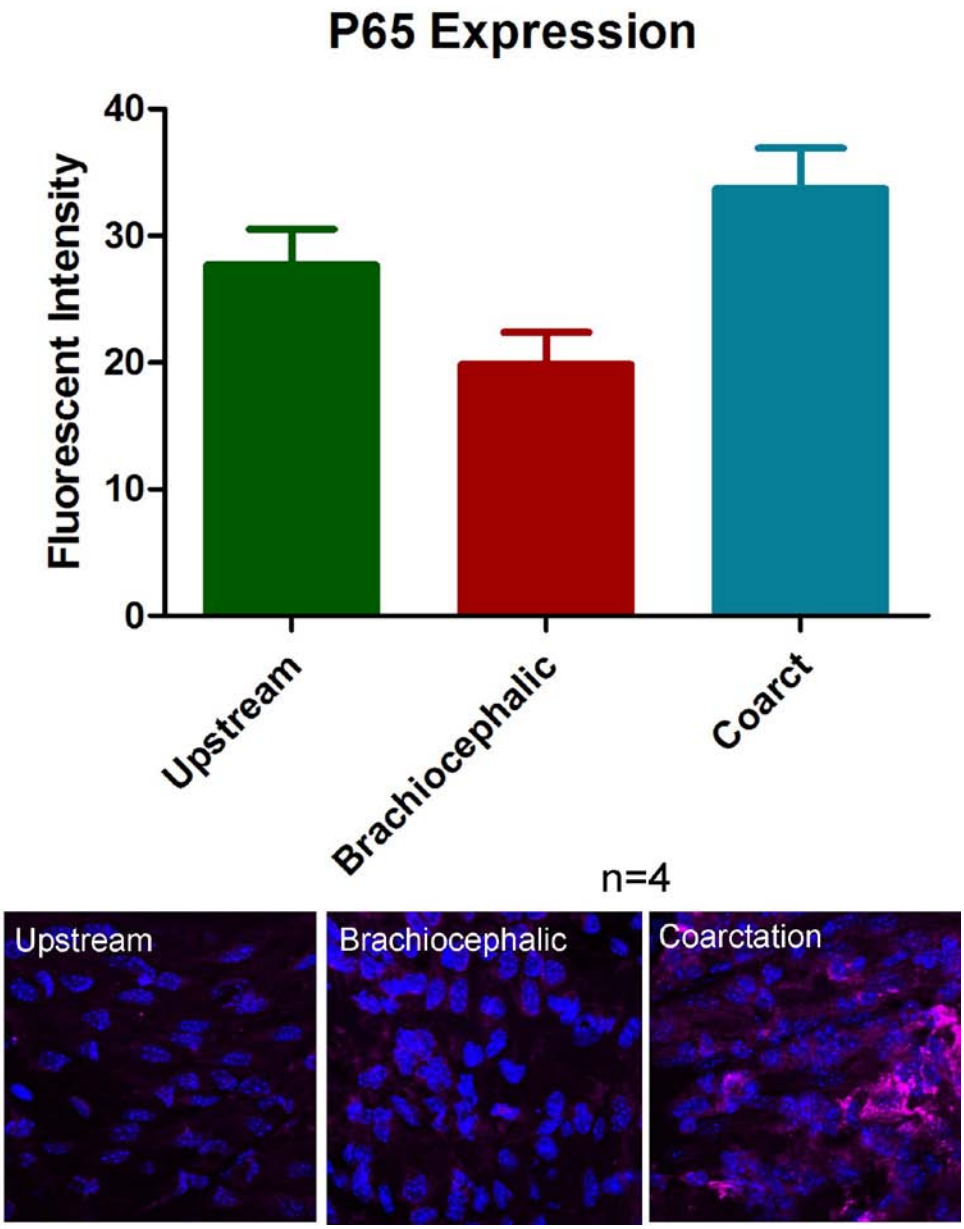

Figure 4.10 – NFκB expression in Coarctation Mice - There as no significant change in p65 expression in any of the three regions, though a slight trend for increased p65 expression in the downstream region was apparent. The lower panels show representative confocal images of p65 staining (pink) and DAPI staining (blue). We observed a trend in the downstream region for increased localization of p65 staining in the nucleus. This is representative of increased NFκB activation. n=4

Superoxide Levels in Response to Low Magnitude Oscillatory WSS

Superoxide levels were quantitatively measured in the endothelium of mice using a novel hydro-Cy3 dye (Figure 4.11). Low basal levels of superoxide were observed in the upstream region of the coarctation, corresponding to high magnitude unidirectional flow. In regions of chronically disturbed flow, such as the brachiocephalic branch, there was a trend for an increase in superoxide generation. Animals with a coarctation experience a region of low magnitude oscillatory WSS downstream from the coarctation. In this downstream region, superoxide levels were increased nearly four-fold in comparison to the control group and nearly two-fold in comparison to the chronically disturbed flow region.

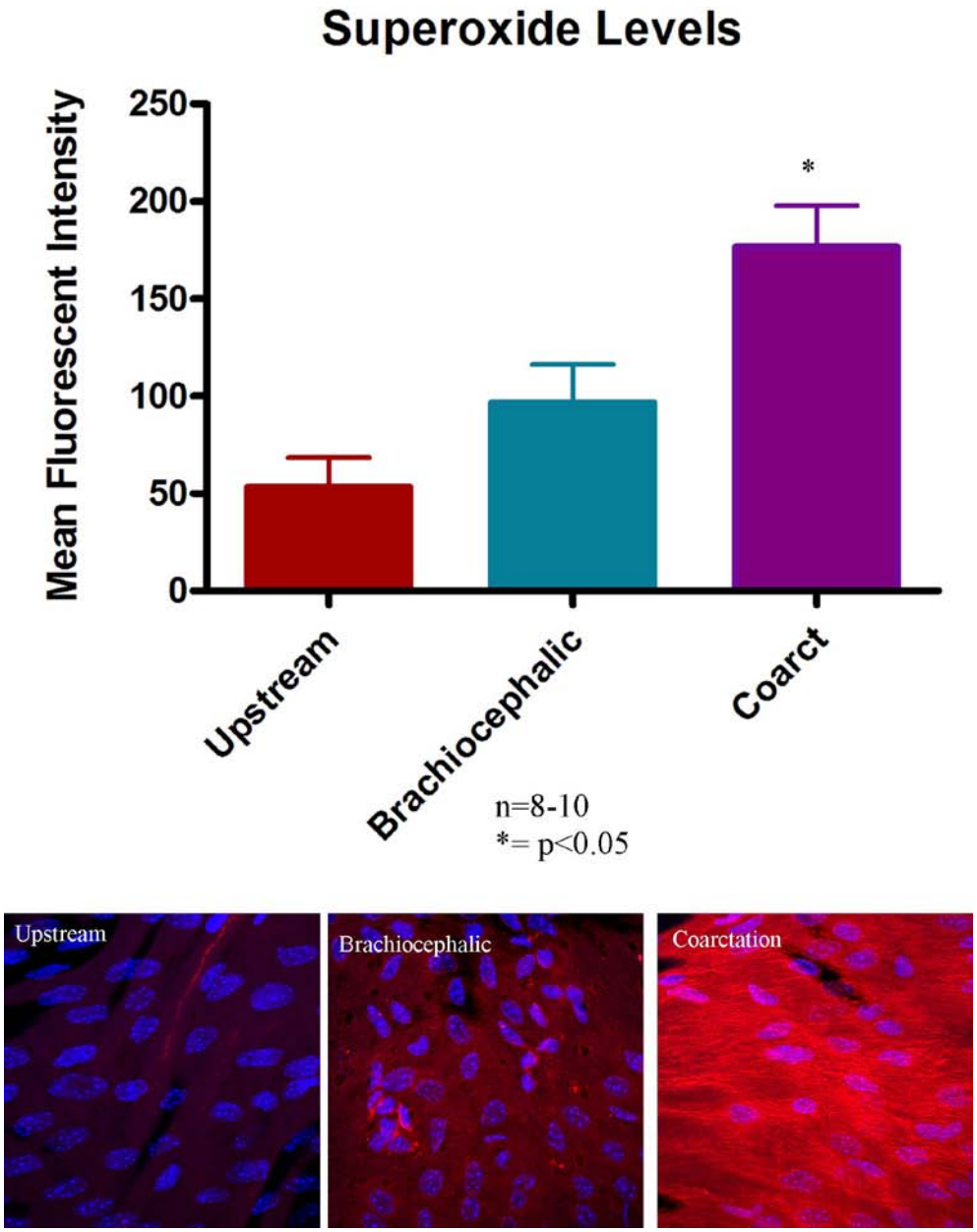

Figure 4.11 – Hydro-Cy3 Measurements of Superoxide Generation in the Endothelium – Superoxide levels are relatively low in the upstream region of the aorta. In areas of chronically disturbed flow, such as the brachiocephalic, there is a trend for an increase in superoxide generation. There is a significant increase in superoxide generation downstream from the coarctation. Representative confocal images from each region are presented.

Fatty Streak Formation

As a model of early lesion formation, we used apoE$^{-/-}$ mice on a normal chow for 2 months with no clip, with a sham (non-constricting) clip, or with coarctation inducing clip. Aortas from these mice were stained with Oil Red O then imaged to quantify fatty streak formation. Low levels of fatty streaks formed in the control animals and animals with a sham, non-constricting, clip. Fatty streak formation significantly increased in the disturbed flow region downstream from the coarctation (figure 4.12).

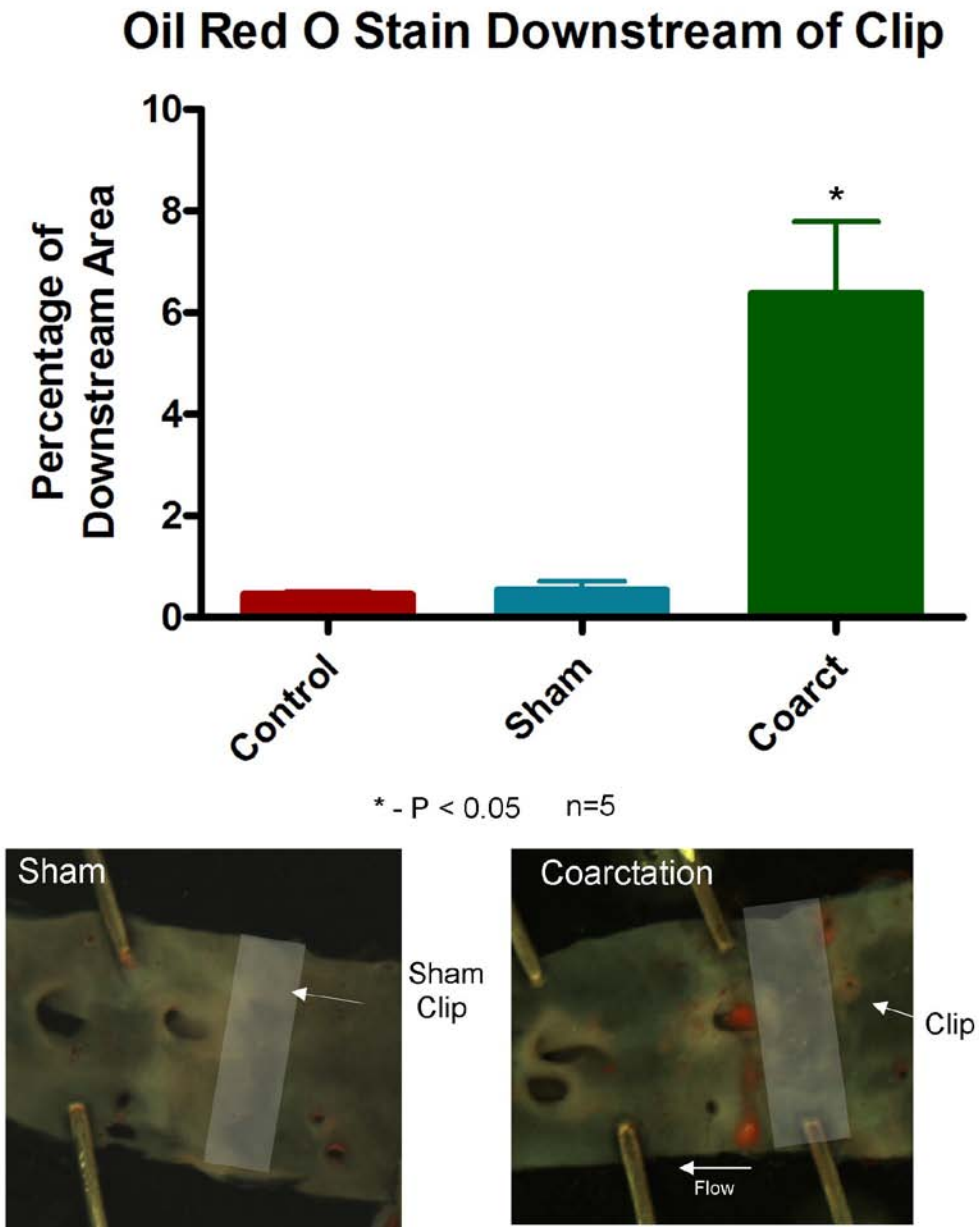

Figure 4.12 – Fatty Streak Formation Measured by Oil Red O Stain - ApoE$^{-/-}$ mice were fed a western diet for eight weeks. Mice either had no surgery, a sham clip, or a coarctation clip. Mice with a coartation clip showed a significant increase in fatty streak formation in the region downstream from the coarctation. The lower panels show representative images of aortas stained with oil red o from animals with a sham clip (lower left panel) or a coarcting clip (lower right panel). n=5 *=p<0.05

Discussion

We developed two hypotheses to address this aim. First, we hypothesized that inflammatory proteins would increase *in vivo*, in the regions of acutely induced low magnitude oscillatory WSS. Additionally, we hypothesized that there would be distinct increases in NFκB and superoxide, that would be present in the acute model, but not in the chronic model. Our objective to address these hypotheses was to characterize the acute and chronic response of atherogenic markers in regions of low magnitude oscillatory WSS. We quantitatively measured expression of VCAM-1, ICAM-1 and NFκB using quantum dot nanoparticles with immunohistochemistry techniques. We also measured superoxide levels using a novel superoxide sensitive dye, hydro-Cy3. We found that in regions of acutely induced low magnitude oscillatory WSS there was an increase in expression of VCAM-1, increased superoxide levels, and increased expression and activation of NFκB. In regions of chronically disturbed flow, superoxide levels were slightly increased, expression of cellular adhesion molecules was upregulated, and there was no change in NFκB expression or activation. Additionally, we show that fatty streaks form in the region downstream from the coarctation over a chronic time course. From these results we determined two main conclusions.

We conclude that the *in vivo* endothelial phenotype associated with acutely disturbed flow is characterized by increased production of superoxide and increased expression of select inflammatory proteins. In comparison, the phenotype associated with chronically disturbed flow is characterized by a more modest increase in superoxide and increased levels of multiple inflammatory proteins.

Utilizing the combination of the coarctation and aortic arch in the same mouse, we have established a powerful technique to analyze mechanotransdcution pathways. Much of the current literature has been obtained using *in vitro*, cell culture, techniques. There are some key limitations; however, a major difference between *in vivo* and *in vitro* settings is the time course involved. Recently, *in vitro* studies have begun extending the time course of experiments to 72 hours [124]. This allows the cells to reach what is considered a stable equilibrium. Most *in vivo* models have drastic differences compared to *in vitro* models, especially with regards to the time course. Our coarctation model is able to analyze the mechanotransduction response on an acute time course similar to the 72 hour *in vitro* studies, as well as the chronic time over the life of the mouse that is consistent with most *in vivo* models. We have shown that there are distinct phenotypic differences between the acute and chronic time course particularly when considering unstable and transiently expressed molecules.

We used a novel superoxide sensitive dye, hydro-Cy3, to look at endothelial superoxide levels in regions of acutely and chronically disturbed flow. The current gold standard for superoxide detection in tissue is with DHE staining; however, DHE requires complex purification prior to use, it has a short half life, and it is light sensitive. Superoxide is a highly unstable and short lived molecule which rapidly reacts with other cellular molecules, such as SOD and NO. It is challenging to employ this unstable dye to detect an unstable molecule, particularly when trying to image small localized regions in the endothelium. Additionally, DHE has not been used for histology of whole tissue preparations of *en face* mounted tissue. Previous attempts by our group to measure superoxide levels using DHE for *en face* histology have proved unsuccessful (data not

shown). One reason is that whole tissue preparations require the tissue, and thus the dye, to be exposed to light during mounting which is not optimal for DHE use. This results in high levels of background noise (poor signal to noise ratio) due to the increased oxidation of DHE. Therefore, we used the hydro-Cy3 dye, which is more stable than DHE, to measure regional tissue levels of endothelial superoxide.

We present a novel use of the hydro-Cy3 dye to quantitatively measure endothelial superoxide levels in regions of varying WSS. We found that superoxide levels increase significantly in regions of low magnitude oscillatory WSS as compared to regions of high unidirectional WSS, similar to published data from *in vitro* studies [59, 60, 66-68]. Previous reports, have demonstrated the specificity of the dye *in vitro* by using tempol as a means to scavenge superoxide molecule [58]. In aim III we will use pharmacological treatments to confirm the specificity of the dye.

Numerous cell culture studies have shown an increase in oxidative markers in response to low magnitude oscillatory WSS [59, 67, 68, 128]. These results better correlate to the results we report from the acute model of disturbed flow than the chronic model of disturbed flow. A clear similarity between the acute model and the *in vitro* studies is the time course: 72 hrs or less for *in vitro* studies compared to 72 hours for acute study, while the chronic time course lasts the entire life of the animal, i.e. months. In a chronic model, the unstable ROS would require continuous production and there would need to be a shift in the balance between oxidative sources and anti-oxidants. On the other hand, the acute model might initiate an immediate increase in oxidative sources with a delayed response of antioxidants. It has been suggested that feedback mechanisms might help to stabilize the system such that it will eventually equilibrate as opposed to

experiencing amplification of oxidative stress. The fact that additional stimulus is needed to progress to lesion development suggests that there may be an equilibration with feedback compensatory mechanisms. Future work to characterize the differences between the acute and chronic response and any compensatory mechanisms would be immensely valuable.

Transcription factors have been shown to be expressed *and activated in vitro* in response to low magnitude oscillatory WSS [98, 99]. Additionally, *in vivo* studies have found increased p65 expression in high prone regions near the aortic sinus and inner curvature of the arch [101, 124]. Our results, however, showed no change in NFκB expression in regions of either acutely or chronically disturbed flow. One difference between our results and the in vitro studies was that the in vitro studies were using 30 minute time course while we used 72 hours for the acute time course and a chronic time course. Transcription factors are very likely transiently expressed, and it is possible that this short time course could account for the differences observed. A difference between our results and previous *in vivo* studies is that we were looking at the brachiocephalic branch while Hajra et al. analyzed the lesion prone region of the lesser curvature of the aortic arch [101]. Though both areas are characterized by low magnitude oscillatory WSS, it is possible that there may be other differences between these locations. Both our study and Hajra et al., however, reported that there was no increase in NFκB activation in regions of chronically disturbed flow [101]. Hajra et al. reported that an additional stimulus, either LPS treatment or high fat diet, resulted in the activation and translocation of NFκB to the nucleus and this response was only observed in regions prone to lesion formation [101]. Other studies have further investigated NFκB in relation to lesion

formation showing that NFκB deficiency in the endothelium results in attenuated lesion area [129]. It is important to note however, that blocking NFκB in other cell types resulted in changes in the composition within the lesion or even increased lesion formation [130, 131]. These results implicate NFκB as an atherogenic molecule in the endothelium; however, the time course involved (30 min to 72 hours to chronic) may influence expression and activation as well as the presence of an additional atherogenic stimulus. It is clear that NFκB plays a complex role in atherosclerosis and mechanotransduction and further research is needed.

NFκB is one of the primary transcription factors leading to increased expression of cellular adhesion molecules. These adhesion molecules are significantly more stable than either transcription factors or ROS, and we therefore expected sustained expression of both VCAM-1 and ICAM-1 in a region of chronically disturbed flow. Our results confirm the previous findings that expression of both VCAM-1 and ICAM-1 is upregulated in the lesser curvature of the aortic arch where flow is chronically disturbed [20]. However, we found that VCAM-1 expression, and not ICAM-1 expression, is upregulated in response to acutely disturbed flow downstream from the coarctation. VCAM-1 has been shown to be a requisite mediator of flow dependent lesion formation in the aortic arch of VCAM-1 deficient (D4D) mice [111]. ICAM-1 knockout mice on the other hand, have been shown to have reduced lesions throughout the entire aorta but not in regions of flow mediated lesion formation [132]. These results, along with our results, implicate VCAM-1 in the early and acute stages of atherogenesis. Additionally, it suggests that VCAM-1 is a requisite mediator for flow induced lesion localization while ICAM-1 is not, at least in the time frame considered for this study.

The acute and chronic time course from the coarctation and aortic arch models respectively, likely provide insight into slightly different pathologies. The chronic time course is likely similar to the progression of atherosclerosis. Atherosclerosis is a multi-stage and multifactoral disease that develops over a long time course. The chronic envrironment in the lesser curvature of the aortic arch has been described as athero-susceptible, though it is in an equilibrated and stable state in the absence of other factors. It is plausible that feedback mechanisms might help to stabilize the system such that it eventually equilibrates as opposed to experiencing an amplification of oxidative stress. This environment is ideal for investigating the progression of lesion formation in a flow dependent manner; however, it does not accurately represent the mechanotransduction mechanisms in response to disturbed flow. Alternatively, the acute model better investigates the *in vivo* mechanotransduction of low magnitude oscillatory WSS. There may still be compensatory mechanisms and parallel pathways, that are not present in the *in vitro* setting, though these may be different then temporal compensatory mechanisms observed in the chronic model. Investigating both the acute and chronic response and, in particular, the compensatory mechnisms that lead to the equilibrated chronic state may provide new directions for treatments of atherosclerosis lesion formation.

There are inherent limitations in using a stenosis/coarctation as our model of disturbed flow, particularly with the assumption that WSS is the primary stimulant to any molecular endothelial response. Using the physical clip prevents any compliance within the stenotic region and alters the strain in the immediately adjacent region. Our area of interest is downstream from the clip in a region where the compliance has returned to the physiologic conditions as determined by our compliance measurements from aim I.

Additionally, we see minimal pressure drop across our coarctation. We therefore assume that we are not producing a large change in strain, either from a change in pressure or from the physical constraint, and therefore, we assume that WSS is the primary mechanical stimulant in our model. Another limitation inherent in the stenosis/coarctation model is that there is a change of the biotransport of both cells and molecules in the lumen of the vessel near the wall. This results in increased exposure time of these molecules and cells to the vessel wall. All regions of low magnitude oscillatory WSS will experience this biotransport phenomena and it is a product of the pathologic disturbed flow environment. We cannot feasibly isolate the mechanical stimulus from the biotransport stimulus, and we must therefore make the assumption that the primary stimulant is from the change in the mechanical force. Another limitation due to the mechanical environment is that the region of interest is very small and limits the available molecular analysis techniques. This model is ideal for use with quantitative staining methods since techniques such as PCR and western blots would be challenging to isolate cells from the region of interest and likely require pooling of a substantial number of mice. We use quantitative analysis techniques with highly stable quantum dots and a novel superoxide sensitive fluorophore.

We are additionally limited in our choice of markers that we can measure. Of particular interest to us would be hydrogen peroxide. NOX family members can directly produce hydrogen peroxide, and SOD scavenges superoxide thereby generating hydrogen peroxide. We therefore would ideally want to investigate the response of hydrogen peroxide in our model. However, we are limited due to the lack of accurate methods for the measurement of hydrogen peroxide. Hydrogen peroxide is challenging to measure *in*

vivo and more challenging to measure specifically in the endothelium. The dye DCF-DA is sometimes used to measure hydrogen peroxide levels; however, recent reviews have shown evidence for the instability of the molecule resulting in high levels of background noise and photobleaching during imaging [54].

In summary, we present a novel model in which we can compare molecular signaling in response to acutely and chronically disturbed flow. We show that there are distinct endothelial phenotypes associated with either chronically disturbed flow or acutely disturbed flow. In conditions of acutely disturbed flow we show an increase in superoxide levels, a trend for an increase in NFκB expression and activation, and an increase in VCAM-1 expression. In regions of chronically disturbed flow we show a trend for an increase in superoxide levels, no change in NFκB, and a significant increase in both VCAM-1 and ICAM-1. NFκB in particular has been implicated as a critical factor in the phenotypic difference between the acute state and the chronic state. Additionally, NFκB may play a role in the transition from an atherosusceptible, but stable, chronic state to a pathologic state progressing to lesion development. There are still many other mediators of mechanosensitive pathways that have been identified *in vitro*. These results demonstrate the importance of confirming *in vitro* findings within *in vivo* settings and in particular to consider the involved time course. This in vivo model additionally allows for the investigation of the functional contribution of various mechanosenstivite markers, which we will analyze in the third aim using genetically altered mice and pharmacologic treatments.

CHAPTER 5

REDOX SIGNALING

Investigate redox signaling mechanisms in the mouse coarctation model

Introduction

For our final aim, our objective was to use a combination of genetic models and pharmacological inhibitors, to investigate if a causal relationship exists by which ROS mediates WSS transduction to induce inflammatory protein expression. ROS have been implicated as important mediators in the flow dependent localization of atherosclerotic lesion formation. In aim II we showed that superoxide levels increase in regions of low magnitude oscillatory WSS. Similar findings have been published from *in vitro* experiments. Endothelial cells acutely exposed to low magnitude oscillatory WSS in cell culture have increased expression of Nox 1, Nox 2, and Nox 4 along with increased superoxide levels [59, 60, 66-68]. This shear dependent superoxide generation is attenuated in cells from p47 phox$^{-/-}$ mice, or by treatment with either siNox1 or 2-DOG, an inhibitor of the pentose shunt pathway for NADPH production [66-68]. Supporting the *in vitro* data, *in vivo* studies have also shown that acute induction of low magnitude oscillatory WSS in a partial carotid ligation model induces atherosclerotic lesion formation, which can be attenuated in p47 phox$^{-/-}$ mice. These data together suggest that superoxide is generated in response to low magnitude oscillatory WSS through an NADPH oxidase mechanism and in particular implicate the involvement of Nox 2. Additional studies have implicated this increase in ROS levels as a critical mechanotransduction signaling event leading to initiation of an inflammatory response and atherosclerotic lesion development.

In aim II we showed that there was increased expression of VCAM-1 in regions of low magnitude oscillatory WSS. There is evidence that antioxidant treatment can attenuate increased expression of VCAM-1, suggesting that ROS mediate VCAM-1 expression in response to low magnitude oscillatory WSS [98, 102, 108]. It is further known that VCAM-1 expression is an important mediator of lesion formation. *In vivo* flow studies have shown that VCAM-1 expression increased in regions of chronically low magnitude oscillatory WSS and that deficiency in VCAM-1 attenuated lesion formation [20, 22, 27, 111, 112]. The *in vitro* data implicate ROS as mediators of shear dependent VCAM-1 expression, while the in vivo data implicate both ROS and VCAM-1 in WSS dependent lesion formation. It is important to note that the data on the involved molecular mechanisms come primarily from *in vitro* studies and little is known about the functional relevance of this data to *in vivo* conditions. The varying cell types (MAECS, HUVECS, or BAECS), time courses (6 hours to 72 hours), flow environments, culture conditions, and environmental factors *in vitro* and *in vivo* study essential for determining the molecular mechanisms that mediate shear induced expression of cell adhesion molecules.

These data led us to hypothesize that in an *in vivo* model of low magnitude oscillatory WSS, superoxide levels would increase in an NADPH oxidase dependent manner and that this increase in superoxide would then mediate shear dependent VCAM-1 expression.

Our primary objective was to investigate whether either superoxide or hydrogen peroxide mediates the increase in VCAM-1 expression observed in regions of low magnitude oscillatory WSS. Our secondary objective for this aim was to determine the

source for WSS induced superoxide generation. We used a combination of transgenic animal models and reagent treatments to investigate the source of endothelial superoxide and show the specificity of the dye hydro-Cy3 dye. We then measured VCAM-1 expression in these same animal models to determine the contribution of ROS to shear dependent VCAM-1 expression. Figure 5.1 shows the proposed pathway and highlights the targets from our transgenic animals and pharmacological inhibitors. We used p47 phox$^{-/-}$ mice, catalase overexpressing mice, mice treated with the SOD mimetic tempol, and mice treated with the glutathione peroxidase mimetic ebselen.

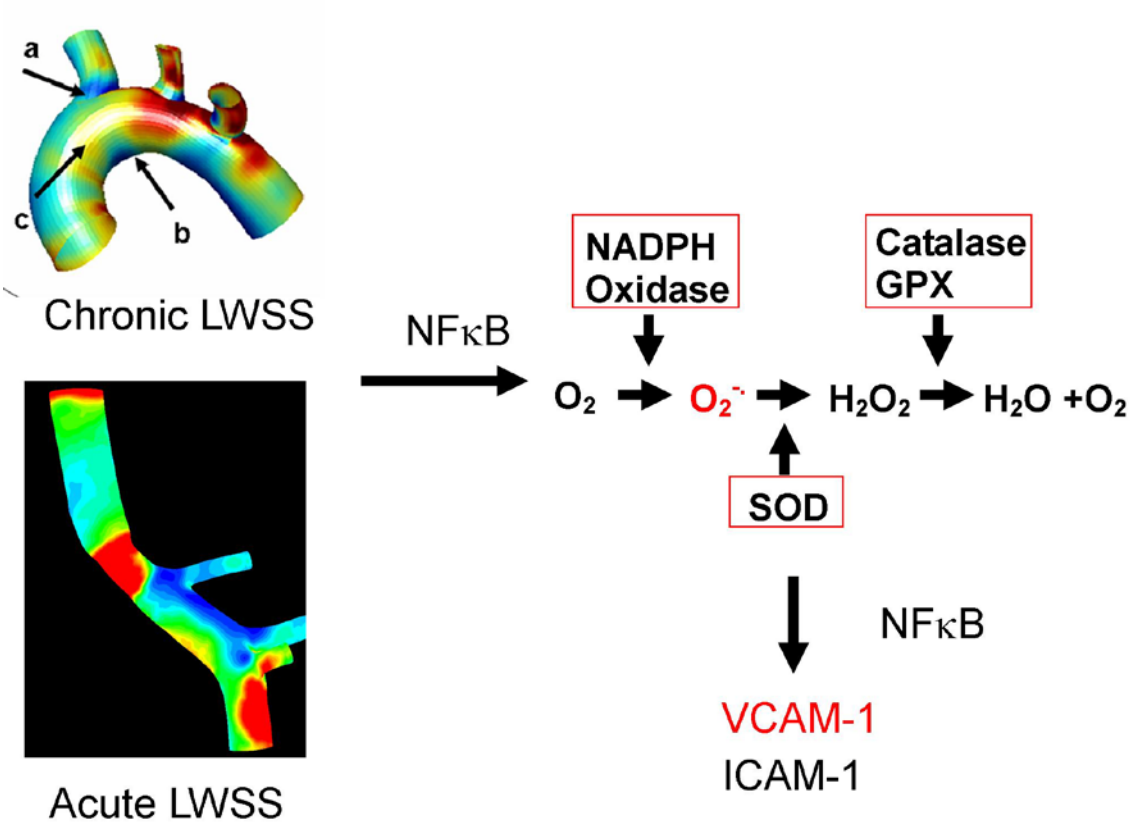

Figure 5.1 – Proposed Pathway of Shear Dependent Mechanotransduction - Transgenic animals and pharmacological inhibitors will be used to diminish ROS levels. The oxidative sources in the red boxes are the targets of the animal models. We measured superoxide levels and VCAM-1 expression in these models.

Methods

Animals

Male C57BL/6 mice were purchased from Jackson Laboratories, (Maine, USA). P47 phox$^{-/-}$ mice and the corresponding C57BL/6 controls were purchased from Taconic Farms, Inc. (New York, USA). Catalase overexpressing mice were bred in house in the Department of Animal Resources at Emory University. These mice have increased expression of human catalase in vascular tissue through the endothelial specific, Tie-2, promoter (These mice come from Dr. Harrison and Dr. Kojda) [133]. Tempol (4-Hydroxy-TEMPO, Sigma Aldrich) was administered in drinking water at a concentration of 1mM, a commonly used dose [134, 135]. In another sample group, tempol was administered intravenously by osmotic mini-pump at a rate of $40*10^{-6}$ mol/kg/min. This dose used the same concentration (100mM) previously used for osmotic mini-pumps, but using a pump with an increased pumping rate of 9.89 μL/hr [135-137]. Both modes of administration were performed with a one day pretreatment, before surgery, and then continued for the 72 hour time course (total of 4 days treatment). Ebselen (Sigma Aldrich) was administered by osmotic mini-pump subcutaneously at a rate of 10 mg/kg/day. To get ebselen into solution it was first dissolved in DMSO which was then mixed with saline to a final concentration of 50% DMSO by volume. Control mice were given mini-pumps with 50% DMSO by volume, the same DMSO concentration used for the ebselen treatment group. Male mice aged 11-13 weeks were used for this study. The animals were housed and cared for according to the guidelines approved by the Emory University Institutional Animal Care and Use Committee.

Osmotic mini-pump implantation

Mice were anesthetized using isoflurane (oxygen delivered at 0.5L/min with 3% isoflurane for induction and 1.5% isoflurane for maintenance). For tempol pumps, fur was removed using a dilapatory (Nair) and an incision was made in the neck to expose the jugular vein. A jugular catheter attached to a primed osmotic mini-pump (Alzet osmotic mini-pump 2ML1, Durect Corporation, Cupertino, CA) was inserted and tied into the jugular vein and the pump inserted subcutaneously at the back of the neck. The neck and back were sutured closed and mice were administered buprenorphine as needed. For ebselen pumps, the fur was removed from the back, a small incision was made, and the pump (Alzet osmotic mini-pump 1007D) was implanted subcutaneously.

Coarctation Surgery

Procedures were performed as described in aim I.

Hydro-Cy3 Staining

Procedures were performed as described in aim II.

***En Face* Quantum Dot Immunohistochemistry**

Procedures were performed as described in aim II.

Microscopy and Quantification of Fluorescence Intensity

Procedures were performed as described in aim II.

Electron Spin Resonance

Plasma tempol concentrations were quantified by electron spin resonance spectrometry. Mouse plasma samples were separated from whole blood by centrifugation

and then stored at -80ºC. Thawed plasma samples were taken up into a glass capillary tube and placed into a Bruker EMX electron spin resonance spectrometer. Tempol produces a characteristic 3-peak spectra and the concentration of tempol is relative to peak intensity. Tempol concentration was quantified by measuring the intensity of the first peak. A standard curve was produced by measuring the intensity of the peak from standard tempol concentrations. Intensity measurements were then obtained for plasma samples and the standard curve was used to accurately quantify the concentration of tempol in the plasma sample. [138]

Statistics

Quantitative results were analyzed with a one-way ANOVA using GraphPad Prism software (GraphPad Software, La Jolla, CA). Results are shown as mean ± SEM. A p-value of <0.05 was considered statistically significant.

Results

Specificity of Hydro-Cy3

Specificity and background noise have been limiting factors in previous attempts to measure superoxide in the endothelium. We administered tempol, an SOD mimetic that scavenges superoxide, to demonstrate the specificity of the hydrocyanine dye. We used ESR to determine the plasma levels of tempol after administration in the drinking water. Tempol administration in drinking water (1mM) resulted in a mean plasma tempol concentration of 46.9 ± 22.6 nM (figure 5.2). Superoxide levels in coarctation mice treated with tempol by drinking water were the same in the upstream and downstream regions, as compared to the respective regions in control mice. In a separate group of mice, tempol was administered intravenously by osmotic mini-pump ($40*10^{-6}$ mol/kg/min). This dose produced a mean tempol plasma concentration of 383.1 ± 45.3 μM, significantly higher than the plasma concentration after drinking water administration. Superoxide levels in coarctation mice in the mini-pump group were significantly attenuated in comparison to the respective regions in control mice; levels in the upstream region were reduced by 79%, levels in the downstream region were reduced by 63% and levels in the brachiocephalic branch opposite the flow divider were reduced by 70% (figure 5.3 & figure 5.4). Downstream superoxide levels after treatment of tempol by mini-pump were comparable to the upstream superoxide levels in the control animals.

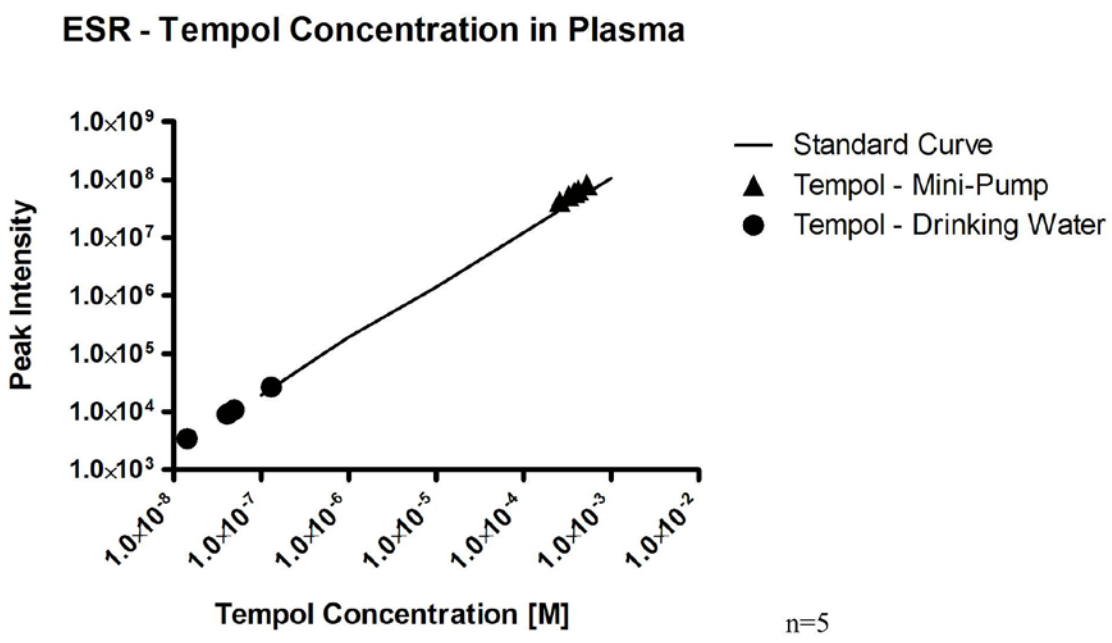

Figure 5.2 – ESR Measurements of Plasma Concentrations of Tempol - Tempol administration through drinking water (1mM) produced plasma tempol concentrations that were significantly lower than the plasma concentrations when tempol was administered by osmotic mini-pump ($40*10^{-6}$ mol/kg/min). n=5

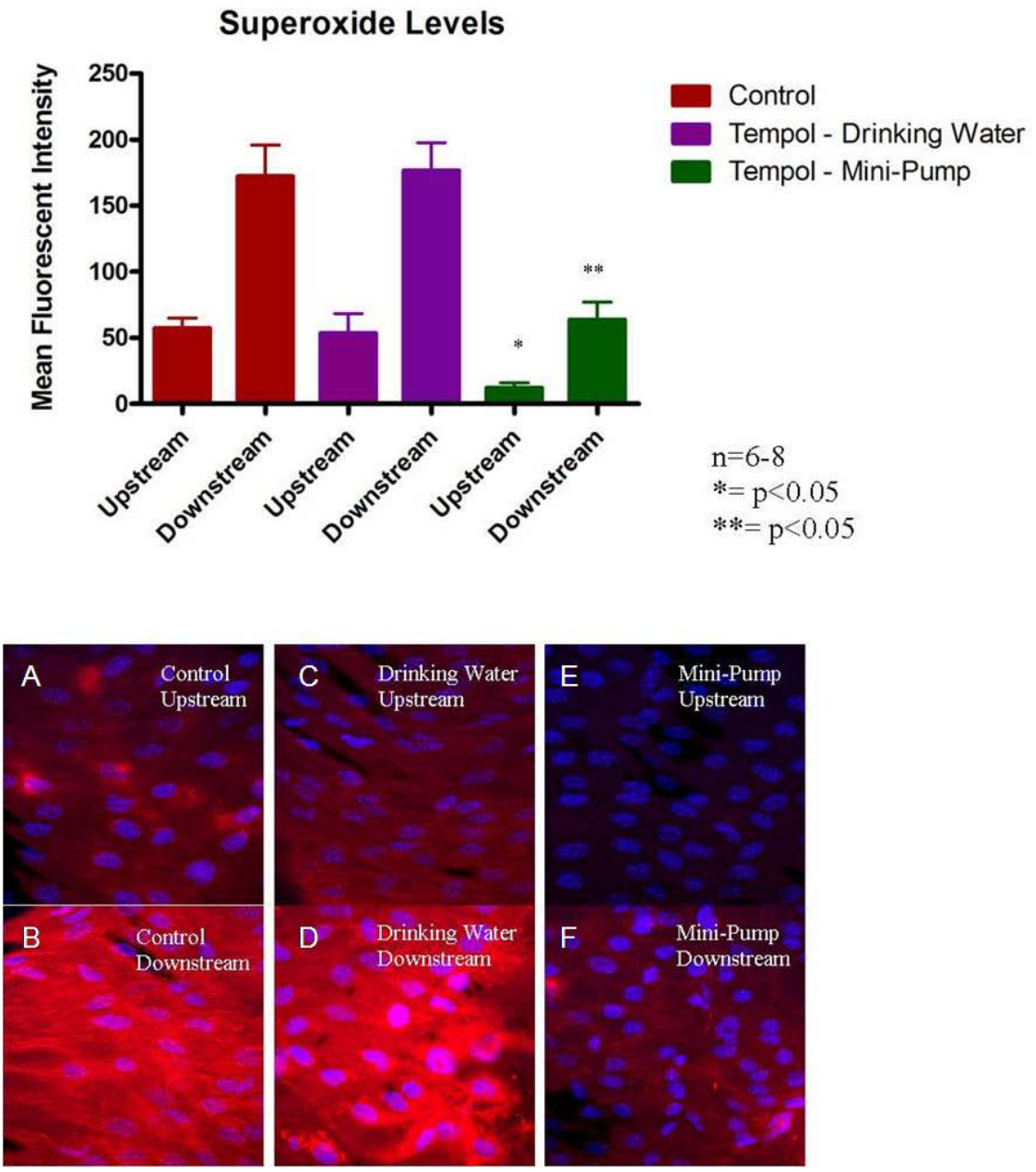

Figure 5.3 – Superoxide Levels in Tempol Treated Mice - Tempol treatment administered through the drinking water produced no change in superoxide levels in either the upstream or downstream region when compared to the control. Tempol treatment by osmotic mini-pump significantly attenuated the superoxide levels in the upstream and downstream regions in comparison to the control. Representative confocal images from *en face* mounted aortas are presented on the bottom of the figure: A,C and E are from the upstream region, B, D, F are from the downstream region from a coarctation aorta, A and B are from control mice, C and D.are from mice treated with tempol administered by drinking water, E and F are from mice treated with tempol administered by mini-pump. n=6-8, *=p<0.05 comparing upstream regions of the three group, **=p<0.05 comparing downstream regions of the three groups.

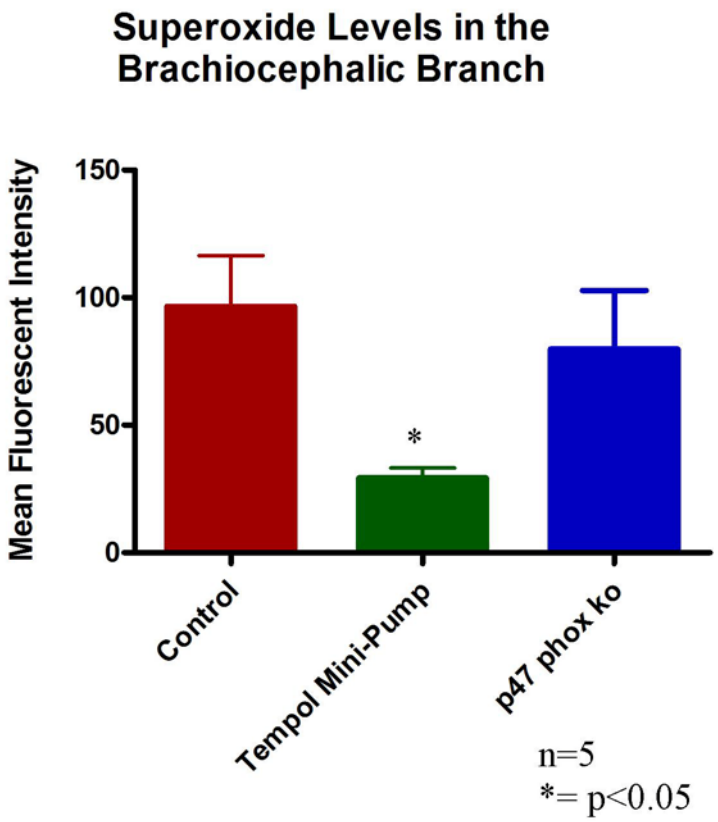

Figure 5.4 – Superoxide Levels in Regions of Chronically Disturbed Flow in Tempol Treated Mice and p47 Phox-/- Mice - Superoxide levels were relatively high in the region of chronically disturbed flow in both control and p47 phox$^{-/-}$ mice. Superoxide levels were significantly decreased in the same region in mice treated with tempol by osmotic mini pump. n=5, *=p<0.05

Superoxide as a Shear Sensitive Signaling Molecule

Tempol treated mice (drinking water and mini-osmotic pump) were used with our coarctation model to investigate the role of superoxide as a mediator of VCAM-1 expression in response to changes in WSS. In control mice with no tempol treatment, VCAM-1 expression was relatively low in the upstream region, where cells were exposed to high magnitude unidirectional WSS (figure 5.5). VCAM-1 expression significantly increased in the downstream region that was acutely exposed to low magnitude

oscillatory WSS. Mice treated with tempol administered through drinking water showed the same VCAM-1 expression in both the upstream and downstream regions as compared to the respective regions in the control, non-tempol treated, mice. Similarly, mice treated with tempol administered intravenously by mini-pump, showed no significant change in VCAM-1 expression in either the upstream or downstream region as compared to control, non-tempol treated, mice. The tempol dose achieved by intravenous infusion was enough to attenuate the endothelial superoxide levels, but had no effect on vascular VCAM-1 expression in the downstream region. There was a trend for a decrease in VCAM-1 expression in the brachiocephalic branch opposite the flow divider in mice treated with tempol by osmotic mini-pump, though this did not reach significance.

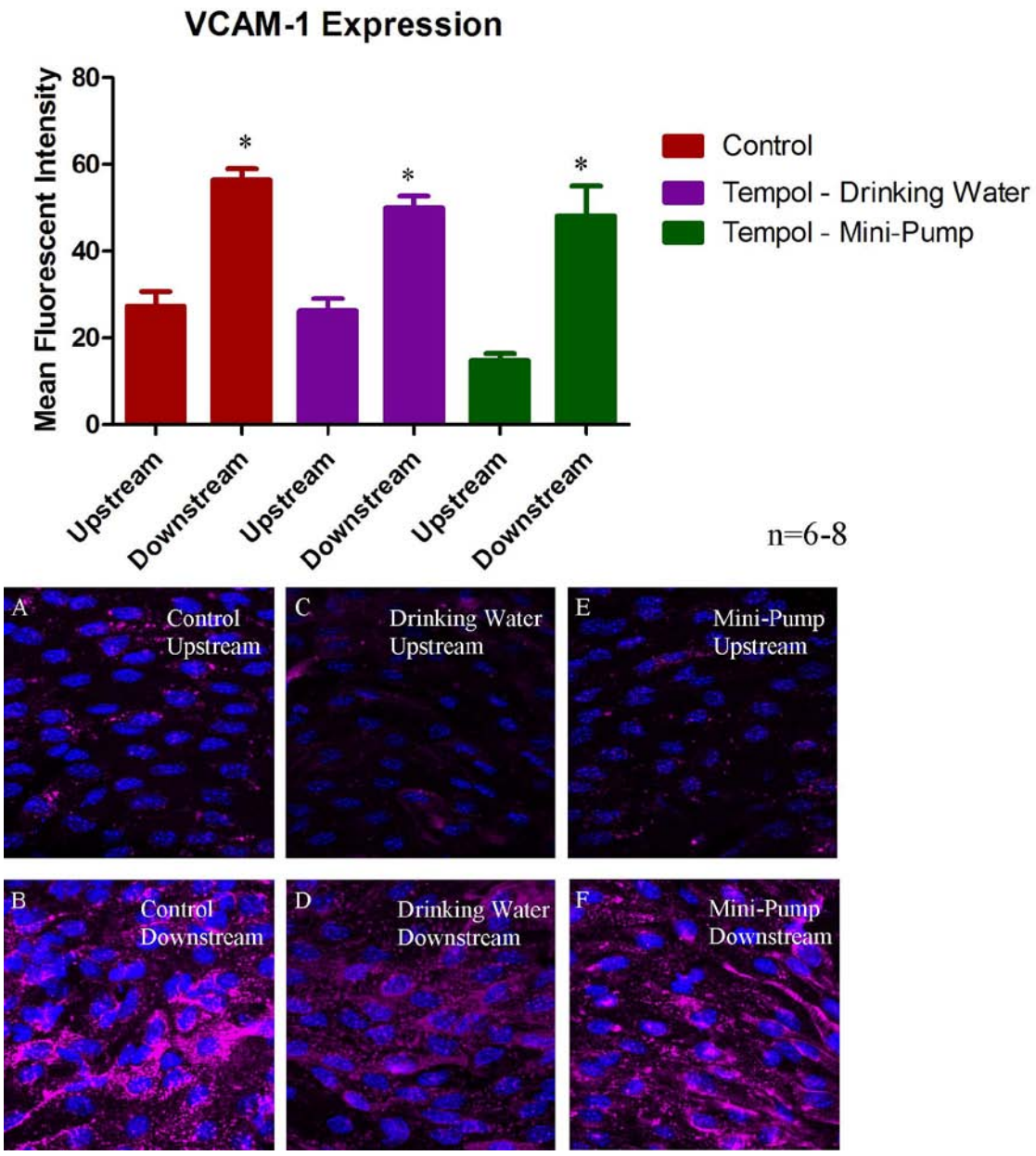

Figure 5.5 – VCAM-1 Expression in Mice Treated with Tempol - Tempol treatment, regardless of mode of administration, had no effect on VCAM-1 expression in either the upstream region or the downstream region when compared to the control. Representative confocal images from *en face* mounted aortas stained for VCAM-1 are presented. A,C, and E are from the upstream region, B, D, F are from the downstream region from a coarctation aorta, A and B are from control mice, C and D.are from mice treated with tempol administered by drinking water, E and F are from mice treated with tempol administered by mini-pump. n=6-8, *=$p<0.05$ comparing upstream region to downstream region.

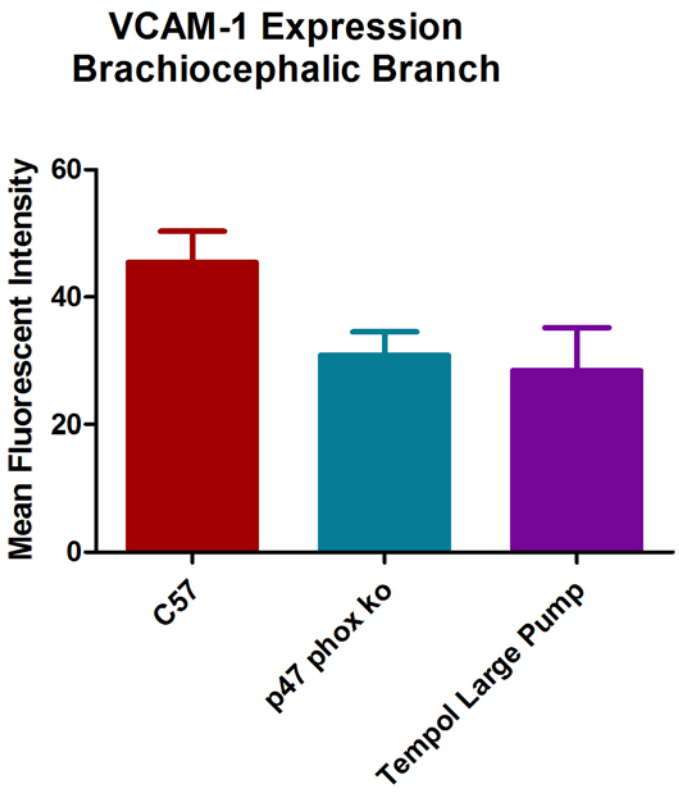

Figure 5.6 – VCAM-1 Expression in Regions of Chronically Disturbed Flow in Tempol Treated Mice and p47 phox-/- Mice - VCAM-1 expression was relatively high in the control mice. There was a trend for attenuated VCAM-1 expression in p47 phox$^{-/-}$ mice and mice treated with tempol by mini-pump, though neither reached significance. n=3 for the p47 phox$^{-/-}$; n=5 for the c57 group; n=5 for the tempol - mini-pump group

Contribution of NADPH Oxidase

The coarctation model was used with p47 phox$^{-/-}$ mice to investigate the contribution of NADPH oxidase to shear-dependent endothelial expression of both superoxide and VCAM-1. There was no significant difference in superoxide levels in the upstream region between the p47 phox$^{-/-}$ mice and the control mice (figure 5.7). The superoxide levels increased significantly in the downstream region in both groups of mice, with a trend for an attenuated signal in the p47 phox$^{-/-}$ mice, which did not reach statistical significance. Similarly, superoxide levels in a region of chronically disturbed flow in p47 phox$^{-/-}$ mice showed no difference between a comparable region in control mice.

VCAM-1 expression followed a similar pattern to that of superoxide. Superoxide expression upstream was comparable between control and p47 phox$^{-/-}$ mice. Expression downstream increased significantly in both groups in comparison to the upstream region. There was a slight trend for attenuated VCAM-1 expression in the downstream region of p47 phox$^{-/-}$ mice as compared to the control, though the attenuation did not reach significance (figure 5.8). Similarly, there was an increase in VCAM-1 levels in the brachiocephalic branch as compared to the upstream region in p47 phox$^{-/-}$ mice (figure 5.6). There was a trend for a slightly attenuated level of VCAM-1 expression in the brachiocephalic region in p47 phox$^{-/-}$ mice as compared to control mice, though this did not reach significance.

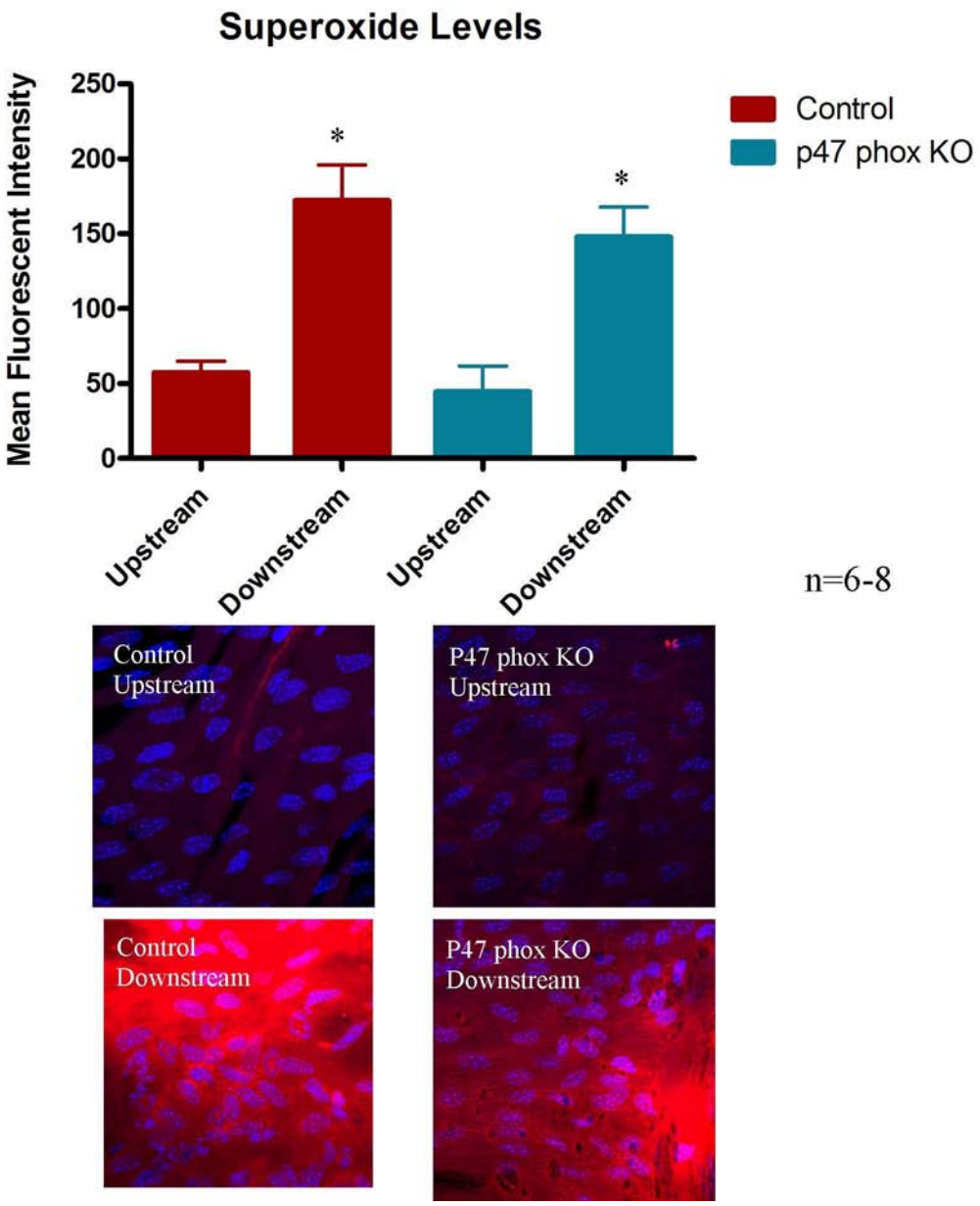

Figure 5.7 – Superoxide Levels in p47 Phox-/- Mice - p47 phox$^{-/-}$ mice showed superoxide levels that were comparable to the control in both the upstream and downstream regions. Representative confocal images from *en face* mounted aortas are presented. n=6-8, *=$p<0.05$ comparing upstream region to downstream region.

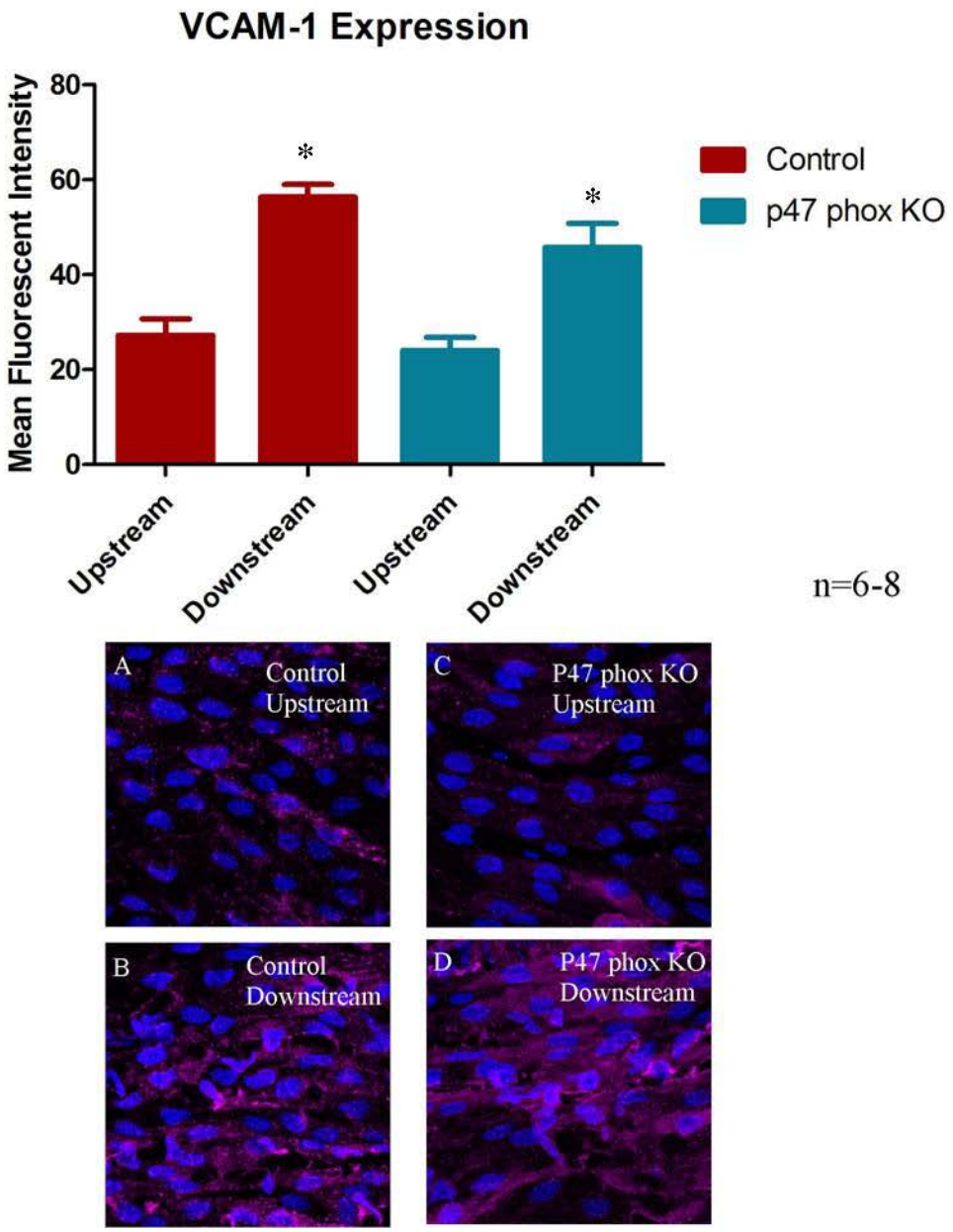

Figure 5.8 – VCAM-1 Expression in p47 Phox-/- Mice - There was no significant change in VCAM-1 expression in either the upstream or downstream regions when compared with the control. Representative confocal images are shown: A and C are from the upstream region, B and D are from the downstream region, A and B are from control mice while C and D are from p47 phox$^{-/-}$ mice. n=6-8, *=$p<0.05$ comparing upstream region to downstream region.

Contribution of Hydrogen Peroxide

We used two complimentary murine models of decreased hydrogen peroxide levels, to further investigate the contribution of ROS to WSS dependent VCAM-1 expression. Transgenic mice over-expressing catalase in the vascular wall, showed a trend for attenuated VCAM-1 expression in the upstream region compared with the control. However, VCAM-1 expression in the downstream region of the catalase overexpressing mice increased significantly compared with the upstream region and was not significantly different from that of the control (Figure 5.9). Similarly, ebselen treated mice, showed attenuated VCAM-1 expression in the upstream region compared to the control, yet expression in the downstream region increased to a level comparable to that of the control. In the region of chronically disturbed flow, VCAM-1 expression increased in comparison to the upstream region in the catalase mice. This level was comparable to the increase observed in the control mice. The ebselen treated mice also showed an increase in the brachiocephalic region in comparison to the upstream region of the ebselen treated mice. However, the VCAM-1 levels were significantly lower in the brachiocephalic branch of the ebselen treated mice in comparison to the same region in the control mice.

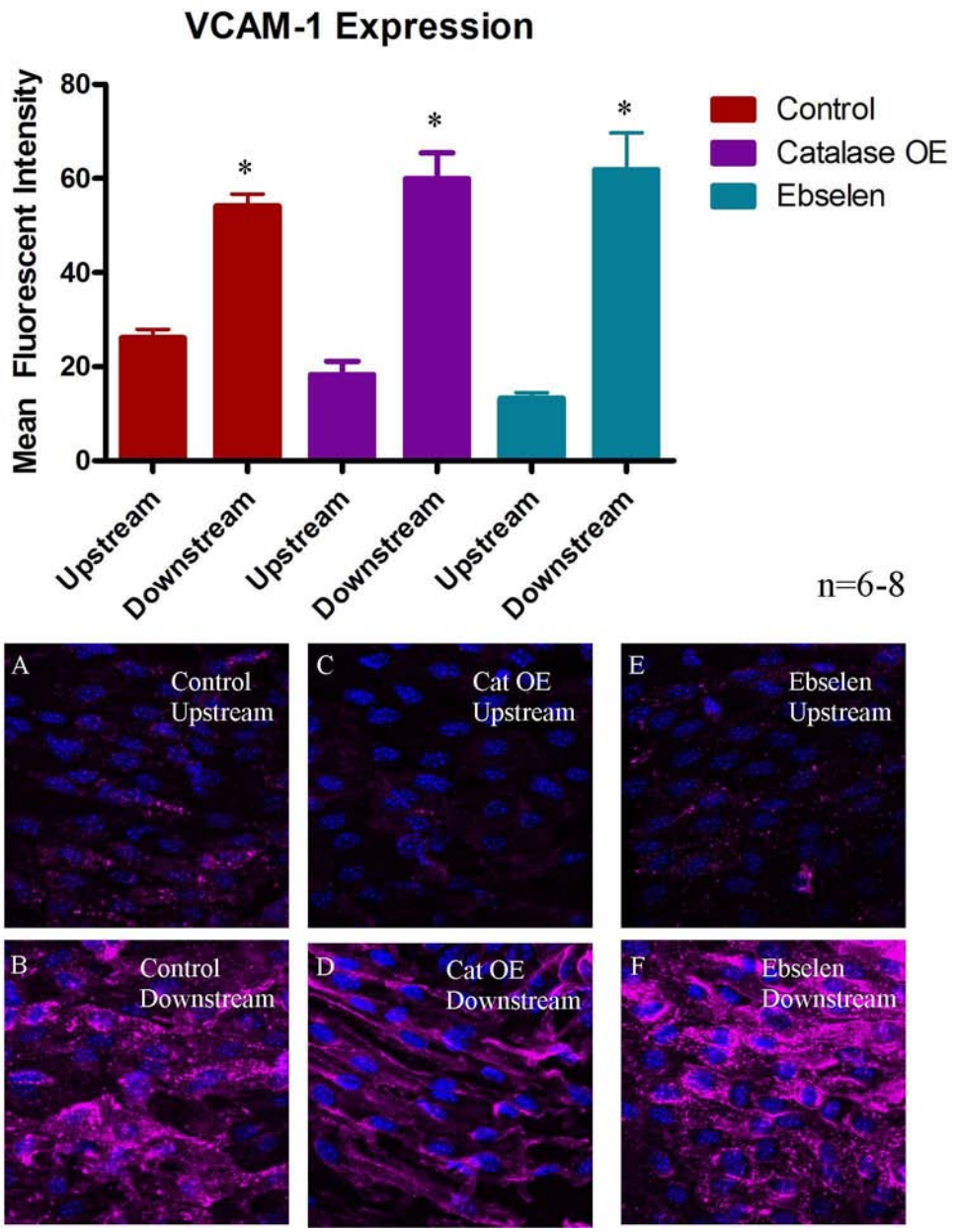

Figure 5.9 – VCAM-1 Expression in Catalase Overexpressing Mice and Ebselen Treated Mice - There was no significant change in VCAM-1 expression in the upstream or downstream regions from either treatment group when compared with the control. Representative confocal images from *en face* mounted aortas stained for VCAM-1 are presented. A,C, and E are from the upstream region, B, D, F are from the downstream region from a coarctation aorta, A and B are from control mice, C and D.are from catalase overexpressing mice, E and F are from mice treated with ebselen. n=6-8, *=$p<0.05$ comparing upstream region to downstream region.

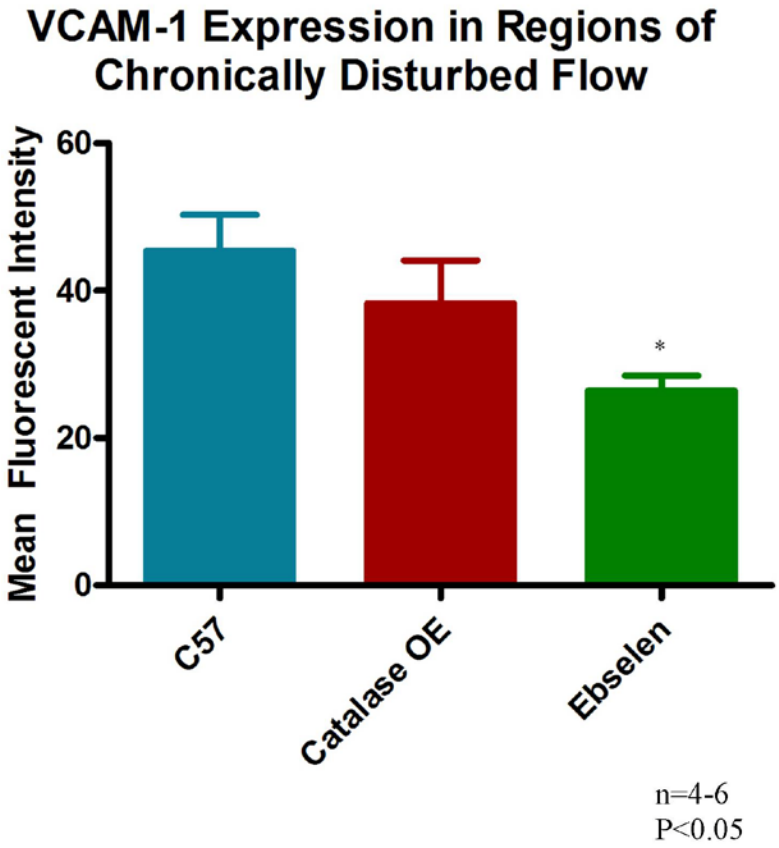

Figure 5.10 – VCAM-1 Expression in Regions of Chronically Disturbed Flow in Animal Models of Decreased Hydrogen Peroxide Levels - The control animals had relatively high levels of VCAM-1 expression in regions of chronically disturbed flow that were comparable to the VCAM-1 expression in the same region of catalase overexpressing mice. Mice treated with ebselen had significantly decreased VCAM-1 expression in regions of chronically disturbed flow. n=4-6 *=$p<0.05$

Contribution of NFκB

NFκB was implicated as a mediator in our hypothesized pathway in which ROS mediated WSS induced VCAM-1 expression. We used $p65^{-/-}$ mice to investigate the contribution of NFκB to VCAM-1 expression in the aortic coarctation model. There were relatively low levels of VCAM-1 expression in the upstream region which significantly increased in the downstream region in both the control and $p65^{-/-}$ mice (figure).

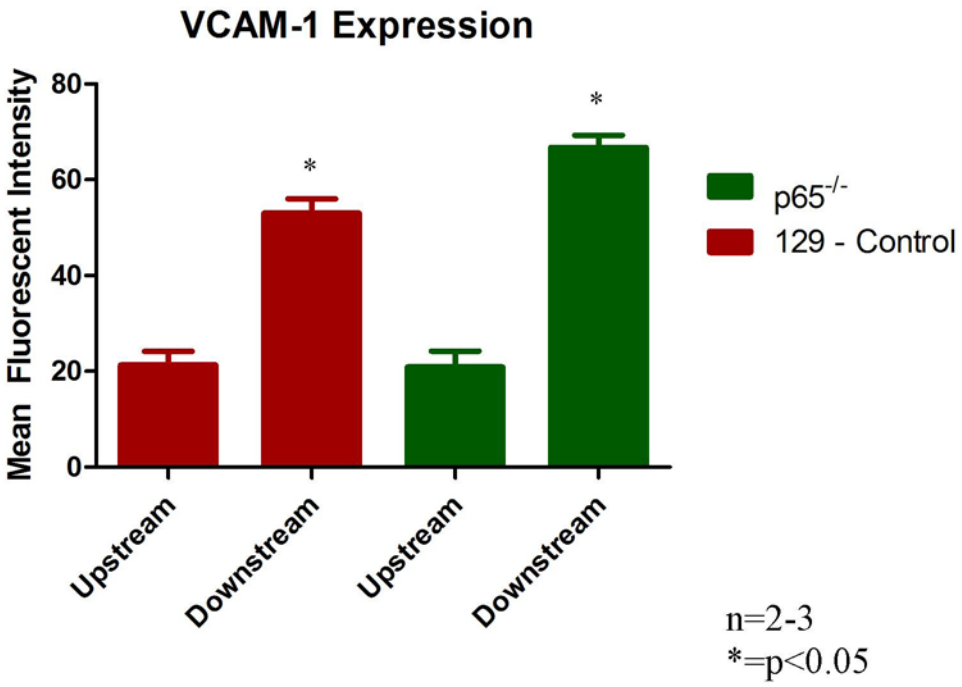

Figure 5.11 – VCAM-1 Expression in $p65^{-/-}$ Mice - VCAM-1 expression increases downstream from the coarctation in control and $p65^{-/-}$ mice. n=2-3 *=p<0.05

Discussion

We hypothesized that in an *in vivo* model of low magnitude oscillatory WSS, superoxide levels would increase in an NADPH oxidase dependent manner and that this increase in superoxide would then mediate shear dependent VCAM-1 expression. Our primary objective was to investigate whether either superoxide or hydrogen peroxide mediates the increase in VCAM-1 expression observed in regions of low magnitude oscillatory WSS. Our secondary objective for this aim was to determine the source for WSS induced superoxide generation. We found that tempol was able to reduce superoxide levels given that tempol was delivered at a sufficient dose. Though tempol was able to reduce superoxide levels, VCAM-1 still increased in regions of low magnitude oscillatory WSS in tempol treated mice. Additionally, we found that p47 phox$^{-/-}$ mice had endothelial superoxide levels and VCAM-1 expression that was comparable to the control mice independent of flow. Finally, in models of decreased hydrogen peroxide levels, we found that VCAM-1 expression still increased in region of acutely disturbed flow. However, ebselen treatment was able to reduce VCAM-1 expression in regions of chronically disturbed flow in comparison to the control. From these results we determined two conclusions.

We conclude that in regions of acutely disturbed flow *in vivo*, VCAM-1 expression is not modulated by reactive oxygen species. Additionally, the NADPH oxidase subunit, p47 phox, does not mediate superoxide generation in response to disturbed flow.

Previous reports have demonstrated the specificity of the hydrocy-3 dye *in vitro* by using tempol as a means to scavenge superoxide [58]. Similarly, we found that hydro-

Cy3 measurements of endothelial superoxide levels could in fact be attenuated by treatment with tempol. However, it was necessary to modify the mode and dose of delivery to increase the plasma concentration to sufficient levels. Previously, an *in vitro* dose response study showed that administration of tempol at a concentration on the order of 1mM inhibited 75% of superoxide production when stimulated with angiotensin II, while tempol concentrations on the order of 100 nM inhibited 10% of superoxide production [87]. Though the stimulus in our study was different (WSS instead of angiotensin II) the findings were similar. Tempol treatment administered intravenously by mini-pump produced plasma concentrations on the order of 1mM and was able to attenuate superoxide levels. However, tempol treatment administered in the drinking water produced plasma levels on the order of 100 nM and had no significant effect on observed endothelial superoxide production. In future studies, it should therefore be taken into account that although tempol treatment in the drinking water has been shown to produce systemic effects, it does not sufficiently increase plasma tempol levels to a concentration where endothelial superoxide production is significantly inhibited.

Though tempol treatment was able to attenuate endothelial superoxide levels in the upstream and downstream regions as compared to the control, it is important to note that there was still a significant increase in superoxide levels in the downstream region as compared to the upstream region. However, the level of superoxide present was equivalent to the baseline levels seen in control animals.

We quantitatively measured VCAM-1 using quantum dot based *en face* immunohistochemistry. This methodology specifically quantifies endothelial protein expression as the quantum dot-antibody conjugates do not penetrate into the media of the

aorta [123]. In aim 2 we reported that VCAM-1 levels increased significantly in the downstream region as compared with the upstream region. Tempol treatment, regardless of mode of administration, had no effect on the upstream or downstream expression of VCAM-1 as compared to the control. Though the data from the region of chronically disturbed flow in tempol treated mice showed a trend for attenuated VCAM-1 expression, this trend did not reach significance. These data suggest that superoxide does not mediate WSS induced changes in endothelial VCAM-1 expression in the aorta.

Since tempol treatment suggests that there may be differences between *in vivo* and *in vitro* signaling pathways, we wanted to investigate the mechanisms of shear dependent superoxide formation by looking at the *in vivo* contribution of the NADPH oxidase subunit, p47 phox. Previous studies found that p47 phox had a functional role in shear dependent superoxide formation and subsequent inflammatory protein expression [27, 67, 68, 128]. Our study, however, found that in p47 phox$^{-/-}$ mice, superoxide levels increased significantly in the downstream region as compared to the upstream region and neither region was significantly different from that of the control. We specifically show this response in the endothelium, whereas previous *in vivo* studies may have been measuring superoxide produced by additional cell types, such as macrophages or smooth muscle cells. Additionally, VCAM-1 expression in p47 phox$^{-/-}$ mice was comparable in all regions to the expression in control mice. These results show that *in vivo* endothelial production of superoxide in response to low magnitude oscillatory WSS is not p47 phox dependent and suggest the presence of compensatory or parallel pathways *in vivo*.

P47 phox$^{-/-}$ mice have some clear limitations with regards to analysis of the entire NOX family. The p47 phox subunit is not present in all NOX family members, of

particular note is NOX 4. NOX 4 in fact, has been shown to be upregulated in p47 phox$^{-/-}$ mice [D. Sorescu, personal communication]. This compensatory mechanism could account for the lack of change in superoxide levels and may even produce an additional increase in other oxidants, primarily hydrogen peroxide. Since *in vitro* studies had shown that p47 phox$^{-/-}$ cells attenuated superoxide production in response to low magnitude oscillatory WSS we chose this model as our focus [68].

Alternative methods for investigating the NADPH oxidase family do exist, primarily the use of the inhibitors apocynin or DPI, yet these have their own limitations. Apocynin has been shown to stimulate ROS production in non-phagocytic cells [79]. In preliminary studies by our group, we saw increased basal VCAM-1 levels throughout the vasculature with apocynin use and thus chose not to pursue this path (data not shown). DPI, on the other hand, inhibits all flavin containing enzymes, including eNOS [50]. eNOS is responsive to WSS and when uncoupled is believed to play a role in endothelial superoxide generation [139]. DPI is therefore not an ideal treatment when trying to isolate molecular mechanisms involving the NOX family from other oxidant producing enzymes. Recent reviews of these treatments have discussed the lack of specificity of both reagents as well as the ability to produce oxidative stress and therefore recommend use of other means to investigate the NOX family [50].

Although compensatory and parallel mechanisms may be directly affecting superoxide levels in this model, it is also feasible that these pathways may also affect other oxidants. Of particular interest is hydrogen peroxide. NOX family members can directly produce hydrogen peroxide and SOD scavenges superoxide producing hydrogen peroxide. We therefore wanted to investigate whether decreasing hydrogen peroxide

levels might inhibit inflammatory protein expression. We found that VCAM-1 expression was not attenuated in the downstream region in either catalase overexpressing mice or mice treated with ebselen. We did however, see attenuated VCAM-1 expression in the chronically disturbed flow region in ebselen treated mice. This level of expression, however, was still higher than upstream levels. A limitation of these experiments is the lack of accurate methods for the measurement of hydrogen peroxide, therefore we cannot confirm the efficacy of the treatments. Hydrogen peroxide is challenging to measure *in vivo* and more challenging to measure specifically in the endothelium. The dye DCF-DA is sometimes used to measure hydrogen peroxide levels; however, recent reviews have shown evidence for the instability of the molecule [54].

The last model that we used investigated the contribution of NFκB to VCAM-1 expression in the coarctation model. As was the trend in the other animal models, the $NF\kappa B^{-/-}$ mice had a significant increase in VCAM-1 expression in the region of acutely disturbed flow, comparable to the control. As described in the discussion for aim II, knocking out NFκB in different cells can have different consequences for atherogenesis. Reports have shown decreased lesion formation, a change in lesion composition or even increased lesion formation [129-131]. These results suggest multiple roles for NFkB *in vivo*, and could likely explain the differences between our data and previous *in vitro* studies.

There were slight differences in the data from aim III in the chronic and acute disturbed flow regions. In the acute disturbed flow region, inflammatory protein expression was completely independent from oxidative stress. This implies that there must be other mechanisms by which shear stress is transduced resulting in inflammatory

protein expression. The data from the chronic region showed a trend for attenuated VCAM-1 expression in the downstream region from each of the models of decreased ROS, though it only reached significance in the ebselen treated group. We therefore, suspect that ROS do play a role in chronically disturbed flow, but other pathways are still activated, whether parallel or compensatory. It is known that oxidative stress contributes to atherosclerosis lesion formation in accelerated atherosclerosis mouse models. However, when specifically considering flow dependent lesion formation in regions such as the arch, there have been some differing results. These data suggest that there may be parallel pathways that are activated during flow dependent lesion formation. These data, along with our data suggest that flow dependent lesion localization occurs through a mechanotransduction mechanism independent of the redox state. Future work might therefore investigate parallel or compensatory pathways by utilizing multiple antioxidants (e.g. target superoxide and hydrogen peroxide).

An obvious limitation of this technique is that it is low throughput and can not look at many different markers. We therefore focused on oxidants that had been shown to be responsive to low magnitude oscillatory WSS in prior studies. Other inflammatory and oxidative markers of interest for future studies may include ICAM-1, BMP-4, eNOS, xanthine oxidase, and peroxynitrite, among others. A recent *in vivo* study gives our group particular interest in investigating eNOS and the AT_1R. It was shown that AT_1R expression increased in atheroprone regions which could be blocked in eNOS overexpressing mice [140]. This implicates another pathway by which low magnitude oscillatory WSS might stimulate an endothelial inflammatory response.

As a result of this study we conclude that shear dependent inflammatory protein expression occurs through a redox independent mechanism. Superoxide is acutely responsive to low magnitude oscillatory WSS, as is VCAM-1. In this model VCAM-1 expression is not dependent on superoxide levels. Furthermore, compensatory mechanisms or parallel pathways appear to exist *in vivo* in the shear dependent production of superoxide, such that this pathway is not dependent on p47 phox. Though *in vitro* studies can provide valuable insight into molecular mechanisms involved in atherogenesis, it is still important to investigate these molecular mechanisms *in vivo* for greater understanding of the development of atherosclerotic plaques. Finally, we show that models of decreased hydrogen peroxide do not inhibit acute shear dependent VCAM-1 expression, but may attenuate VCAM-1 expression partially in a chronic time course. These data suggest that hydrogen peroxide may be involved in VCAM-1 upregulation as a result of disturbed flow, but it is not a critical component. Mechanically induced oxidative stress is clearly a complex mechanism and further research is required to determine the many pathways that are likely involved.

CHAPTER 6

DISCUSSION AND FUTURE DIRECTIONS

Discussion

Aim I

Our objective for this aim was to develop a novel mouse model of acutely disturbed flow. We thoroughly characterized the hemodynamic environment associated with the coarctation induced by the nitinol clip. Using a combination of techniques, *in situ* μCT and *ex vivo* pressure inflation, we showed that we can effectively constrict the aortic diameter at the clip with minimal variability. We further showed that this constriction produced a minor stenosis with no significant pressure loss. The CFD model showed that the coarctation produced low magnitude oscillatory WSS in the distal region.

We concluded that coarctation of the descending aorta using a nitinol clip uniquely created a hemodynamic environment of low magnitude oscillatory WSS without a significant change in blood pressure.

We found that the nitinol clip model produced an idealized stenosis. We used μCT and *ex vivo* pressure inflation to demonstrate the efficacy of the nitnol clip. The pressure inflation showed that we were able to induce an ideal stenosis under *ex vivo* conditions without interference from surrounding tissue. However, after fixation at 100 mmHg the tissue remained largely compliant and the unpressurized aortic diameter correlated to a diameter at a pressure of 10 mmHg as determined by the pressure diameter curves. We speculate that the tissue was not fixed at the morphology corresponding to the fixation pressure because the mouse aorta is very thin and the composition of the

vessel is high in elastin compared to collagen. To correct for this error, we determined an expansion factor from the pressure diameter curves. We applied these expansion factors *in silico* to the aortic diameter of the μCT reconstruction. When the expansion factor was applied to expand the tissue to an aortic diameter comparable to the diameter during diastole, about 60 mmHg, a significant stenosis was observed. We used the *in silico* expanded aorta for the CFD modeling.

The CFD model showed results as predicted by the idealized stenosis model. Flow was unidirectional during the upstroke of systole, flow separation occurred during the downstroke of systole, and then was again unidirectional during diastole. WSS was high upstream from the coarctation, increased further in the stenotic region, then decreased significantly downstream from the coarctation. Additionally, we showed that there was no significant pressure loss produced by the coarctation. Therefore we predict that there is no significant change in strain on the endothelial cells and that the primary mechanical stimulus of the model is the change in WSS. These results demonstrate a model with significant advantages over current *in vivo* murine models of WSS.

The comparable murine flow models are the carotid coarctation reported by Cheng et al. and the carotid partial ligation reported by Nam et al. [25, 27]. Our model produces a unique model of low oscillatory WSS with minimal disturbances to pressure and therefore strain. The carotid coarctation model reports a region of low magnitude unidirectional WSS and a region of high magnitude oscillatory WSS [25]. Furthermore, this model does not characterize any alterations to pressure and/or strain. The partial ligation model reports low magnitude oscillatory WSS, but does not characterize pressure and/or strain. The low flow in this model likely produces a moderate change in strain

which could modulate the biological response. These distinct differences in the mechanical environments of the three models and the limitations of each model provide unique *in vivo* models to investigate different biological responses.

We conclude that this study presents a novel model of acutely disturbed flow. The model utilizes the shape memory response of a nitinol clip to induce an aortic coarctation with high reproducibility. We showed low magnitude oscillatory WSS in the region distal to the coarctation. This model can be used in future studies without the need for further validation of the flow environment and will significantly increase the accessibility of *in vivo* experiments addressing mechanical transduction. This model provides a number of advantages over existing *in vivo* mouse models of disturbed flow including: ease of use, high reproducibility, low mortality rate, an acute time course, and a fully defined hemodynamic environment exhibiting low magnitude oscillatory WSS.

Aim II

We developed two hypotheses for aim II. First, we hypothesized that inflammatory proteins would increase *in vivo*, in the regions of acutely induced low magnitude oscillatory WSS. Additionally, we hypothesized that there would be a distinct increases in NFκB and superoxide, that would be present in the acute model, but not in the chronic model. Our objective to address these hypotheses was to characterize the acute and chronic response of atherogenic markers in regions of low magnitude oscillatory WSS. We found that in regions of acutely induced low magnitude oscillatory WSS there was an increase in expression of VCAM-1 and a large increase in superoxide levels. In regions of chronically disturbed flow, superoxide levels were moderately increased, while expression of cellular adhesion molecules, both VCAM-1 and ICAM-1

was significantly increased. Additionally we show that fatty streaks form in the region downstream from the coarctation over a chronic time course. From these results we determined two main conclusions.

We conclude that the *in vivo* endothelial phenotype associated with acutely disturbed flow is characterized by increased production of superoxide and increased expression of select inflammatory proteins. In comparison, the phenotype associated with chronically disturbed flow is characterized by a more modest increase in superoxide and increased levels of multiple inflammatory proteins.

We used a novel superoxide sensitive dye, hydro-cyanine 3, to quantitatively measure endothelial superoxide levels in regions of acutely and chronically disturbed flow. The current gold standard for superoxide detection in tissue is with DHE staining; however, DHE requires complex purification prior to use, it has a short half life, and it is light sensitive. Therefore, we used the hydro-Cy3 dye, which is more stable than DHE, to measure regional tissue levels of endothelial superoxide [58]. We found that superoxide levels increase significantly in regions of low magnitude oscillatory WSS as compared to regions of high unidirectional WSS, similar to published data from *in vitro* studies [59, 60, 66-68]. Contrary to these results, there was only a moderate increase under chronically disturbed flow.

Transcription factors are similarly transiently expressed and activated in response to low magnitude oscillatory WSS [98, 99, 101]. Our results show no significant change in NFκB expression in either the chronic or acute time course. Our findings are contradictory to previous studies that found increased p65 expression in "high prone" regions near the aortic sinus and inner curvature of the arch [101, 124]. Hajra et al.

additionally reported that an additional stimulus, either LPS treatment or high fat diet, resulted in the activation and translocation of NFκB to the nucleus and this response was only observed in regions prone to lesion formation [101]. Previous *in vitro* studies had reported that low magnitude oscillatory WSS was sufficient to increase p65 expression and NFκB activation and that an additional stimulus was not needed. Other studies have further investigated NFκB in relation to lesion formation showing that NFκB deficiency in the endothelium results in attenuated lesion area [129]. It is important to note however, that blocking NFκB in other cell types resulted in changes in the composition within the lesion or even increased lesion formation [130, 131]. These results investigating the response of NFκB to WSS and the eventual contribution to lesion formation are not consistent with one another. It is likely that the time course involved plays an important role. A recent mechanistic model predicted that in response to oscillatory WSS there was an immediate increase in NFκB activation, which decreased by ten hours and increased again by 24 hours [141]. Further analysis of the persistent activation and expression of NFκB will be valuable in determining the *in vivo* response of NFκB to WSS and contribution to lesion formation.

NFκB is one of the primary transcription factors that produce increased expression of cellular adhesion molecules. Our results confirmed the previous findings that expression of both VCAM-1 and ICAM-1 is upregulated in the lesser curvature of the aortic arch where flow is chronically disturbed [20]. However, we found that VCAM-1 expression, and not ICAM-1 expression, is upregulated in response to acutely disturbed flow downstream from the coarctation. VCAM-1 has been shown to be a requisite mediator of flow dependent lesion formation in the aortic arch of VCAM-1

deficient (D4D) mice [111]. ICAM-1 knockout mice on the other hand, have been shown to have reduced lesions throughout the entire aorta but not in regions of flow mediated lesion formation [132]. These results along with our results implicate VCAM-1 in the early and acute stages of atherogenesis. Additionally, it suggests that VCAM-1 is a requisite mediator for flow induced lesion localization while ICAM-1 is not, though ICAM-1 might be involved in later stage lesion formation. These data could explain our results in which we did not observe an acute increase in ICAM-1 expression.

The results presented in aim II show a distinct difference between the acute and chronic response of atherogenic markers *in vivo* and additionally show differences between the *in vivo* and *in vitro* settings. Much of the current literature has been obtained using *in vitro*, cell culture, techniques which often utilize a time course on the order of minutes to hours. Recently, *in vitro* studies have begun extending the time course of experiments to 72 hours allowing the cells to reach what is considered a stable equilibrium, though even this is still significantly different from the time course often used *in vivo* [124]. Our coarctation model is able to provide an acute time course similar to the 72 hour *in vitro* studies, as well as the chronic time over the life of the mouse that is consistent with most *in vivo* models.

The acute and chronic time course from the coarctation and aortic arch models, provide insight into slightly different pathologies. The chronic time course is similar to the progression of atherosclerosis. Atherosclerosis is a multi-stage and multifactoral disease that develops over a long time course. The chronic environment in the lesser curvature of the aortic arch has been described as atherosusceptible, though it is in an equilibrated and stable state in the absence of other factors. It is plausible that feedback

mechanisms might help to stabilize the system such that it eventually equilibrates as opposed to experiencing an amplification of oxidative stress. This environment is ideal for investigating the progression of lesion formation in a flow dependent manner; however, it does not accurately represent the mechanotransduction mechanisms in response to disturbed flow. Alternatively, the acute coarctation model better investigates the *in vivo* mechanotransduction of low magnitude oscillatory WSS. There may still be compensatory mechanisms and parallel pathways, that are not present in the *in vitro* setting, though these may be different then temporal compensatory mechanisms observed in the chronic model. Investigating both the acute and chronic response and in particular, the compensatory mechnisms that lead to the equilibrated chronic state may provide new directions for treatments of atherosclerosis lesion formation.

In summary, we present a novel model in which we can compare molecular signaling in response to acutely and chronically disturbed flow. We show that there are distinct endothelial phenotypes associated with either chronically disturbed flow or acutely disturbed flow. In conditions of acutely disturbed flow we show and increase in superoxide levels and an increase in VCAM-1 expression. In regions of chronically disturbed flow we show a trend for an increase in superoxide levels and a significant increase in both VCAM-1 and ICAM-1. There are still many other mediators of mechanosensitive pathways that have been identified *in vitro*. These results demonstrate the importance of confirming *in vitro* findings to *in vivo* settings and in particular to consider the involved time course. This *in vivo* model additionally allows for the investigation of the functional contribution of various mechanosenstivite markers, which

we analyzed in the third aim using genetically altered mice and pharmacologic treatments.

Aim III

We hypothesized that in an *in vivo* model of low magnitude oscillatory WSS, superoxide levels would increase in an NADPH oxidase dependent manner and that this increase in superoxide would then mediate shear dependent VCAM-1 expression. Our primary objective was to investigate whether either superoxide or hydrogen peroxide mediates the increase in VCAM-1 expression observed in regions of low magnitude oscillatory WSS. Our secondary objective for this aim was to determine the source for WSS induced superoxide generation. We found that tempol was able to reduce superoxide levels given that tempol was delivered at a sufficient dose. Though tempol was able to reduce superoxide levels, VCAM-1 still increased in regions of low magnitude oscillatory WSS in tempol treated mice. Additionally, we found that in our flow models, p47 phox$^{-/-}$ mice had endothelial superoxide levels and VCAM-1 expression that was comparable to the control mice. Finally, in models of decreased hydrogen peroxide levels, we found that VCAM-1 expression still increased in regions of acutely disturbed flow. However, ebselen treatment was able to reduce VCAM-1 expression in regions of chronically disturbed flow in comparison to the control. From these results we determined two conclusions.

We conclude that in regions of acutely disturbed flow *in vivo*, VCAM-1 expression is not modulated by reactive oxygen species. Additionally, we conclude that p47 phox-dependent NADPH Oxidase activity does not have a functional role in WSS induced superoxide generation in the endothelium.

We investigated the mechanisms of shear dependent superoxide formation and in particular the *in vivo* contribution of p47-dependent NADPH oxidase activity. Previous studies found that p47 phox had a functional role in shear dependent superoxide formation and subsequent inflammatory protein expression [27, 67, 68, 128]. Our study, however, found that in p47 phox$^{-/-}$ mice, superoxide levels increased significantly in the downstream region as compared to the upstream region and neither region was significantly different from that of the control. Additionally, VCAM-1 expression in p47 phox$^{-/-}$ mice was comparable in all regions to the expression in control mice. Though a previous *in vivo* study showed shear dependent increases in superoxide generation in a p47 phox dependent manner, the study may have been measuring superoxide produced by additional cell types, such as macrophages or smooth muscle cells [27]. We specifically show that endothelial cells do not produce superoxide in response to disturbed flow through a p47 phox dependent mechanism. These results show that *in vivo* endothelial production of superoxide in response to low magnitude oscillatory WSS is not p47 phox dependent and suggest the presence of compensatory or parallel pathways *in vivo*.

p47 phox$^{-/-}$ mice have some clear limitations with regards to analysis of the entire NOX family. The p47 phox subunit is not present in all NOX family members particularly NOX 4. NOX 4 in fact, has been shown to be upregulated in p47 phox$^{-/-}$ mice [D. Sorescu, personal communication]. This compensatory mechanism could account for the lack of change in superoxide levels and may even produce an additional increase in other oxidants, primarily hydrogen peroxide.

We then investigated the contribution of superoxide to WSS dependent VCAM-1 expression. After confirming the efficacy of tempol treatment, we found that animals with attenuated superoxide levels had comparable VCAM-1 expression in the upstream and downstream regions when compared to the control. These data show that superoxide does not mediate WSS induced changes in endothelial VCAM-1 expression in the aorta.

NADPH oxidase family members can directly produce hydrogen peroxide, we therefore wanted to investigate whether decreasing hydrogen peroxide levels might inhibit inflammatory protein expression. To analyze the contribution of hydrogen peroxide to shear dependent inflammatory protein expression, we utilized ebselen treated mice and catalase overexpressing mice. We found that VCAM-1 expression was not attenuated in the downstream region in either catalase overexpressing mice or mice treated with ebselen. We did, however, see attenuated VCAM-1 expression in the chronically disturbed flow region in ebselen treated mice. This level of expression, however, was still higher than upstream levels. A limitation of these experiments is the lack of accurate methods for the measurement of hydrogen peroxide, therefore we cannot confirm the efficacy of the treatments. Hydrogen peroxide is challenging to measure *in vivo* and more challenging to measure specifically in the endothelium. The dye DCF-DA is sometimes used to measure hydrogen peroxide levels; however, recent reviews have shown evidence for the instability of the molecule [54].

The last model that we used investigated the contribution of NFκB to VCAM-1 expression in the coarctation model. As was the trend in the other animal models, the $NF\kappa B^{-/-}$ mice had a significant increase in VCAM-1 expression in the region of acutely disturbed flow, comparable to the control. Studies have previously shown that a shear

dependent increase and activation of NFκB occurs through a redox mechanism *in vitro* [127]. Our data, therefore, suggest the presence of an *in vivo* pathway that is independent of NFκB and also independent of redox signaling.

There were slight differences in the data from aim III in the chronic and acute disturbed flow regions. In the acute disturbed flow region, inflammatory protein expression was completely independent from oxidative stress. This implies that *in vivo* there must be other mechanotransduciton mechanisms by which shear stress is able to produce inflammatory protein expression. The data from the chronic region showed a trend for attenuated VCAM-1 expression in the downstream region from each of the models of decreased ROS, though it only reached significance in the ebselen treated group. We therefore, suspect that ROS do play a role in chronically disturbed flow, but other pathways are still activated, whether parallel or compensatory. It is known that oxidative stress contributes to atherosclerosis lesion formation in accelerated atherosclerosis mouse models. However, when specifically considering flow dependent lesion formation in regions like the arch, there have been some differing results [69]. These data suggest that there may be parallel pathways that are activated in a flow dependent lesion formation. These data, along with our data suggest that flow dependent lesion localization occurs through a mechanotransduction mechanism independent of the redox state. Future work might therefore investigate parallel or compensatory pathways.

As a result of this study we conclude that shear dependent inflammatory protein expression occurs through a redox independent mechanism. Superoxide is acutely responsive to low magnitude oscillatory WSS, as is VCAM-1. In this model VCAM-1 expression is not dependent on superoxide levels. Furthermore, compensatory

mechanisms or parallel pathways appear to exist *in vivo* in the shear dependent production of superoxide, such that this pathway is not dependent on p47 phox. Though *in vitro* studies can provide valuable insight into molecular mechanisms involved in atherogenesis, it is still important to investigate these molecular mechanisms *in vivo* for greater understanding of the development of atherosclerotic plaques. Finally, we show that models of decreased hydrogen peroxide do not inhibit acute shear dependent VCAM-1 expression, but may attenuate VCAM-1 expression partially in a chronic time course. These data suggest that hydrogen peroxide may be involved in VCAM-1 upregulation as a result of disturbed flow, but it is not a critical component. Mechanically induced oxidative stress is clearly a complex mechanism and further research is required to determine the many pathways that are involved.

Limitations and Future Directions

A major limitation for the first aim was the lack of ability to image the morphology *in vivo*. We utilized three different imaging modalities, μCT, MRI, and *ex vivo* perfusion, to best approximate the morphology of the aorta surrounding the coarctation. However, the ideal imaging modality would directly measure the aortic morphology *in vivo*. The most promising direction to achieve this would be *in vivo* μCT. This could theoretically be accomplished by pursuing two different directions. The first would be improved μCT technology. Investigators have utilized improved algorithms that measure the phase shift in X-ray refraction as opposed to attenuation of X-rays to obtain better vascular contrast[142]. Additionally, recent advances using flat panel detectors have reduced acquisition time and improved sensitivity and signal to noise ratio [143, 144]. The second technique would be improved contrast agents. Investigators have been working on developing contrast agents with improved circulating time [145]. There is now a commercially available blood pool contrast agent, Fenestra VC (Alerion Biomedical, Inc., San Diego, CA), which has been used to image the aorta [146]. Improved *in vivo* angiography in mice would have additional applications particularly involving imaging of vessels at multiple time points over an extended time course. This could theoretically be used to monitor the progression of diseases such as aneurysm formation or monitor angiogensis.

Though this technology would be immensely useful for numerous applications, we do not believe it would alter the outcome of our findings. We have quite thoroughly characterized the hemodynamic environment associated with the aortic coarctation and show that it produces a region of low magnitude oscillatory WSS. Additionally,

improved μCT would still have interference from the material of the nitinol and have a halo effect distorting the image immediately surrounding the clip. Nevertheless, this would still be a very useful direction for further research.

Another limitation for the first aim involves the WSS profile, which we wanted to be low magnitude and oscillatory WSS. This WSS profile has been correlated to lesion formation. However, it is unknown which parameters dictate the development of the disease. We characterized our flow environments under two parameters: magnitude, i.e. low vs high, and directionality, i.e. oscillatory vs unidirectional. This is a very basic characterization of the stresses that are imparted on the endothelium. With regards to the magnitude it is currently unknown whether this is a simple binary mechanism, such that crossing a threshold activates atherogenic signaling. It is plausible that there is a balance between an atherogenic state and an atheroprotective state, and the magnitude can gradually shift the phenotype along this scale. With regards to directionality, there are still questions about what constitutes oscillatory or unidirectional. Flow occurs in three dimensions with primary flows that tend to move axially along the vessel and secondary flows that move circumferentially. The shear stress vector is therefore not simply forwards or backwards but also includes a second dimension. Investigators have attempted to quantify directionality using the OSI [5, 147, 148]. OSI provides a more substantial measure of directionality than simply oscillatory or unidirectional. Similar to the magnitude issue, this raises the question of whether this is a binary mechanism that is on or off, or a gradual mechanism that can shift along a scale. There are also other parameters that may be involved in lesion localization, such as the gradient of shear.

Improved models that allow for further analysis of the parameters of WSS will be valuable in better understanding endothelial mechanotransduction. The coarctation model could be modified to investigate some of these questions using different sized clips. Different sized clips would result in a different degree of stenosis which would impart a different WSS profile upon the endothelial cells. The sensitivity analysis in aim I demonstrates this effect (figure 3.22). With a smaller degree of stenosis there is a smaller region of flow separation and a smaller change in magnitude, while a larger stenosis would create a larger separation region and a larger change in WSS magnitude. Different sized clips could be used to investigate the gradual change in the parameters of magnitude, OSI, and gradient of shear. A different approach to this problem might be to step back to the *in vitro* environment. There are currently improved cell culture flow set ups that allow for excellent control over the WSS profile [149]. Similar cell culture systems could allow for improved *in vitro* analysis of the various parameters of WSS.

A main limitation for aim II is the access to adequate probes for desired targets. The study raises a particular interest in hydrogen peroxide. As discussed in Chapter 4, the dye DCF-DA can be used to measure hydrogen peroxide levels, but DCF-DA is very unstable [54]. We show a novel fluorophore that is specific to superoxide, a similar type of fluorophore that specifically measures hydrogen peroxide, would also be useful. Other targets of interest for future studies include BMP-4, eNOS, xanthine oxidase, peroxynitrite, and AT_1R. The AT_1R is of particular interest as a recent study showed that AT_1R expression increased in atheroprone regions and was blocked in eNOS overexpressing mice [140]. Furthermore, we have some preliminary *en face* data that links expression of the AT_1R to regions of disturbed flow and AAA formation. Another

target of interest might be micro-RNA. A collaborator recently showed *in vitro* that some mirs, including mir-21, are regulated in response to WSS. We are currently working with them to develop an *en face* staining protocol for mir-21 using *in situ* hybridization.

Another limitation for aim II was the determination of a time course. We originally determined 72 hours from a pilot study in which we measured VCAM-1 expression after numerous time points. All time points in our pilot study showed increased VCAM-1 expression with little variability. However, other markers are likely to have more variability, particularly NFκB. NFκB is believed to be very transiently expressed and activated. Therefore 72 hours may not be the optimal time point for the measurement of an acute NFκB response. Additionally, ICAM-1 showed that there was a chronic increase in expression but not an acute increase in expression in response to low magnitude oscillatory WSS. We looked at ICAM-1 expression after 7 days with a coarctation and still saw no change. These results raise the question of the difference between the chronic and acute phenotype. It is likely that this is a gradual change in which the cell is attempting to equilibrate and reach a stable state. This would imply that there are compensatory mechanisms that are activated and help to stabilize the state of the cell. A future direction could utilize the coarctation model using more time points to investigate any compensatory mechanisms. This information might provide a means not only to stabilize atherosclerotic lesion progression but possibly even reverse the progression.

There are a number of limitations for aim III. The primary limitation of concern is the lack of a NADPH oxidase specific inhibitor or knockout model. NADPH oxidase is a primary source of superoxide in the endothelium and has been shown to be

responsive to WSS *in vitro* [67]. We, however, found that superoxide was produced in a p47 phox independent manner in regions of low magnitude oscillatory WSS *in vivo*. We therefore would like to further investigate the source of the superoxide generation in the endothelium in response to low magnitude WSS. Other possible animal models to investigate NADPH oxidases could include gp91 phox$^{-/-}$ mice, p22 phox$^{-/-}$ mice or DPI treated mice. Additionally we would like to look at enzymatic ROS sources other than NADPH oxidase, primarily uncoupled eNOS. Using eNOS$^{-/-}$ mice, DPI treated mice, or L-NAME treated mice could provide insight into the contribution of uncoupled eNOS to endothelial superoxide generation in our model. Lastly, we would like to use these models to investigate other inflammatory markers, particularly ICAM-1. We found that ICAM-1 expression did not increase in the acute model, but did increase in the chronic model. Future directions could investigate this difference and utilize knockout models and pharmacological inhibitors to investigate the ICAM-1 response to chronically disturbed flow.

Additionally none of our animal models of decreased ROS looked at compensatory mechanisms or parallel pathways. It would be of interest to utilize a model of dual treatments to decrease both superoxide and hydrogen peroxide. This could be done using catalase overexpressing mice treated with tempol or mice treated with both ebselen and tempol. Additionally looking at eNOS models with a secondary treatment might give insight into parallel pathways. Lastly it would be interesting to investigate other signaling pathways that may be parallel to the redox signaling pathway. As mentioned previously, the angiotensin pathway is of particular interest. Other directions

might include cytokines such as TNF-alpha or IL-1, or growth factors, such as PDGF all of which have been shown to increase in response to disturbed flow (REF).

Additional future directions might investigate the coarctation model as it relates to atherosclerotic lesion formation. Previous future directions discussed the time course between acute and chronic oxidative stress and inflammatory protein expression. The next progression in the time course would be to the beginning of lesion formation. After lesion formation is intiated there are a series of events that result in the progression of the lesion, but little is understood about the contribution of WSS to this progression. We have shown that superoxide can be decreased in the regions of low magnitude oscillatory WSS, but that this does not alter VCAM-1 expression. A future direction could investigate whether a decrease in superoxide, but not VCAM-1, would be sufficient to attenuate lesion formation. Additionally, it would be interesting to investigate the contribution of WSS after the intitiaon of lesion formation, by removing the nitinol clip at various time points part of the way through the lesion formation study. This model could be used to distinguish whether disturbed flow continues to be involved in middle and later stages of lesion formation, or if it is only involved in the initiation and localization of the disease.

A final future direction might utilize the coarctation model to investigate the mechanical environment that contributes to aneurysm formation. There are many similarities between abdominal aortic aneurysm formation and atherosclerosis formation. Both are focally localized diseases, though they localize to different regions. It is believed that flow disturbances might contribute to AAA formation. Preliminary data from our lab showed that AT_1R was upregulated at the celiac branch where there were

flow disturbances. Aneurysms form in AngII treated animals at this same location. It would be interesting to see if other factors could shift the balance of the coarctation model from atherosclerosis formation to aneurysm formation. A possible means to do this might be treatment with the lysyl oxidase inhibitor βAPN. This would prevent crosslinking of the extracellular matrix which in combination with the mechanical inflammatory and oxidative stimulus produced by the coarctation might produce an aneurysm. A separate direction related to aneurysm formation might be to use the clip as a therapeutic. Placing the clip around the aorta of the mouse provides a mechanical support for the vessel wall. This might be able to be used to prevent or treat aneurysm formation when the vessel wall loses mechanical integrity.

Conclusion

The overall objective for this thesis was to develop an *in vivo* flow model that produces low magnitude oscillatory WSS. To achieve this objective, we created a novel aortic coarctation model using a shape memory nitinol clip. The clip reproducibly constricts the aorta creating a narrowing of the lumen resulting in a stenosis. This mechanical constraint produces a region of flow separation downstream from the coarctation. We have characterized the coarctation in terms of the efficacy, pressure loss, and fluid dynamics. We then measured the endothelial response of shear sensitive redox and inflammatory markers. Lastly, we utilized genetically modified mice and mice treated with pharmacological inhibitors to investigate the mechanisms involved in the expression of WSS induced inflammatory and redox markers. From these experiments we have reached the following conclusions:

1) Coarctation of the descending aorta using a nitinol clip uniquely created a hemodynamic environment of low magnitude oscillatory WSS without a significant change in blood pressure.
2) The *in vivo* endothelial phenotype associated with acutely disturbed flow is characterized by increased production of superoxide and increased expression of select inflammatory proteins. In comparison, the phenotype associated with chronically disturbed flow is characterized by a more modest increase in superoxide and increased levels of multiple inflammatory proteins.
3) In regions of acutely disturbed flow *in vivo*, VCAM-1 expression is not modulated by reactive oxygen species. Additionally, we conclude that p47

phox-dependent NADPH Oxidase activity does not have a functional role in WSS induced superoxide generation in the endothelium.

In summary, we have created a novel murine model of low magnitude oscillatory WSS that can be used to investigate the *in vivo* molecular mechanisms associated with atherogenesis. While previous data obtained *in vitro* indicated that depletion of an individual ROS was sufficient to inhibit flow-induced inflammatory protein expression, our findings, to the contrary, showed that antioxidant treatment *in vivo* does not inhibit shear-dependent inflammatory protein expression. Our results suggest that atherogenesis in the *in vivo* environment is significantly more complicated than the *in vitro* environment and that parallel pathways and compensatory mechanisms are likely activated *in vivo* in response to WSS. These results could have significant implications in the efficacy of antioxidant treatment of atherosclerosis and could explain the complexity of results observed in clinical trials.

APPENDIX A

HYDRO-CY3 STAINING PROTOCOL

1. Prepare hydro-Cy3 for pressure perfusion
    a. It is preferable to use freshly made dye (made within a week or so) – when you break the seal and open the bottle you want to see minimal pink (some is ok but it should not be bright pink)
    b. Dissolve hydro-Cy3 in methanol to a final stock concentration of 1 mg/ml
    c. I use a working dilution of: 500 uL stock hydro-Cy3: 100 mL saline
2. Fill a Viaflex IV bag (250 uL) with the above solution and cover with aluminum foil
3. Sacrifice mouse with CO2 – expose heart and place a butterfly needle in the left ventricle
4. Pressure perfuse @ 100mmHg using Viaflex IV bags 1m above the mouse (turn off the lights in the room - though hydrocyanine is stable it is still somewhat light sensitive)
    a. Perfuse for 5 min with saline
    b. Perfuse for 5 min with working dilution hydro-Cy3 as described above (note: hydro-Cy3 is membrane permeable and detergent is not needed)
    c. Perfuse for 5 min with 10% formalin
    d. Perfuse for 5 min with saline
5. Harvest the aorta

6. Wash aorta in PBS in a 24 well plate until visibly clean (i.e. no blood), and then mount *en face* in Vectashield mounting medium w/DAPI
7. Control
    a. Negative control – Add a pressure perfusion step after the first saline wash and before the hydro-Cy3 with tempol. Perfuse with tempol at 5mM for 5 min.
    b. Positive control - Treat the mouse with 0.5 mg LPS the evening before sacrificing the mouse.

APPENDIX B

AORTIC COARCTATION SURGERY PROTOCOL

Materials

1. Small surgical scissors
2. Hemostat forceps
3. 2 small, micro-forceps
4. Self retaining retractors
5. Nitinol Clip

Procedure

1. Sterilize instruments with glass bead sterilizer.
2. Anesthetize mouse - oxygen delivered through inhalation at a flow rate of 0.5L/min mixed with isoflurane at 3% for induction and 1.5% for maintenance.
3. Shave the abdomen of the mouse.
4. Remove the remainder of hair in this region with depilatory cream (Nair).
5. Wipe skin with gauze to remove excess cream and hair and then cleanse skin with
6. Betadine.
7. Make a single incision along the midline of the skin and peritoneum of the abdomen.
8. Expose the abdominal cavity using a self-retaining retractor to push open the skin and peritoneum.
9. Locate the abdominal aorta using a dissecting microscope. Remove the peridaventitial fatby performing a blunt dissection with the micro-forceps. Push the micro-forceps underneath the aorta to ensure a clear path for the clip.

10. Deform the clip to an open state and insert underneath the aorta. The clip should recover to its orginal state, but warmed saline can help assist the process if needed.
11. Return the intestines to the abdominal cavity and suture the peritoneum and skin together with absorbable sutures.
12. Apply surgical staples along the incision line to ensure proper healing.
13. Keep animals on a heating pad during recovery and give buprenorphine (0.01 mg/kg intraperitoneal) as necessary.

REFERENCES

1. Lloyd-Jones, D., et al., *Heart disease and stroke statistics--2009 update: a report from the American Heart Association Statistics Committee and Stroke Statistics Subcommittee.* Circulation, 2009. **119**(3): p. 480-6.

2. Lloyd-Jones, D., et al., *Heart Disease and Stroke Statistics--2010 Update. A Report From the American Heart Association.* Circulation, 2009.

3. Thom, T., et al., *Heart disease and stroke statistics--2006 update: a report from the American Heart Association Statistics Committee and Stroke Statistics Subcommittee.* Circulation, 2006. **113**(6): p. e85-151.

4. Caro, C.G., J.M. Fitz-Gerald, and R.C. Schroter, *Atheroma and arterial wall shear. Observation, correlation and proposal of a shear dependent mass transfer mechanism for atherogenesis.* Proc R Soc Lond B Biol Sci, 1971. **177**(46): p. 109-59.

5. Ku, D.N., et al., *Pulsatile flow and atherosclerosis in the human carotid bifurcation. Positive correlation between plaque location and low oscillating shear stress.* Arteriosclerosis, 1985. **5**(3): p. 293-302.

6. Ross, R., *Atherosclerosis--an inflammatory disease.* N Engl J Med, 1999. **340**(2): p. 115-26.

7. Stary, H.C., *Natural history and histological classification of atherosclerotic lesions: an update.* Arterioscler Thromb Vasc Biol, 2000. **20**(5): p. 1177-8.

8. Stary, H.C., et al., *A definition of initial, fatty streak, and intermediate lesions of atherosclerosis. A report from the Committee on Vascular Lesions of the Council on Arteriosclerosis, American Heart Association.* Arterioscler Thromb, 1994. **14**(5): p. 840-56.

9. Stary, H.C., et al., *A definition of advanced types of atherosclerotic lesions and a histological classification of atherosclerosis. A report from the Committee on Vascular Lesions of the Council on Arteriosclerosis, American Heart Association.* Circulation, 1995. **92**(5): p. 1355-74.

10. Davies, P.F., *Flow-mediated endothelial mechanotransduction.* Physiol Rev, 1995. **75**(3): p. 519-60.

11. Braunwald, E., *Braunwald's Heart Disease: A Textbook of Cardiovascular Medicine*. ebook ed, ed. R.O.B.M. r Libby MD, Douglas P. Zipes MD, Douglas L. Mann MD. Vol. Eighth 2009, Philadelphia: SAUNDERS ELSEVIER.

12. Wootton, D.M. and D.N. Ku, *Fluid mechanics of vascular systems, diseases, and thrombosis.* Annu Rev Biomed Eng, 1999. **1**: p. 299-329.

13. Glagov, S., et al., *Hemodynamics and atherosclerosis. Insights and perspectives gained from studies of human arteries.* Arch Pathol Lab Med, 1988. **112**(10): p. 1018-31.

14. Perktold, K. and G. Rappitsch, *Computer simulation of local blood flow and vessel mechanics in a compliant carotid artery bifurcation model.* J Biomech, 1995. **28**(7): p. 845-56.

15. Moore, J.E., Jr., et al., *Fluid wall shear stress measurements in a model of the human abdominal aorta: oscillatory behavior and relationship to atherosclerosis.* Atherosclerosis, 1994. **110**(2): p. 225-40.

16. Bargeron, C.B., et al., *Effect of flow partition on wall shear in a cast of a human coronary artery.* Cardiovasc Res, 1988. **22**(5): p. 340-4.

17. Davies, P.F., *Hemodynamic shear stress and the endothelium in cardiovascular pathophysiology.* Nat Clin Pract Cardiovasc Med, 2009. **6**(1): p. 16-26.

18. Cheng, C., et al., *Large variations in absolute wall shear stress levels within one species and between species.* Atherosclerosis, 2007. **195**(2): p. 225-35.

19. Amirbekian, S., et al., *In vivo assessment of blood flow patterns in abdominal aorta of mice with MRI: implications for AAA localization.* Am J Physiol Heart Circ Physiol, 2009. **297**(4): p. H1290-5.

20. Suo, J., et al., *Hemodynamic shear stresses in mouse aortas: implications for atherogenesis.* Arterioscler Thromb Vasc Biol, 2007. **27**(2): p. 346-51.

21. Iiyama, K., et al., *Patterns of vascular cell adhesion molecule-1 and intercellular adhesion molecule-1 expression in rabbit and mouse atherosclerotic lesions and at sites predisposed to lesion formation.* Circ Res, 1999. **85**(2): p. 199-207.

22. Cheng, C., et al., *Atherosclerotic lesion size and vulnerability are determined by patterns of fluid shear stress.* Circulation, 2006. **113**(23): p. 2744-53.

23. Wu, J.H., et al., *Aortic constriction exacerbates atherosclerosis and induces cardiac dysfunction in mice lacking apolipoprotein E.* Arterioscler Thromb Vasc Biol, 2002. **22**(3): p. 469-75.

24. Vaziri, N.D. and Z. Ni, *Expression of NOX-I, gp91phox, p47phox and P67phox in the aorta segments above and below coarctation.* Biochim Biophys Acta, 2005. **1723**(1-3): p. 321-7.

25. Cheng, C., et al., *Shear stress affects the intracellular distribution of eNOS: direct demonstration by a novel in vivo technique.* Blood, 2005. **106**(12): p. 3691-8.

26. Korshunov, V.A. and B.C. Berk, *Flow-induced vascular remodeling in the mouse: a model for carotid intima-media thickening.* Arterioscler Thromb Vasc Biol, 2003. **23**(12): p. 2185-91.

27. Nam, D., et al., *Partial carotid ligation is a model of acutely induced disturbed flow, leading to rapid endothelial dysfunction and atherosclerosis.* Am J Physiol Heart Circ Physiol, 2009. **297**(4): p. H1535-43.

28. Ando, J., et al., *Wall shear stress rather than shear rate regulates cytoplasmic Ca++ responses to flow in vascular endothelial cells.* Biochem Biophys Res Commun, 1993. **190**(3): p. 716-23.

29. Nilius, B. and G. Droogmans, *Ion channels and their functional role in vascular endothelium.* Physiol Rev, 2001. **81**(4): p. 1415-59.

30. Olesen, S.P., D.E. Clapham, and P.F. Davies, *Haemodynamic shear stress activates a K+ current in vascular endothelial cells.* Nature, 1988. **331**(6152): p. 168-70.

31. Li, Y.S., J.H. Haga, and S. Chien, *Molecular basis of the effects of shear stress on vascular endothelial cells.* J Biomech, 2005. **38**(10): p. 1949-71.

32. Wang, Y., et al., *Interplay between integrins and FLK-1 in shear stress-induced signaling.* Am J Physiol Cell Physiol, 2002. **283**(5): p. C1540-7.

33. Shay-Salit, A., et al., *VEGF receptor 2 and the adherens junction as a mechanical transducer in vascular endothelial cells.* Proc Natl Acad Sci U S A, 2002. **99**(14): p. 9462-7.

34. Wang, Y., et al., *Shear Stress Regulates the Flk-1/Cbl/PI3K/NF-kappaB Pathway Via Actin and Tyrosine Kinases.* Cell Mol Bioeng, 2009. **2**(3): p. 341-350.

35. Gudi, S., et al., *Rapid activation of Ras by fluid flow is mediated by Galpha(q) and Gbetagamma subunits of heterotrimeric G proteins in human endothelial cells.* Arterioscler Thromb Vasc Biol, 2003. **23**(6): p. 994-1000.

36. Jo, H., et al., *Differential effect of shear stress on extracellular signal-regulated kinase and N-terminal Jun kinase in endothelial cells. Gi2- and Gbeta/gamma-dependent signaling pathways.* J Biol Chem, 1997. **272**(2): p. 1395-401.

37. Gudi, S.R., C.B. Clark, and J.A. Frangos, *Fluid flow rapidly activates G proteins in human endothelial cells. Involvement of G proteins in mechanochemical signal transduction.* Circ Res, 1996. **79**(4): p. 834-9.

38. Rizzo, V., et al., *Rapid mechanotransduction in situ at the luminal cell surface of vascular endothelium and its caveolae.* J Biol Chem, 1998. **273**(41): p. 26323-9.

39. Hierck, B.P., et al., *Primary cilia sensitize endothelial cells for fluid shear stress.* Dev Dyn, 2008. **237**(3): p. 725-35.

40. Nauli, S.M., et al., *Endothelial cilia are fluid shear sensors that regulate calcium signaling and nitric oxide production through polycystin-1.* Circulation, 2008. **117**(9): p. 1161-71.

41. Van der Heiden, K., et al., *Endothelial primary cilia in areas of disturbed flow are at the base of atherosclerosis.* Atherosclerosis, 2008. **196**(2): p. 542-50.

42. Osawa, M., et al., *Evidence for a role of platelet endothelial cell adhesion molecule-1 in endothelial cell mechanosignal transduction: is it a mechanoresponsive molecule?* J Cell Biol, 2002. **158**(4): p. 773-85.

43. Davies, P.F., A. Robotewskyj, and M.L. Griem, *Quantitative studies of endothelial cell adhesion. Directional remodeling of focal adhesion sites in response to flow forces.* J Clin Invest, 1994. **93**(5): p. 2031-8.

44. McCue, S., S. Noria, and B.L. Langille, *Shear-induced reorganization of endothelial cell cytoskeleton and adhesion complexes.* Trends Cardiovasc Med, 2004. **14**(4): p. 143-51.

45. Shyy, J.Y. and S. Chien, *Role of integrins in endothelial mechanosensing of shear stress.* Circ Res, 2002. **91**(9): p. 769-75.

46. Cunningham, K.S. and A.I. Gotlieb, *The role of shear stress in the pathogenesis of atherosclerosis.* Lab Invest, 2005. **85**(1): p. 9-23.

47. Chatzizisis, Y.S., et al., *Role of endothelial shear stress in the natural history of coronary atherosclerosis and vascular remodeling: molecular, cellular, and vascular behavior.* J Am Coll Cardiol, 2007. **49**(25): p. 2379-93.

48. Taniyama, Y. and K.K. Griendling, *Reactive oxygen species in the vasculature: molecular and cellular mechanisms.* Hypertension, 2003. **42**(6): p. 1075-81.

49. Thomas, S.R., P.K. Witting, and G.R. Drummond, *Redox control of endothelial function and dysfunction: molecular mechanisms and therapeutic opportunities.* Antioxid Redox Signal, 2008. **10**(10): p. 1713-65.

50. Aldieri, E., et al., *Classical inhibitors of NOX NAD(P)H oxidases are not specific.* Curr Drug Metab, 2008. **9**(8): p. 686-96.

51. Chen, K., S.R. Thomas, and J.F. Keaney, Jr., *Beyond LDL oxidation: ROS in vascular signal transduction.* Free Radic Biol Med, 2003. **35**(2): p. 117-32.

52. Claiborne, A., et al., *Protein-sulfenic acid stabilization and function in enzyme catalysis and gene regulation.* FASEB J, 1993. **7**(15): p. 1483-90.

53. Klotz, L.O., P. Schroeder, and H. Sies, *Peroxynitrite signaling: receptor tyrosine kinases and activation of stress-responsive pathways.* Free Radic Biol Med, 2002. **33**(6): p. 737-43.

54. Dikalov, S., K.K. Griendling, and D.G. Harrison, *Measurement of reactive oxygen species in cardiovascular studies.* Hypertension, 2007. **49**(4): p. 717-27.

55. Liochev, S.I. and I. Fridovich, *Lucigenin (bis-N-methylacridinium) as a mediator of superoxide anion production.* Arch Biochem Biophys, 1997. **337**(1): p. 115-20.

56. Fink, B., et al., *Detection of intracellular superoxide formation in endothelial cells and intact tissues using dihydroethidium and an HPLC-based assay.* Am J Physiol Cell Physiol, 2004. **287**(4): p. C895-902.

57. Marchesi, E., et al., *Photoreduction of the fluorescent dye 2'-7'-dichlorofluorescein: a spin trapping and direct electron spin resonance study with implications for oxidative stress measurements.* Free Radic Biol Med, 1999. **26**(1-2): p. 148-61.

58. Kundu, K., et al., *Hydrocyanines: a class of fluorescent sensors that can image reactive oxygen species in cell culture, tissue, and in vivo.* Angew Chem Int Ed Engl, 2009. **48**(2): p. 299-303.

59. Sorescu, D., et al., *Superoxide production and expression of nox family proteins in human atherosclerosis.* Circulation, 2002. **105**(12): p. 1429-35.

60. Li, J.M. and A.M. Shah, *Endothelial cell superoxide generation: regulation and relevance for cardiovascular pathophysiology.* Am J Physiol Regul Integr Comp Physiol, 2004. **287**(5): p. R1014-30.

61. Cai, H. and D.G. Harrison, *Endothelial dysfunction in cardiovascular diseases: the role of oxidant stress.* Circ Res, 2000. **87**(10): p. 840-4.

62. Liu, Y., et al., *Mitochondrial sources of H2O2 generation play a key role in flow-mediated dilation in human coronary resistance arteries.* Circ Res, 2003. **93**(6): p. 573-80.

63. Griendling, K.K. and G.A. FitzGerald, *Oxidative stress and cardiovascular injury: Part I: basic mechanisms and in vivo monitoring of ROS.* Circulation, 2003. **108**(16): p. 1912-6.

64. Topper, J.N., et al., *Identification of vascular endothelial genes differentially responsive to fluid mechanical stimuli: cyclooxygenase-2, manganese superoxide*

dismutase, and endothelial cell nitric oxide synthase are selectively up-regulated by steady laminar shear stress. Proc Natl Acad Sci U S A, 1996. **93**(19): p. 10417-22.

65. Lehoux, S., *Redox signalling in vascular responses to shear and stretch.* Cardiovasc Res, 2006. **71**(2): p. 269-79.

66. Hwang, J., et al., *Pulsatile versus oscillatory shear stress regulates NADPH oxidase subunit expression: implication for native LDL oxidation.* Circ Res, 2003. **93**(12): p. 1225-32.

67. Hwang, J., et al., *Oscillatory shear stress stimulates endothelial production of O2- from p47phox-dependent NAD(P)H oxidases, leading to monocyte adhesion.* J Biol Chem, 2003. **278**(47): p. 47291-8.

68. Sorescu, G.P., et al., *Bone morphogenic protein 4 produced in endothelial cells by oscillatory shear stress induces monocyte adhesion by stimulating reactive oxygen species production from a nox1-based NADPH oxidase.* Circ Res, 2004. **95**(8): p. 773-9.

69. Barry-Lane, P.A., et al., *p47phox is required for atherosclerotic lesion progression in ApoE(-/-) mice.* J Clin Invest, 2001. **108**(10): p. 1513-22.

70. McNally, J.S., et al., *Role of xanthine oxidoreductase and NAD(P)H oxidase in endothelial superoxide production in response to oscillatory shear stress.* Am J Physiol Heart Circ Physiol, 2003. **285**(6): p. H2290-7.

71. Brooks, A.R., P.I. Lelkes, and G.M. Rubanyi, *Gene expression profiling of human aortic endothelial cells exposed to disturbed flow and steady laminar flow.* Physiol Genomics, 2002. **9**(1): p. 27-41.

72. McNally, J.S., et al., *Regulation of xanthine oxidoreductase protein expression by hydrogen peroxide and calcium.* Arterioscler Thromb Vasc Biol, 2005. **25**(8): p. 1623-8.

73. Mueller, C.F., et al., *The role of the multidrug resistance protein-1 in modulation of endothelial cell oxidative stress.* Circ Res, 2005. **97**(7): p. 637-44.

74. Barbieri, S.S., et al., *Apocynin prevents cyclooxygenase 2 expression in human monocytes through NADPH oxidase and glutathione redox-dependent mechanisms.* Free Radic Biol Med, 2004. **37**(2): p. 156-65.

75. Stefanska, J. and R. Pawliczak, *Apocynin: molecular aptitudes.* Mediators Inflamm, 2008. **2008**: p. 106507.

76. Holland, J.A., et al., *Thrombin stimulated reactive oxygen species production in cultured human endothelial cells.* Endothelium, 1998. **6**(2): p. 113-21.

77. Ghosh, M., H.D. Wang, and J.R. McNeill, *Role of oxidative stress and nitric oxide in regulation of spontaneous tone in aorta of DOCA-salt hypertensive rats.* Br J Pharmacol, 2004. **141**(4): p. 562-73.

78. Beswick, R.A., et al., *NADH/NADPH oxidase and enhanced superoxide production in the mineralocorticoid hypertensive rat.* Hypertension, 2001. **38**(5): p. 1107-11.

79. Ximenes, V.F., et al., *The oxidation of apocynin catalyzed by myeloperoxidase: proposal for NADPH oxidase inhibition.* Arch Biochem Biophys, 2007. **457**(2): p. 134-41.

80. Heumuller, S., et al., *Apocynin is not an inhibitor of vascular NADPH oxidases but an antioxidant.* Hypertension, 2008. **51**(2): p. 211-7.

81. Tew, D.G., *Inhibition of cytochrome P450 reductase by the diphenyliodonium cation. Kinetic analysis and covalent modifications.* Biochemistry, 1993. **32**(38): p. 10209-15.

82. Xia, Y., et al., *Inducible nitric-oxide synthase generates superoxide from the reductase domain.* J Biol Chem, 1998. **273**(35): p. 22635-9.

83. Stuehr, D.J., et al., *Inhibition of macrophage and endothelial cell nitric oxide synthase by diphenyleneiodonium and its analogs.* FASEB J, 1991. **5**(1): p. 98-103.

84. Bedard, K. and K.H. Krause, *The NOX family of ROS-generating NADPH oxidases: physiology and pathophysiology.* Physiol Rev, 2007. **87**(1): p. 245-313.

85. Suzuki, K., *Anti-oxidants for therapeutic use: why are only a few drugs in clinical use?* Adv Drug Deliv Rev, 2009. **61**(4): p. 287-9.

86. Simonsen, U., F.H. Christensen, and N.H. Buus, *The effect of tempol on endothelium-dependent vasodilatation and blood pressure.* Pharmacol Ther, 2009. **122**(2): p. 109-24.

87. Luo, Z., et al., *Comparison of inhibitors of superoxide generation in vascular smooth muscle cells.* Br J Pharmacol, 2009. **157**(6): p. 935-43.

88. Kimura, S., et al., *Mitochondria-derived reactive oxygen species and vascular MAP kinases: comparison of angiotensin II and diazoxide.* Hypertension, 2005. **45**(3): p. 438-44.

89. Xu, H., G.D. Fink, and J.J. Galligan, *Tempol lowers blood pressure and sympathetic nerve activity but not vascular O2- in DOCA-salt rats.* Hypertension, 2004. **43**(2): p. 329-34.

90. Fang, J., et al., *Ebselen: a thioredoxin reductase-dependent catalyst for alpha-tocopherol quinone reduction.* Toxicol Appl Pharmacol, 2005. **207**(2 Suppl): p. 103-9.

91. Zhao, R., H. Masayasu, and A. Holmgren, *Ebselen: a substrate for human thioredoxin reductase strongly stimulating its hydroperoxide reductase activity and a superfast thioredoxin oxidant.* Proc Natl Acad Sci U S A, 2002. **99**(13): p. 8579-84.

92. Musaev, D.G., et al., *Can the ebselen derivatives catalyze the isomerization of peroxynitrite to nitrate?* J Am Chem Soc, 2003. **125**(13): p. 3877-88.

93. Maulik, N., T. Yoshida, and D.K. Das, *Oxidative stress developed during the reperfusion of ischemic myocardium induces apoptosis.* Free Radic Biol Med, 1998. **24**(5): p. 869-75.

94. Heitzer, T., et al., *Tetrahydrobiopterin improves endothelium-dependent vasodilation in chronic smokers : evidence for a dysfunctional nitric oxide synthase.* Circ Res, 2000. **86**(2): p. E36-41.

95. Heitzer, T., et al., *Tetrahydrobiopterin improves endothelium-dependent vasodilation by increasing nitric oxide activity in patients with Type II diabetes mellitus.* Diabetologia, 2000. **43**(11): p. 1435-8.

96. Creager, M.A., et al., *L-arginine improves endothelium-dependent vasodilation in hypercholesterolemic humans.* J Clin Invest, 1992. **90**(4): p. 1248-53.

97. Kauser, K., et al., *Role of endogenous nitric oxide in progression of atherosclerosis in apolipoprotein E-deficient mice.* Am J Physiol Heart Circ Physiol, 2000. **278**(5): p. H1679-85.

98. Mohan, S., et al., *IkappaBalpha-dependent regulation of low-shear flow-induced NF-kappa B activity: role of nitric oxide.* Am J Physiol Cell Physiol, 2003. **284**(4): p. C1039-47.

99. Nagel, T., et al., *Vascular endothelial cells respond to spatial gradients in fluid shear stress by enhanced activation of transcription factors.* Arterioscler Thromb Vasc Biol, 1999. **19**(8): p. 1825-34.

100. Orr, A.W., et al., *The subendothelial extracellular matrix modulates NF-kappaB activation by flow: a potential role in atherosclerosis.* J Cell Biol, 2005. **169**(1): p. 191-202.

101. Hajra, L., et al., *The NF-kappa B signal transduction pathway in aortic endothelial cells is primed for activation in regions predisposed to atherosclerotic lesion formation.* Proc Natl Acad Sci U S A, 2000. **97**(16): p. 9052-7.

102. Pueyo, M.E., et al., *Angiotensin II stimulates endothelial vascular cell adhesion molecule-1 via nuclear factor-kappaB activation induced by intracellular oxidative stress.* Arterioscler Thromb Vasc Biol, 2000. **20**(3): p. 645-51.

103. Hernandez-Presa, M., et al., *Angiotensin-converting enzyme inhibition prevents arterial nuclear factor-kappa B activation, monocyte chemoattractant protein-1 expression, and macrophage infiltration in a rabbit model of early accelerated atherosclerosis.* Circulation, 1997. **95**(6): p. 1532-41.

104. Han, Y., M.S. Runge, and A.R. Brasier, *Angiotensin II induces interleukin-6 transcription in vascular smooth muscle cells through pleiotropic activation of nuclear factor-kappa B transcription factors.* Circ Res, 1999. **84**(6): p. 695-703.

105. Iademarco, M.F., et al., *Characterization of the promoter for vascular cell adhesion molecule-1 (VCAM-1).* J Biol Chem, 1992. **267**(23): p. 16323-9.

106. Lawson, C. and S. Wolf, *ICAM-1 signaling in endothelial cells.* Pharmacol Rep, 2009. **61**(1): p. 22-32.

107. Chappell, D.C., et al., *Oscillatory shear stress stimulates adhesion molecule expression in cultured human endothelium.* Circ Res, 1998. **82**(5): p. 532-9.

108. Basta, G., et al., *At least 2 distinct pathways generating reactive oxygen species mediate vascular cell adhesion molecule-1 induction by advanced glycation end products.* Arterioscler Thromb Vasc Biol, 2005. **25**(7): p. 1401-7.

109. Chiu, J.J., et al., *Shear stress increases ICAM-1 and decreases VCAM-1 and E-selectin expressions induced by tumor necrosis factor-[alpha] in endothelial cells.* Arterioscler Thromb Vasc Biol, 2004. **24**(1): p. 73-9.

110. Mohan, S., et al., *Regulation of low shear flow-induced HAEC VCAM-1 expression and monocyte adhesion.* Am J Physiol, 1999. **276**(5 Pt 1): p. C1100-7.

111. Cybulsky, M.I., et al., *A major role for VCAM-1, but not ICAM-1, in early atherosclerosis.* J Clin Invest, 2001. **107**(10): p. 1255-62.

112. Jongstra-Bilen, J., et al., *Low-grade chronic inflammation in regions of the normal mouse arterial intima predisposed to atherosclerosis.* J Exp Med, 2006. **203**(9): p. 2073-83.

113. Nakashima, Y., et al., *Upregulation of VCAM-1 and ICAM-1 at atherosclerosis-prone sites on the endothelium in the ApoE-deficient mouse.* Arterioscler Thromb Vasc Biol, 1998. **18**(5): p. 842-51.

114. Collins, R.G., et al., *P-Selectin or intercellular adhesion molecule (ICAM)-1 deficiency substantially protects against atherosclerosis in apolipoprotein E-deficient mice.* J Exp Med, 2000. **191**(1): p. 189-94.

115. Gall, K., et al., *Thermomechanics of the shape memory effect in polymers for biomedical applications.* J Biomed Mater Res A, 2005. **73**(3): p. 339-48.

116. Frick, C.P., et al., *Thermal processing of polycrystalline NiTi shape memory alloys.* Materials Science and Engineering a-Structural Materials Properties Microstructure and Processing, 2005. **405**(1-2): p. 34-49.

117. Garg, P., et al., *Effect of the Na-K-2Cl cotransporter NKCC1 on systemic blood pressure and smooth muscle tone.* Am J Physiol Heart Circ Physiol, 2007. **292**(5): p. H2100-5.

118. Duvall, C.L., et al., *Quantitative microcomputed tomography analysis of collateral vessel development after ischemic injury.* Am J Physiol Heart Circ Physiol, 2004. **287**(1): p. H302-10.

119. Weiss, D., J.J. Kools, and W.R. Taylor, *Angiotensin II-induced hypertension accelerates the development of atherosclerosis in apoE-deficient mice.* Circulation, 2001. **103**(3): p. 448-54.

120. Ritman, E.L., *Micro-computed tomography-current status and developments.* Annu Rev Biomed Eng, 2004. **6**: p. 185-208.

121. Oshinski, J.N., et al., *Effects of acceleration on the accuracy of MR phase velocity measurements.* J Magn Reson Imaging, 1992. **2**(6): p. 665-70.

122. Oshinski, J.N., D.N. Ku, and R.I. Pettigrew, *Turbulent fluctuation velocity: the most significant determinant of signal loss in stenotic vessels.* Magn Reson Med, 1995. **33**(2): p. 193-9.

123. Ferrara, D.E., et al., *Quantitative 3D fluorescence technique for the analysis of en face preparations of arterial walls using quantum dot nanocrystals and two-photon excitation laser scanning microscopy.* Am J Physiol Regul Integr Comp Physiol, 2006. **290**(1): p. R114-23.

124. Won, D., et al., *Relative reduction of endothelial nitric-oxide synthase expression and transcription in atherosclerosis-prone regions of the mouse aorta and in an in vitro model of disturbed flow.* Am J Pathol, 2007. **171**(5): p. 1691-704.

125. Getz, G.S. and C.A. Reardon, *Diet and murine atherosclerosis.* Arterioscler Thromb Vasc Biol, 2006. **26**(2): p. 242-9.

126. Meir, K.S. and E. Leitersdorf, *Atherosclerosis in the apolipoprotein-E-deficient mouse: a decade of progress.* Arterioscler Thromb Vasc Biol, 2004. **24**(6): p. 1006-14.

127. Mohan, S., et al., *Low shear stress preferentially enhances IKK activity through selective sources of ROS for persistent activation of NF-kappaB in endothelial cells.* Am J Physiol Cell Physiol, 2007. **292**(1): p. C362-71.

128. Sorescu, G.P., et al., *Bone morphogenic protein 4 produced in endothelial cells by oscillatory shear stress stimulates an inflammatory response.* J Biol Chem, 2003. **278**(33): p. 31128-35.

129. Gareus, R., et al., *Endothelial cell-specific NF-kappaB inhibition protects mice from atherosclerosis.* Cell Metab, 2008. **8**(5): p. 372-83.

130. Kanters, E., et al., *Hematopoietic NF-kappaB1 deficiency results in small atherosclerotic lesions with an inflammatory phenotype.* Blood, 2004. **103**(3): p. 934-40.

131. Kanters, E., et al., *Inhibition of NF-kappaB activation in macrophages increases atherosclerosis in LDL receptor-deficient mice.* J Clin Invest, 2003. **112**(8): p. 1176-85.

132. Nageh, M.F., et al., *Deficiency of inflammatory cell adhesion molecules protects against atherosclerosis in mice.* Arterioscler Thromb Vasc Biol, 1997. **17**(8): p. 1517-20.

133. Lauer, N., et al., *Critical involvement of hydrogen peroxide in exercise-induced up-regulation of endothelial NO synthase.* Cardiovasc Res, 2005. **65**(1): p. 254-62.

134. San Martin, A., et al., *Reactive oxygen species-selective regulation of aortic inflammatory gene expression in Type 2 diabetes.* Am J Physiol Heart Circ Physiol, 2007. **292**(5): p. H2073-82.

135. Wilcox, C.S. and A. Pearlman, *Chemistry and antihypertensive effects of tempol and other nitroxides.* Pharmacol Rev, 2008. **60**(4): p. 418-69.

136. Kawada, N., et al., *A mouse model of angiotensin II slow pressor response: role of oxidative stress.* J Am Soc Nephrol, 2002. **13**(12): p. 2860-8.

137. Dikalova, A., et al., *Nox1 overexpression potentiates angiotensin II-induced hypertension and vascular smooth muscle hypertrophy in transgenic mice.* Circulation, 2005. **112**(17): p. 2668-76.

138. Saito, K., et al., *Two reaction sites of a spin label, TEMPOL (4-hydroxy-2,2,6,6-tetramethylpiperidine-N-oxyl), with hydroxyl radical.* J Pharm Sci, 2003. **92**(2): p. 275-80.

139. Harrison, D.G., et al., *Endothelial mechanotransduction, nitric oxide and vascular inflammation.* J Intern Med, 2006. **259**(4): p. 351-63.

140. Ramkhelawon, B., et al., *Shear stress regulates angiotensin type 1 receptor expression in endothelial cells.* Circ Res, 2009. **105**(9): p. 869-75.

141. Yin, W., H. Jo, and E.O. Voit, *Systems analysis of the role of bone morphogenic protein 4 in endothelial inflammation.* Ann Biomed Eng. **38**(2): p. 291-307.

142. Ritman, E.L., *Micro-computed tomography of the lungs and pulmonary-vascular system.* Proc Am Thorac Soc, 2005. **2**(6): p. 477-80, 501.

143. Schambach, S.J., et al., *Ultrafast high-resolution in vivo volume-CTA of mice cerebral vessels.* Stroke, 2009. **40**(4): p. 1444-50.

144. Kiessling, F., et al., *Volumetric computed tomography (VCT): a new technology for noninvasive, high-resolution monitoring of tumor angiogenesis.* Nat Med, 2004. **10**(10): p. 1133-8.

145. Mukundan, S., Jr., et al., *A liposomal nanoscale contrast agent for preclinical CT in mice.* AJR Am J Roentgenol, 2006. **186**(2): p. 300-7.

146. Schambach, S.J., et al., *Application of micro-CT in small animal imaging.* Methods. **50**(1): p. 2-13.

147. Taylor, C.A., T.J. Hughes, and C.K. Zarins, *Finite element modeling of three-dimensional pulsatile flow in the abdominal aorta: relevance to atherosclerosis.* Ann Biomed Eng, 1998. **26**(6): p. 975-87.

148. Les, A.S., et al., *Quantification of Hemodynamics in Abdominal Aortic Aneurysms During Rest and Exercise Using Magnetic Resonance Imaging and Computational Fluid Dynamics.* Ann Biomed Eng.

149. Conway, D.E., et al., *Endothelial cell responses to atheroprone flow are driven by two separate flow components: low time-average shear stress and fluid flow reversal.* Am J Physiol Heart Circ Physiol. **298**(2): p. H367-74.

VITA

NICK J WILLETT

Nick was born in Boston, MA on May 4th 1983. He grew up in Newton, MA where he went to Angier Elementary, Brown Middle school and Newton South high school. He was particularly engaged in the sciences. He complemented school with an active interest sports including soccer, tennis, and skiing.He went on to pursue a Bachelors degree in Mechanical Engineering from the University of Colorado in Boulder, CO. There he developed an interest in the biological applications of engineering in part from the engineering school and in part from emergency medical training (EMT) and ski patrol at Winter Park ski resort. Nick graduated from the University of Colorado in 2005 and went on the graduate school in the biomedical engineering program at Emory University and Georgia Institute of Technology in Atlanta, GA. He is now finishing up his PhD and planning to continue research doing a post-doc at Georgia Tech.